Journal of Mathematical Biology (2026) 92:12
https://doi.org/10.1007/s00285-025-02326-6

Mathematical Biology

# Spatio-temporal evolution of cooperation: multistability, pattern formation, and chaos in resource-driven eco-evolutionary games

Haihui Cheng [1,2,3] · Hao Wang [3] · Xinzhu Meng [2]

Received: 21 October 2024 / Revised: 9 August 2025 / Accepted: 30 November 2025


**Abstract**

In biological systems, cooperative behavior forms the foundation for the survival and prosperity of many organisms. However, the finite nature of resources often drives selfish individuals to exploit resources through deceptive tactics, thereby instigating conflicts between collective and individual interests. These strategic interactions not only alter the availability of environmental resources but also feedback on the strategic choices of populations, leading to the co-evolution of environmental resources and behavioral strategies. By integrating population dynamics with replicator dynamics, we develop models for both well-mixed and spatially heterogeneous distributions that incorporate resource feedback mechanisms to analyze the intricate interplay between cooperative behavior and resource dynamics across temporal and spatial scales. Our findings reveal complex evolutionary dynamics, including rich multistability, transcritical and Hopf bifurcations in the temporal system, alongside spatial stability, Turing instability, Turing-Hopf bifurcation, and chaotic behavior in the spatial diffusion system. In homogeneous distributions, payoffs result in stable periodic solutions, while heterogeneous distributions disrupt stable periodicity and lead to chaotic dynamics. Notably, increasing the initial density of cooperators, the rate of resource growth, and reducing the initial resource stock are favorable for sustaining cooperation. Interestingly, high payoffs for cooperators and low payoffs for defectors do not necessarily promote cooperative behavior, as evolutionary outcomes also depend on resource abundance. We provide the conditions that sustain cooperation, revealing the critical

✉ Hao Wang
hao8@ualberta.ca

✉ Xinzhu Meng
mxz721106@sdust.edu.cn

1 School of Mathematics and Statistics, Northeastern University at Qinhuangdao, Qinhuangdao 066004, China

2 College of Mathematics and Systems Science, Shandong University of Science and Technology, Qingdao 266590, People's Republic of China

3 Department of Mathematical and Statistical Sciences, University of Alberta, Edmonton T6G 2G1, Alberta, Canada

Published online: 11 December 2025

role of resource dynamics and spatial diffusion in shaping the evolution of cooperative strategies. Our findings have important implications for studying ecosystem management, conservation biology, and animal social behavior.

**Keywords** Evolutionary game theory · Multistability · Turing-Hopf bifurcation · Pattern formation · Chaos

**Mathematics Subject Classification** 91A22

## 1 Introduction

Cooperative behavior serves as the cornerstone of complex ecosystems, enabling organisms to develop advanced capabilities and stronger adaptations. However, scarce resources within a population drive individuals to prioritize their own interests, often at the expense of the collective good. This self-serving behavior can lead to social dilemmas, where cooperation erodes and the tragedy of the commons emerges as the most damaging outcome. This dynamic is vividly illustrated in group hunts by predators such as African wild dogs (Dugatkin 2001), wolves (MacNulty et al. 2012), chimpanzees (Boesch 1994), and lions (Scheel and Packer 1991). Cooperative members expend significant effort to secure resources, while defectors, who contribute little or nothing, benefit from the collective's success. Similarly, certain bird species, including grouse, waterfowl, and grebes, avoid the burden of rearing offspring by laying their eggs in the nests of others (Lyon and Eadie 2008). Even among vampire bats, free-riders exploit the resources shared by cooperative individuals (Riehl and Frederickson 2016; Wilkinson 1984). Despite the risks associated with such deception, cooperation persists across biological, economic, and social systems (Jousset et al. 2013; Rand and Nowak 2013; Haselhuhn and Mellers 2005). The tension between individual and collective interests poses a significant challenge for evolutionary game theory. Understanding why cooperation endures, identifying the conditions and mechanisms that sustain it, and exploring the evolutionary processes that govern it are complex yet critical tasks. Replicator dynamics (Hofbauer and Sigmund 1998) provide a robust framework for investigating the evolution of cooperation, offering insights into how cooperative strategies can survive despite the presence of deceitful individuals.

Classic evolutionary game theory often assumes a fixed and unchanging environment, focusing solely on the internal frequency-varying properties of replicator dynamics while overlooking the impact of renewable environmental resources. However, in reality, the interaction of strategies affects the stock of environmental resources, which in turn influences players' strategic choices. This dynamic interplay results in eco-evolutionary games, where strategies and the environment mutually influence each other. Such eco-evolutionary games are prevalent in complex systems like biological and social environments (Lion 2018; Hauert et al. 2019; Jiang et al. 2023). For example, in the fishing industry, fish stock directly impacts the efficacy of fishing strategies, while the intensity of fishing practices affects the fish stock (Tilman et al. 2016). In the realm of infectious diseases, the virus transmission rate influences individuals' choices regarding vaccination strategies and public health measures, and vice versa

(Yamin et al. 2016; Yong and Choy 2021; Wagner et al. 2022). In climate dynamics, the strategies of individuals, businesses, and nations shape global climate change, while the long-term effects of environmental changes, in turn, modify these strategies, creating a feedback loop (Nordhaus 2015; Kolk and Pinkse 2005). Individual strategic choices such as foraging behavior (Cheng et al. 2022; Auger et al. 2002), territorial competition (Valdaliso and Wilson 2015), and cooperation and defection are directly linked to changes in environmental resources. The distribution and stock of resources are critical to the survival of individual strategies, and the collective outcome of these strategies affects the long-term availability of resources (Tilman 1982; Schoener 1983). For example, excessive resource utilization may result in resource depletion, thus forcing individuals to readjust their strategies to new resource conditions (Nowak and Sigmund 2004; Smith 1982). Therefore, understanding the feedback mechanisms between resources and strategies is important for predicting ecosystem dynamics and evolutionary trends. Previous works focus on the internal interactions of strategies in replicator dynamics models, such as stability, adaptability, and evolutionary stability of strategies (Hofbauer and Sigmund 1998; van Veelen 2011; Garay et al. 2018). These studies typically assume that strategy interactions take place in a fixed resource environment, with less consideration paid to dynamic changes in resources and external feedback on strategies. We introduce a nonlinear feedback mechanism between renewable resources and strategic choices, modeling how resources affect strategic choices while accounting for the effects of strategic changes on the distribution of resources.

In recent years, the mutual feedback between environments and strategies has attracted increasing attention from researchers. Weitz et al. (2016) developed a coevolutionary game framework in which the environment and the strategies of players depending on it co-evolve. Their study demonstrated that the system exhibits oscillations between cooperation and defection, accompanied by cyclic fluctuations in environmental quality from depleted to abundant states. Building upon this work, Lin and Weitz (2019) proposed a stochastic model incorporating individual interactions on a two-dimensional grid, introducing the diffusion of resources. Their simulations revealed the emergence of spatiotemporal oscillations in spatial evolutionary games. Hauert et al. (2019) investigated the evolution of strategies in heterogeneous environments, where individuals engage in asymmetric games influenced by local environmental conditions. They examined the bistability of such feedback systems and found that rapid ecological changes can lead to the collapse of cooperation. Tilman et al. (2020) developed an ecological evolutionary game framework, deriving conditions for equilibrium stability and highlighting that the coevolution of strategies and environments is shaped by their relative timescales. Building on this line of research, Cheng et al. (2024) extended the framework of Tilman et al. by incorporating spatial diffusion through partial differential equations and proposed an evolutionary game model featuring decaying public goods. While Cheng et al. (2024) investigated resource degradation in a biological setting with public goods, our study focuses on logistically growing renewable resources, which are widely observed across ecological systems. Most existing studies assume linear environmental feedback, wherein resource dynamics follow constant rates of growth or depletion. To more accurately capture biological realism and account for saturation effects in resource consump-

tion, we introduce a nonlinear Holling type II functional response. This formulation enables us to investigate how nonlinear feedback mechanisms shape the evolution of cooperation and give rise to both complex temporal behaviors and rich spatial pattern formation.

As our understanding of ecosystem complexity deepens, eco-evolutionary game theory has emerged as an invaluable tool for investigating resource sustainability and the evolution of strategies. Within this framework, spatial diffusion is increasingly recognized as a crucial factor influencing strategy dynamics and ecological processes. Traditional evolutionary games often assume that individuals interact randomly in homogeneous environments, either explicitly or implicitly. However, this assumption overlooks the significant impact of spatial heterogeneity on interaction patterns and strategic choices (Nowak and May 1992; Nanda and Durrett 2017; Schreiber and Killingback 2013). In biology, spatial diffusion models are widely employed to depict species distributions, population dynamics, and ecosystem stability (Song et al. 2017; Yang et al. 2021; Yuan et al. 2013). For instance, in epidemiology, spatial diffusion is used to model disease transmission pathways, revealing how individual movement patterns affect the rate and extent of disease spread (Keeling and Rohani 2011). In studies of biological invasions, spatial dispersal helps predict the expansion routes and ecological impacts of invasive species, providing a theoretical foundation for management and control (Hastings et al. 2004). Additionally, spatial dispersal can lead to non-uniform distributions of prey and predators in the environment, revealing complex dynamic equilibria in ecosystems by modeling the spatial interactions between these groups (Wang et al. 2022; Gou et al. 2023). The application of spatial diffusion in biology and evolutionary games offers new perspectives for analyzing the evolution and stability of strategies within ecosystems. Previous studies of eco-evolutionary games (Weitz et al. 2016; Tilman et al. 2020; Hauert et al. 2019; Cheng et al. 2023), particularly those utilizing replicator dynamics, have primarily focused on variations in strategic frequency, often overlooking changes in player density. This oversight limits the understanding of how spatial diffusion affects the spatial distribution and stabilization of strategies. To address these limitations, we innovate by transforming strategy frequency changes in replicator dynamics into population density changes, skillfully integrating these with spatial diffusion to more comprehensively reveal the profound effects of heterogeneous distribution on strategy evolution.

Patterns, as a self-organizing phenomenon, have garnered significant attention and in-depth exploration across various fields, including economics, biology, and physics. The study of patterns in these systems unveils complex spatial structures and dynamic behaviors, shedding light on phenomena such as market fluctuations, species distributions, and nonlinear chemical reactions (Alfarano et al. 2005; Manna et al. 2021; Halatek and Frey 2018). However, despite the wealth of research findings in these areas, the application and exploration of patterns within eco-evolutionary games remain relatively underdeveloped. Eco-evolutionary game theory focuses on the dynamics of strategies among species, particularly how these strategies interact and evolve within their environment. The introduction of pattern-based models into this field offers a novel perspective, enabling scholars to investigate the spatial distribution of strategies and their evolution over time. This approach can reveal

intricate patterns within ecosystems that are not yet fully understood, offering deeper insights into how cooperative and defective strategies coexist and maintain spatial balance (Newth and Cornforth 2009; Szabó and Szolnoki 2012; Cheng et al. 2024). Despite the significant potential of pattern analysis in eco-evolutionary games, related studies are still relatively scarce. To address this gap, we combine spatial diffusion with eco-evolutionary games to explore the spatial distribution and dynamic evolution of different strategies in the context of renewable resources, aiming to uncover the intrinsic mechanisms by which cooperators and resources form complex patterns.

This paper is organized as follows. In Section 2, we develop the temporal and spatial diffusion models. Section 3 focuses on the analysis of the temporal system (2.5), where we investigate the local stability, bi-stability, and multi-stability of equilibria. We also derive the conditions for Hopf and transcritical bifurcations and further examine the stability of periodic solutions and the direction of Hopf bifurcation. In Section 4, we shift our focus to the spatial diffusion system (2.6), exploring spatial stability, Hopf bifurcation, and Turing-Hopf bifurcation. Section 5 addresses the complex spatial distributions of cooperation and renewable resources, while Section 6 uncovers chaotic dynamics driven by payoffs in the diffusion system. Finally, in Section 7, we summarize our findings and discuss their broader implications.

## 2 Model formulation

### 2.1 Temporal model

In biological systems, cooperators typically invest significant effort to extract resources from the environment, whereas defectors avoid such efforts and instead acquire resources through deception. A quintessential example is the female cuckoo, which notoriously lays its eggs in the nests of other birds. The unsuspecting hosts expend their energy raising offspring that are not their own-a deceptive strategy that is also found in other species, including certain brood-parasitic ducks and cowbirds. This dynamic is not limited to avian species. In group hunting scenarios involving lions, wolves, African wild dogs, and even certain species of dolphins, deceivers may intentionally withhold effort, cheating cooperators out of their hard-earned prey. Additionally, in social insects like ants (Lenoir et al. 2001), certain individuals may refrain from foraging, instead benefiting from the labor of others. In vampire bat communities, some individuals may feign cooperative behavior to gain access to food shared by genuine cooperators. These examples exemplify a widespread biological phenomenon in which cooperators invest substantial effort in acquiring and sharing resources, whereas defectors benefit through deceptive means without exerting comparable effort. Tilman et al. (2020) proposed a renewable resource model in which players consume resources in a linear fashion. However, in biological systems, particularly under resource-abundant conditions, individuals are often constrained not by resource availability but by their capacity to process or utilize what they acquire. To capture this nonlinear saturation effect, we build upon the research by Tilman et al. (2020) by introducing a Holling type II functional response, replacing the constant-rate linear consumption assump-

tion with a saturating nonlinear mechanism. To describe the behavior of players under the biological scenarios outlined above, we construct a model in which a renewable resource grows logistically and is consumed by cooperators and defectors according to a Holling type II functional response. The dynamics of the resource is governed by

$$\frac{\mathrm{d}n}{\mathrm{d}t} = rn\left(1-\frac{n}{k}\right) - \frac{p\widehat{e}un}{1+gn} - \frac{p\widetilde{e}(N-u)n}{1+gn}, \tag{2.1}$$

where $n$ is resource stock, $N$ is total player density, $k$ is carrying capacity of $n$, $r$ is intrinsic growth rate, $u \in [0, N]$ is cooperator density, and $p$ is a parameter that maps the harvesting efforts $\widehat{e}$ and $\widetilde{e}$ to the resource capture rates of cooperators and defectors. The parameter $g$ represents the handling time, reflecting the non-linear saturation mechanism when players capture resources. The last two terms describe the resource consumption by cooperators and defectors, respectively–both governed by the Holling type II response, in which consumption saturates as resource availability increases.

In our model, cooperators exert effort to directly access and consume the resource, and thus $\widehat{e} > 0$. Defectors, by contrast, invest no effort and cannot directly consume the resource. Instead, they gain indirect benefits by exploiting the cooperative framework without participating in resource acquisition. As a result, we set $\widetilde{e} = 0$ to reflect their lack of contribution. Such scenarios can be observed in biological systems. For example, consider a cooperative hunting system where prey density decreases only through direct predation by cooperators; if only defectors are present, prey density remains unaffected by predation because defectors do not invest the effort required to capture or consume prey. Letting $e_1 = p\widehat{e}$, we obtain

$$\frac{\mathrm{d}n}{\mathrm{d}t} = rn\left(1-\frac{n}{k}\right) - \frac{e_1un}{1+gn}. \tag{2.2}$$

Notably, a previous investigation (Cheng et al. 2024) based on public goods evolutionary games considers scenarios in which public goods are produced by cooperators and linearly consumed by all players. These public goods are modeled as decaying resources–that is, they gradually degrade over time in the absence of production. In contrast to this form of environmental feedback, our model considers logistically growing resources that are nonlinearly consumed by cooperators through their own harvesting efforts. Defectors, lacking the necessary effort, are unable to access the resources directly. This shift from linear to nonlinear feedback introduces a saturation effect in resource consumption, potentially offering a more biologically realistic representation of cooperative dynamics.

The payoffs for individuals using cooperation ($C$) and defection ($D$) strategies depend not only on the strategies they employ but also on the feedback from the resource. The payoff matrix is structured as follows:

$$\Pi = (\theta - n)\begin{matrix} C \\ D \end{matrix}\begin{pmatrix} a_0 & b_0 \\ c_0 & d_0 \end{pmatrix} + n\begin{matrix} C \\ D \end{matrix}\begin{pmatrix} a_1 & b_1 \\ c_1 & d_1 \end{pmatrix},$$

where the first and second matrix entries represent the payoffs of individuals in the game when resources are poor and abundant, respectively. In particular, $a_0$ and $b_0$ denote the payoffs of a cooperator interacting with a cooperator and a defector, respectively, while $c_0$ and $d_0$ represent the payoffs of a defector interacting with a cooperator and a defector, respectively. The parameters $a_1$, $b_1$, $c_1$, and $d_1$ follow a similar interpretation under abundant resources. Here, $\theta > 0$ represents the baseline payoff when $n = 0$. Then, the fitness of cooperators and defectors is given by

$$\begin{aligned} f_C(u,n) =& \frac{1}{N}\left[(\theta a_0 + (a_1 - a_0)n)u + (\theta b_0 + (b_1 - b_0)n)\,(N-u)\right], \\ f_D(u,n) =& \frac{1}{N}\left[(\theta c_0 + (c_1 - c_0)n)u + (\theta d_0 + (d_1 - d_0)n)\,(N-u)\right]. \end{aligned} \tag{2.3}$$

The incentives driving behavioral change can be interpreted from the following parameter combinations derived from the payoff matrix.

$$\begin{aligned} \Lambda_1 &= f_C(0,\theta) - f_D(0,\theta) = (b_1 - d_1)\theta, \\ \Lambda_2 &= f_C(N,\theta) - f_D(N,\theta) = (a_1 - c_1)\theta, \\ \Upsilon_1 &= f_D(N,0) - f_C(N,0) = (c_0 - a_0)\theta, \\ \Upsilon_2 &= f_D(0,0) - f_C(0,0) = (d_0 - b_0)\theta. \end{aligned}$$

Parameter $\Lambda_1$ characterizes the incentive for individuals to adopt the cooperation strategy when the entire population consists of defectors and the environment is favorable. In contrast, $\Lambda_2$ reflects the incentive to cooperate when the population is composed entirely of cooperators under similarly favorable environmental conditions. Parameter $\Upsilon_1$ captures the incentive for individuals to abandon cooperation strategy in favor of defection when all individuals are cooperators but the environment deteriorates. Conversely, $\Upsilon_2$ represents the incentive for individuals in a defecting population to continue imitating defectors under poor environmental conditions.

By coupling the replicator dynamics with the resource dynamics from equation (2.1), we obtain the following eco-evolutionary game system:

$$\begin{cases} \varepsilon \frac{\mathrm{d}u}{\mathrm{d}T} = \frac{u}{N}\,(N-u)\,(f_C - f_D)\,, \\ \frac{\mathrm{d}n}{\mathrm{d}T} = rn\left(1 - \frac{n}{k}\right) - \frac{e_1 n u}{1+gn}, \end{cases} \tag{2.4}$$

where $\varepsilon$ is the relative timescale utilized to characterize the relative evolutionary rates of resources and cooperators. Cooperators evolve faster (slower) than resources when $\varepsilon < 1$ ($\varepsilon > 1$). Players' strategic choices influence resource consumption, which in turn affects the overall resource stock. The resource stock then feeds back into the system by influencing players' fitness. This bidirectional feedback between resource dynamics and player strategies is captured in equations (2.3) and (2.4). In replicator dynamics, a player's fitness reflects its reproductive success. When cooperators have higher fitness than defectors, they reproduce more successfully, leading to an increase

in cooperator density. Conversely, when cooperators have lower fitness, their population declines. Combining equation (2.3) and rescaling time by $t = \frac{T}{\varepsilon}$, we obtain

$$\begin{cases} \dfrac{\mathrm{d}u}{\mathrm{d}t} = \dfrac{u}{N^2}(N-u)\left[((d_1 - d_0 - a_0 + a_1 - b_1 + b_0 + c_0 - c_1)u \right. \\ \qquad \left. + N(d_0 - d_1 - b_0 + b_1))n - \theta((b_0 + c_0 - d_0 - a_0)u + N(d_0 - b_0))\right], \\ \dfrac{\mathrm{d}n}{\mathrm{d}t} = \varepsilon\left(rn\left(1 - \dfrac{n}{k}\right) - \dfrac{e_1 n}{1 + gn}u\right). \end{cases} \tag{2.5}$$

### 2.2 Diffusion model

Spatial diffusion plays a vital role in eco-evolutionary games by influencing the distribution and dynamics of resources and strategies in space and time. In social insects such as ants, pheromone-guided foraging creates spatial structures that can be exploited by deceptive individuals, especially in environments where resources are scarce (Gordon 2010). Predator-prey interactions also exhibit spatial diffusion effects, with heterogeneous distributions of predators and prey leading to spatio-temporal patterns that stabilize cooperation or encourage deception (Cantrell and Cosner 2004). Similarly, territorial animals such as wolves (Kittle et al. 2015) and lions (Mosser et al. 2015) develop distinct spatial distributions through competition and cooperation, which may be disrupted by individual deception. In plant communities (Press and Phoenix 2005), spatial distributions shaped by seed dispersal and resource allocation can drive both cooperative and exploitative strategies, with parasitic plants mimicking cooperative partners to steal nutrients. Considering the movement of cooperators and resources in spatial locations, we obtain the following higher-order eco-evolutionary game system incorporating spatial diffusion:

$$\begin{cases} \dfrac{\partial u(\mathbf{x},t)}{\partial t} = \dfrac{u}{N^2}(N-u)\left[((d_1 - d_0 - a_0 + a_1 - b_1 + b_0 + c_0 - c_1)u \right. \\ \qquad \left. + N(d_0 - d_1 - b_0 + b_1))n - \theta((b_0 + c_0 - d_0 - a_0)u \right. \\ \qquad \left. + N(d_0 - b_0))\right] + d_u\nabla^2 u, & \mathbf{x} \in \Omega, t > 0, \\ \dfrac{\partial n(\mathbf{x},t)}{\partial t} = \varepsilon\left(rn\left(1 - \dfrac{n}{k}\right) - \dfrac{e_1 n}{1 + gn}u\right) + d_n\nabla^2 n, & \mathbf{x} \in \Omega, t > 0, \\ \dfrac{\partial u(\mathbf{x},t)}{\partial \nu} = \dfrac{\partial n(\mathbf{x},t)}{\partial \nu} = 0, & \mathbf{x} \in \partial\Omega, t > 0, \\ u(\mathbf{x},0) = u_0(\mathbf{x}) \geq 0,\ n(\mathbf{x},0) = n_0(\mathbf{x}) \geq 0, & \mathbf{x} \in \Omega, \end{cases} \tag{2.6}$$

in which $u(\mathbf{x}, t)$ and $n(\mathbf{x}, t)$ represent the densities of cooperators and resources at time $t$ and location $\mathbf{x}$, respectively; $\nabla^2 = \frac{\partial^2}{\partial x^2} + \frac{\partial^2}{\partial y^2}$ is the Laplacian operator; $\mathbf{x} \in \Omega \subseteq \mathbb{R}^2$ is a 2-dimensional bounded domain with smooth boundary $\partial\Omega$; $\nu$ is the outward unit normal vector of $\partial\Omega$; Neumann boundary conditions are adopted since players and resources are assumed to not enter and leave the boundary; $d_u$ and $d_n$ denote the diffusion coefficients of cooperators and resources, respectively.

## 3 Dynamics of temporal system (2.5)

The possible outcomes of evolution are reflected by equilibria. It is essential to discuss the existence and stability of equilibria for the system (2.5). Different factors such as payoffs, relative timescales, player density, and initial status result in various evolutionary outcomes for players' choices of strategies and resource stocks. Next, we reveal these factors affecting evolution by analyzing multistability, transcritical bifurcations, and Hopf bifurcations.

### 3.1 Existence of equilibria

The equilibria of system (2.5) are denoted as $E_0(0,0)$, $E_1(N,0)$, $E_2\left(\frac{N(d_0-b_0)}{a_0+d_0-b_0-c_0},0\right)$, $E_3(0,k)$, $E_4^+(N,n_4^+)$, $E_4^-(N,n_4^-)$, and $E^*(u^*,n^*)$. The boundary equilibria $E_0(0,0)$, $E_1(N,0)$, and $E_3(0,k)$ always exist. Define the following conditions.

**(H1)**: $a_0 > c_0$ and $d_0 > b_0$, or $a_0 < c_0$ and $d_0 < b_0$.
**(H2)**: $gk > 1$ and $r(1+gk)^2 > 4Ngke_1$.
**(H3)**: $gk < 1$ and $r > \max\{\frac{Ngke_1}{(1+gk)^2}, Ne_1\}$.
**(H4)**: $gk > 1$ and $r(1+gk)^2 > 4Ngke_1$ and $Ne_1 > r$.
**(H5)**: $\gamma_1(\gamma_2 r + Ne_1(b_0-d_0)) < 0$, $\delta_2^2 < 3\delta_1\delta_3$, $k > n^*$, and $N > \frac{r(k-n^*)(gn^*+1)}{ke_1}$.

If (H1) holds, then $\frac{N(d_0-b_0)}{a_0+d_0-b_0-c_0} \in (0,N)$. Hence, boundary equilibrium $E_2\left(\frac{N(d_0-b_0)}{a_0+d_0-b_0-c_0},0\right)$ exists when (H1) is satisfied. From (2.5), we have

$$n_4^{\pm} = \frac{r(gk-1) \pm \sqrt{r^2(1+gk)^2 - 4Ngke_1 r}}{2gr}.$$

Thus, $E_4^+$ exists ( i.e., $n_4^+ > 0$) when either (H2) or (H3) is met. $E_4^-$ exists ( i.e., $n_4^- > 0$) exists if (H4) is true. We now explore the existence of positive equilibria $E^*(u^*,n^*)$. From equations (2.5),we know $u^*$ and $n^*$ satisfy

$$\delta_1 n^{*3} + \delta_2 n^{*2} + \delta_3 n^* + \delta_4 = 0, \tag{3.1}$$

and

$$u^* = \frac{r(k-n^*)(gn^*+1)}{ke_1}, \tag{3.2}$$

where

$$\begin{aligned}
\delta_1 =& gr\gamma_1,\\
\delta_2 =& -r[(\gamma_1 k + \theta\gamma_2)g - \gamma_1],\\
\delta_3 =& [(g\theta\gamma_2 - \gamma_1)r + Ne_1\gamma_3]k - \theta r\gamma_2,\\
\delta_4 =& k\theta(\gamma_2 r + Ne_1(b_0-d_0)),\\
\gamma_1 =& a_0 - a_1 - b_0 + b_1 - c_0 + c_1 + d_0 - d_1,
\end{aligned}$$

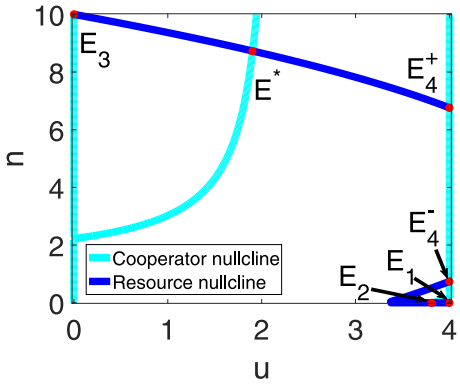


**Fig. 1** Existence of equilibria for temporal system (2.5). The cyan and blue curves are the nullclines for cooperators and resources, respectively, where $\frac{du}{dt} = 0$ and $\frac{dn}{dt} = 0$. Equilibria are marked by red dots, occurring where the cyan and blue curves intersect. Parameters: $\varepsilon = 3$, $a_0 = 3.1$, $a_1 = 2.9$, $b_0 = 2$, $b_1 = 1.3$, $c_0 = 3.2$, $c_1 = 1.5$, $d_0 = 0$, $d_1 = 1.1$, $r = 0.1$, $k = 10$, $e_1 = 0.03$, $g = 0.4$, $\theta = 2$, $N = 4$. The values of the parameters are presented in Table 1

$$\begin{aligned}\gamma_2 =& a_0 - c_0 - b_0 + d_0,\\ \gamma_3 =& d_0 - d_1 - b_0 + b_1.\end{aligned}$$

Denote

$$F_1(n) = \delta_1 n^3 + \delta_2 n^2 + \delta_3 n + \delta_4. \tag{3.3}$$

When $\delta_1 > 0$ and $\delta_4 < 0$, $F_1(0) = \delta_4 < 0$ and $\lim\limits_{n\to+\infty} F(n) = +\infty$. In this case, equation (3.1) has at least one positive root $n^*$ on the interval $(0, +\infty)$, and at most three positive roots may exist in total. Similarly, $F_1(0) = \delta_4 > 0$ and $\lim\limits_{n\to+\infty} F(n) = -\infty$ when $\delta_1 < 0$ and $\delta_4 > 0$. Hence, $n^* > 0$ when $\delta_1\delta_4 < 0$. The condition $\gamma_1(\gamma_2 r + Ne_1(b_0 - d_0)) < 0$ ensures $\delta_1\delta_4 < 0$. From (3.2), we conclude that if $k > n^*$ and $N > \frac{r(k-n^*)(gn^*+1)}{ke_1}$, then $u^* \in (0, N)$. Therefore, the internal equilibrium $E^*(u^*, n^*)$ exists if condition (H5) holds.

The existence of the internal equilibrium is affected by the joint effect of the strategies' payoff differences, carrying capacity, internal growth rate, and player density. Fig. 1 illustrates the existence of equilibria for the temporal system (2.5) and the potential location of the equilibria. The parameters are chosen to satisfy the above conditions for the existence of equilibria.

### 3.2 Local stability and multistability analysis

We can recognize feasible evolutionary outcomes of cooperators from local stability, bistability, and multistability. Here, we discuss local stability, bistability, and multistability mathematically to predict the evolution of cooperators accurately. Denote

$$\tilde{r} = \frac{e_1 N(d_0 - b_0)}{a_0 + d_0 - b_0 - c_0},\ \tilde{d}_1 = \frac{\theta(b_0 - d_0)}{k} + b_1 - b_0 + d_0,$$

**Table 1** The parameter values are as follows: (1) for Figs. 1, 2(b), (c), (d), and 3(e); (2) for Figs. 2(a) and 3(d); (3) for Figs. 2(e) and Figs. 14-26; (4) for Fig. 3(a); (5) for Fig. 3(b); (6) for Fig. 3(c); and (7) for Figs. 4-13.

| | $a_1$ | $b_1$ | $c_1$ | $d_1$ | $a_0$ | $b_0$ | $c_0$ | $d_0$ | $r$ | $k$ | $e_1$ | $g$ | $\theta$ | $\varepsilon$ | $N$ |
|---|---|---|---|---|---|---|---|---|---|---|---|---|---|---|---|
| (1) | 2.9 | 1.3 | 1.5 | 1.1 | 3.1 | 2 | 3.2 | 0 | 0.1 | 10 | 0.03 | 0.4 | 2 | 3 | 4 |
| (2) | 2 | 1.3 | 1.5 | 1.1 | 1.3 | −2 | 1.2 | −3 | 0.25 | 10 | 0.03 | 0.4 | 2 | 1 | 10 |
| (3) | 1 | 3 | −4 | 3 | 4 | 1.1 | 10 | 3.9 | 0.5 | 4.7 | 0.1 | 0.1 | 3 | 20 | 6 |
| (4) | 2.9 | 3 | 3 | 2 | 4 | 2 | 2.4 | 1.7 | 0.6 | 5 | 0.2 | 0.6 | 2 | 2 | 5 |
| (5) | −2 | 4 | 5 | 1.4 | 1 | 3 | 2 | 1 | 0.2 | 6 | 0.1 | 0.4 | 3 | 1 | 5 |
| (6) | 2 | 1.3 | 1.5 | 1.1 | −1 | −2 | 1.2 | −3 | 0.4 | 3 | 0.3 | 0.4 | 2 | 1 | 4 |
| (7) | 1 | 2 | −4 | 3 | 4 | 1.1 | 10 | 3.9 | 0.5 | 4.7 | 0.1 | 0.1 | 3 | 2 | 30 |

$$\tilde{a}_1 = \frac{\theta(c_0 - a_0)}{n_4^+} + a_0 - c_0 + c_1,\ \tilde{N} = \frac{r(k - 2n_4^+)(gn_4^+ + 1)^2}{e_1 k},$$

$$\hat{a}_1 = \frac{\theta(c_0 - a_0)}{n_4^-} + a_0 - c_0 + c_1,\ \hat{N} = \frac{r(k - 2n_4^-)(gn_4^- + 1)^2}{e_1 k},$$

$$\tilde{\theta} = \frac{(a_0 - a_1 - c_0 + c_1)n_4^+}{a_0 - c_0},\ \tilde{\varepsilon} = \frac{ku^*(N - u^*)(gn^* + 1)^2(\theta\gamma_2 - \gamma_1 n^*)}{N^2[(gn^* + 1)^2(2n^* - k)r + u^* e_1 k]},$$

$$\delta_5 = \frac{u^*(N - u^*)}{N^2}(\gamma_2\theta - \gamma_1 n^*),\ \delta_6 = r\left(\frac{2n^*}{k} - 1\right) + \frac{e_1 u^*}{(gn^* + 1)^2},$$

$$\delta_7 = (\gamma_2\theta - \gamma_1 n^*)\left(r\left(1 - \frac{2n^*}{k}\right) - \frac{e_1 u^*}{(gn^* + 1)^2}\right) + (\gamma_1 u^* + N\gamma_3)\frac{e_1 n^*}{gn^* + 1}.$$

Theorem 3.1 outlines the conditions for local stability of complex multiple equilibria.

**Theorem 3.1**

*(I)* $E_0(0,0)$ *is unstable node if* $b_0 > d_0$; $E_0(0,0)$ *is a saddle point if* $b_0 < d_0$.

*(II)* $E_1(N,0)$ *is a locally asymptotically stable node if* $c_0 < a_0$ *and* $r < Ne_1$; $E_1(N,0)$ *is an unstable node if* $c_0 > a_0$ *and* $r > Ne_1$; $E_1(N,0)$ *is a saddle point if* $c_0 > a_0$ *and* $r < Ne_1$, *or* $c_0 < a_0$ *and* $r > Ne_1$.

*(III)* $E_2(u_2,0)$ *is a locally asymptotically stable node if* $a_0 < c_0$ *and* $r < \tilde{r}$; $E_2(u_2,0)$ *is an unstable node if* $a_0 > c_0$ *and* $r > \tilde{r}$; $E_2(u_2,0)$ *is a saddle point if* $a_0 > c_0$ *and* $r < \tilde{r}$, *or* $a_0 < c_0$ *and* $r > \tilde{r}$.

*(IV)* $E_3(0,k)$ *is a locally asymptotically stable node if* $d_1 > \tilde{d}_1$; $E_3(0,k)$ *is a saddle point if* $d_1 < \tilde{d}_1$.

*(V)* $E_4^+(N,n_4^+)$ *is a locally asymptotically stable node if* $a_1 > \tilde{a}_1$ *and* $N > \tilde{N}$; $E_4^+(N,n_4^+)$ *is an unstable node if* $a_1 < \tilde{a}_1$ *and* $N < \tilde{N}$; $E_4^+(N,n_4^+)$ *is a saddle point if* $a_1 < \tilde{a}_1$ *and* $N > \tilde{N}$, *or* $a_1 > \tilde{a}_1$ *and* $N < \tilde{N}$.

*(VI)* $E_4^-(N,n_4^-)$ *is a locally asymptotically stable node if* $a_1 > \hat{a}_1$ *and* $N > \hat{N}$; $E_4^-(N,n_4^-)$ *is an unstable node if* $a_1 < \tilde{a}_1$ *and* $N < \hat{N}$; $E_4^-(N,n_4^-)$ *is a saddle point if* $a_1 < \hat{a}_1$ *and* $N > \hat{N}$, *or* $a_1 > \hat{a}_1$ *and* $N < \hat{N}$.

*(VII)* $E^*(u^*, n^*)$ *is a locally asymptotically stable node or focus if* $\varepsilon\delta_6 > \delta_5$ *and* $\delta_7 > 0$*;* $E^*(u^*, n^*)$ *is an unstable node or focus if* $\varepsilon\delta_6 < \delta_5$ *and* $\delta_7 > 0$*;* $E^*(u^*, n^*)$ *is a saddle point if* $\delta_7 < 0$.

***Proof*** See Appendix A. □

From the analysis provided in Appendix A, we derive conditions for bistability and multistability of system (2.5).

**Corollary 3.1** *(I)* $E_1(N, 0)$ *and* $E^*(u^*, n^*)$ *are stable when* $c_0 < a_0$, $r < Ne_1$, $\varepsilon\delta_6 > \delta_5$, *and* $\delta_7 > 0$.

*(II)* $E_2\left(\frac{N(d_0-b_0)}{a_0+d_0-b_0-c_0}, 0\right)$ *and* $E^*(u^*, n^*)$ *are stable when* $a_0 < c_0$, $r < \tilde{r}$, $\varepsilon\delta_6 > \delta_5$, *and* $\delta_7 > 0$.

*(III)* $E_3(0, k)$ *and* $E^*(u^*, n^*)$ *are stable when* $d_1 > \tilde{d}_1$, $\varepsilon\delta_6 > \delta_5$, *and* $\delta_7 > 0$.

*(IV)* $E_1(N, 0)$, $E_3(0, k)$, *and* $E_4^-(N, n_4^-)$ *are stable when* $c_0 < a_0$, $r < Ne_1$, $d_1 > \tilde{d}_1$, $a_1 > \hat{a}_1$, *and* $N > \hat{N}$.

*(V)* $E_2\left(\frac{N(d_0-b_0)}{a_0+d_0-b_0-c_0}, 0\right)$, $E_3(0, k)$, *and* $E_4^-(N, n_4^-)$ *are stable when* $a_0 < c_0$, $r < \tilde{r}$, $d_1 > \tilde{d}_1$, $a_1 > \hat{a}_1$, *and* $N > \hat{N}$.

Fig. 2 depicts local stability via time series for the temporal system (2.5), where the parameters are chosen to satisfy the conditions of local stability. The combination of smaller payoffs from defector-cooperator encounters than from cooperative encounters and a lower growth rate of the resource gives the opportunity to fill the population with cooperators. In contrast, if the payoffs of defector-collaborator encounters are greater than the benefits of cooperator encounters, and the resource grows at a higher growth rate, then cooperators and defectors coexist in a barren resource. The same parameters but different initial situations result in drastically different evolutionary outcomes. With relatively abundant resource reserves, the initial density of cooperators determines the survival of both cooperators and defectors if the payoffs from cooperator encounters and defector encounters are both relatively large ($a_1 > \tilde{a}_1$ and $d_1 > \tilde{d}_1$). Cooperators eventually become extinct if the initial density of cooperators is small. Higher initial densities of cooperators allow cooperators to have an evolutionary advantage over defectors in the end. The case with a medium initial density of cooperators and a poor initial resource stock is characterized by the coexistence of eventual cooperators and defectors in poor resources. Fig. 2(b) and (e) keep the initial state the same, varying parameters such as payoffs and relative timescales to permit a modest amount of resources to be shared between cooperators and defectors.

Fig. 3 presents five multistability, including three bi-stability and two tri-stability. The choice of parameters depends on Corollary 3.1. When resource reserves are impoverished, higher densities of cooperators favor the survival of cooperators, which is reflected in the victory of cooperators over defectors if the population evolves from having higher densities of cooperators. If the initial stock of resources is abundant, the initial density of cooperators will no longer affect the evolutionary outcome. In this case, defectors survive because the initial abundance of the resource stock allows defectors to exploit the resource by deceiving cooperators. Defectors have a better opportunity to survive, and even defectors are able to dominate the population when

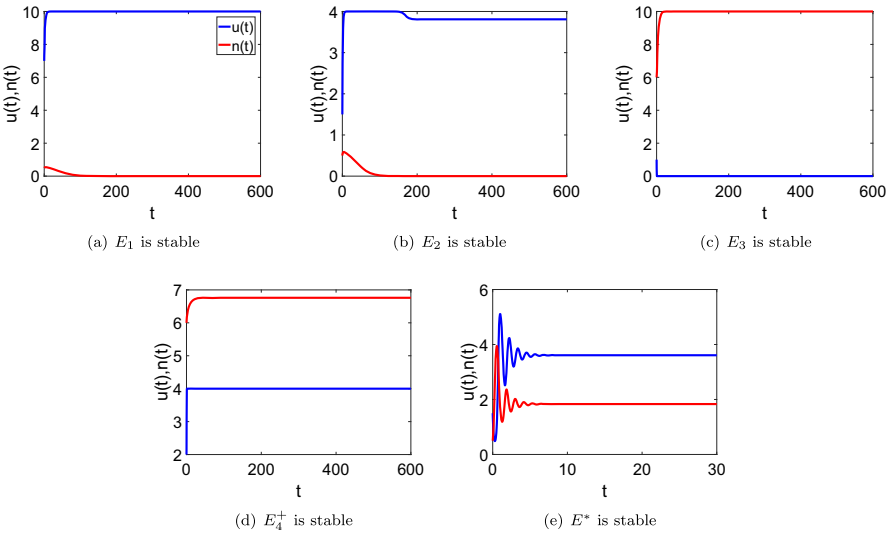


(a) $E_1$ is stable (b) $E_2$ is stable (c) $E_3$ is stable

(d) $E_4^+$ is stable (e) $E^*$ is stable

**Fig. 2** Temporal dynamics of cooperators and resources for non-diffusion system (2.5). The blue and red curves demonstrate the specific evolution of cooperators and resources, respectively. The initial conditions $(u(0), n(0))$ for (a), (b), (c), (d), and (e) are set to (7,0.5), (1.5,0.5), (1,6), (2,6), and (1.5,0.5), respectively. Parameters: (a) $\varepsilon = 1$, $a_0 = 1.3$, $a_1 = 2$, $b_0 = -2$, $b_1 = 1.3$, $c_0 = 1.2$, $c_1 = 1.5$, $d_0 = -3$, $d_1 = 1.1$, $r = 0.25$, $k = 10$, $e_1 = 0.03$, $g = 0.4$, $\theta = 2$, $N = 10$. (e) $\varepsilon = 20$, $a_0 = 4$, $a_1 = 1$, $b_0 = 1.1$, $b_1 = 3$, $c_0 = 10$, $c_1 = -4$, $d_0 = 3.9$, $d_1 = 3$, $r = 0.5$, $k = 4.7$, $e_1 = 0.1$, $g = 0.1$, $\theta = 3$, $N = 6$. The parameters of (b), (c), and (d) are identical to those of Fig. 1

the initial stock of resources is abundant. When the initial stock of resources is low, cooperators have a more favorable chance to survive and reproduce. No matter what the initial density of cooperators is, cooperators can eventually survive after evolution. The developmental advantage of a cooperator depends on the initial density of cooperators if the initial reserve of resources is large. If the initial density of cooperators is high, then cooperators can have the opportunity to grow and prosper or even dominate the entire population. Choosing the same parameters, differences in the initial state of cooperators and resource reserves yield numerous and varied evolutionary outcomes. In addition, even if the initial density of the population's cooperators and the initial reserves of resources remain consistent, alterations in factors such as payoffs, environmental growth rates, and player densities can bring diverse evolutionary outcomes.

### 3.3 Bifurcation analysis

Next, we explore the transcritical and Hopf bifurcations of system (2.5). The right hand side of system (2.5) is defined as $G_1$ and $G_2$, respectively.

(I) The eigenvalues of $J_1$ are zero and $\varepsilon(r - Ne_1)$ when $c_0 = a_0$. The eigenvectors of $J_1$ and $J_1^T$ regarding eigenvalue zero are $V_1 = (1, 0)^T$ and $W_1 = (1, 0)^T$, respectively. Then, we have

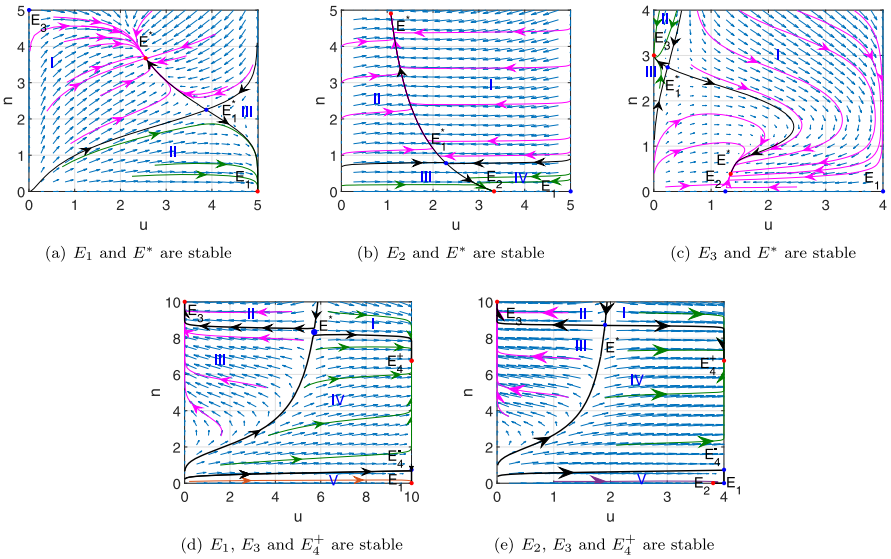


(a) $E_1$ and $E^*$ are stable (b) $E_2$ and $E^*$ are stable (c) $E_3$ and $E^*$ are stable

(d) $E_1$, $E_3$ and $E_4^+$ are stable (e) $E_2$, $E_3$ and $E_4^+$ are stable

**Fig. 3** Multistability of the temporal system (2.5). The phase portraits present a variety of multistability, including three kinds of bistability and two kinds of tristability. The red dots and blue dots indicate stable and unstable equilibria, respectively. Magenta, green, brown, and purple curves from different initial values eventually converge to distinct stable equilibria. The black curve separates the $u-n$ phase plane into three, four, or five regions. Parameters: (a) $\varepsilon = 2, a_0 = 4, a_1 = 2.9, b_0 = 2, b_1 = 3, c_0 = 2.4, c_1 = 3, d_0 = 1.7, d_1 = 2, r = 0.6, k = 5, e_1 = 0.2, g = 0.6, \theta = 2, N = 5$. (b) $\varepsilon = 1, a_0 = 1, a_1 = -2, b_0 = 3, b_1 = 4, c_0 = 2, c_1 = 5, d_0 = 1, d_1 = 1.4, r = 0.2, k = 6, e_1 = 0.1, g = 0.4, \theta = 3, N = 5$. (c) $\varepsilon = 1, a_0 = -1, a_1 = 2, b_0 = -2, b_1 = 1.3, c_0 = 1.2, c_1 = 1.5, d_0 = -3, d_1 = 1.1, r = 0.4, k = 3, e_1 = 0.3, g = 0.4, \theta = 2, N = 4$. The parameters of (d) and (e) coincide with those of Fig. 2(a) and Fig. 1, respectively

$$G_{c_0}(E_1; a_0) = \begin{pmatrix} \frac{u^2(N-u)(n-\theta)}{N^2} \\ 0 \end{pmatrix}_{(E_1;a_0)} = \begin{pmatrix} 0 \\ 0 \end{pmatrix},$$

$$DG_{c_0}(E_1; a_0)V_1 = \begin{pmatrix} \frac{(2uN-3u^2)(n-\theta)}{N^2} & \frac{u^2N-u^3}{N^2} \\ 0 & 0 \end{pmatrix} \begin{pmatrix} 1 \\ 0 \end{pmatrix}_{(E_1;a_0)} = \begin{pmatrix} \theta \\ 0 \end{pmatrix},$$

$$D^2G(E_1; a_0)(V_1, V_1) = \begin{pmatrix} \frac{(2N-6u)(n-\theta)}{N^2} \\ 0 \end{pmatrix}_{(E_1;a_0)} = \begin{pmatrix} \frac{4}{N} \\ 0 \end{pmatrix}.$$

Furthermore,

$$W_1^T G_{c_0}(E_1; a_0) = (1, 0) \begin{pmatrix} 0 \\ 0 \end{pmatrix} = 0,$$

$$W_1^T DG_{c_0}(E_1; a_0)V_1 = (1, 0) \begin{pmatrix} \theta \\ 0 \end{pmatrix} = \theta \neq 0,$$

$$W_1^T D^2G(E_1; a_0)(V_1, V_1) = (1, 0) \begin{pmatrix} \frac{4}{N} \\ 0 \end{pmatrix} = \frac{4}{N} \neq 0.$$

Thus, system (2.5) experiences transcritical bifurcation at $E_1(N, 0)$ when $c_0 = a_0$.

(II) When $r = \tilde{r}$, the eigenvalues of $J_2$ are $\frac{(a_0-c_0)\theta u_2}{N}$ and zero. The eigenvectors of $J_2$ and $J_2^T$ with respect to eigenvalue zero are

$$V_2 = \left(1, \frac{\theta u_2(c_0 - a_0)}{N\gamma_4}\right)^T,$$
$$W_2 = (0, 1)^T,$$

where

$$\gamma_4 = \frac{N(d_0 - b_0)(a_0 - c_0)}{(a_0 - c_0 - b_0 + d_0)^3}((c_1 - d_1)(a_0 - c_0) + (a_1 - c_1)(d_0 - b_0)).$$

We then derive that

$$G_r(E_2; \tilde{r}) = \begin{pmatrix} 0 \\ \varepsilon n\left(1 - \frac{n}{k}\right) \end{pmatrix}_{(E_2;\tilde{r})} = \begin{pmatrix} 0 \\ 0 \end{pmatrix},$$
$$DG_r(E_2; \tilde{r})V_2 = \begin{pmatrix} 0 & 0 \\ 0 & \varepsilon\left(1 - \frac{2n}{k}\right) \end{pmatrix} \begin{pmatrix} 1 \\ \frac{\theta u_2(c_0-a_0)}{N\gamma_4} \end{pmatrix}_{(E_2;\tilde{r})} = \begin{pmatrix} 0 \\ \frac{\varepsilon\theta u_2(c_0-a_0)}{N\gamma_4} \end{pmatrix},$$
$$D^2G(E_2; \tilde{r})(V_2, V_2) = \begin{pmatrix} 0 \\ -\frac{2\varepsilon\theta^2(a_0-c_0)^2u_2^2}{kN^2\gamma_4^2} \end{pmatrix}.$$

Further,

$$W_2^T G_r(E_2; \tilde{r}) = (0, 1)\begin{pmatrix} 0 \\ 0 \end{pmatrix} = 0,$$
$$W_2^T DG_r(E_2; \tilde{r})V_2 = (0, 1)\begin{pmatrix} 0 \\ \frac{\varepsilon\theta u_2(c_0-a_0)}{N\gamma_4} \end{pmatrix} = \frac{\varepsilon\theta u_2(c_0 - a_0)}{N\gamma_4} \neq 0,$$
$$W_2^T D^2G(E_2; \tilde{r})(V_2, V_2) = (0, 1)\begin{pmatrix} 0 \\ -\frac{2\varepsilon\theta^2(a_0-c_0)^2u_2^2}{kN^2\gamma_4^2} \end{pmatrix} = -\frac{2\varepsilon\theta^2(a_0 - c_0)^2u_2^2}{kN^2\gamma_4^2} \neq 0.$$

Hence, the transcritical bifurcation occurs at $E_2\left(\frac{N(d_0-b_0)}{a_0+d_0-b_0-c_0}, 0\right)$ of system (2.5).

(III) If $d_1 = \tilde{d_1}$, then $-\varepsilon r$ and zero are eigenvalues of $J_3$. After calculations, $V_3 = \left(1, \frac{-ke_1}{(gk+1)r}\right)$ and $W_3 = (1, 0)^T$ are the eigenvectors of $J_3$ and $J_3^T$, respectively. Then, we obtain

$$G_{d_1}(E_3; \tilde{d_1}) = \begin{pmatrix} \frac{un(N-u)^2}{N^2} \\ 0 \end{pmatrix}_{(E_3;\tilde{d_1})} = \begin{pmatrix} 0 \\ 0 \end{pmatrix},$$
$$DG_{d_1}(E_3; \tilde{d_1})V_3 = \begin{pmatrix} \frac{(N-u)(3u-N)n}{N^2} & \frac{-u(N-u)^2}{N^2} \\ 0 & 0 \end{pmatrix} \begin{pmatrix} 1 \\ \frac{-ke_1}{r(gk+1)} \end{pmatrix}_{(E_3;\tilde{d_1})} = \begin{pmatrix} -k \\ 0 \end{pmatrix},$$

$$D^2G(E_3;\tilde{d_1})(V_3,V_3)=\begin{pmatrix} n(4N-6u)+2\frac{4uN-3u^2-N^2}{r(gk+1)} \\ 0 \end{pmatrix}_{(E_3;\tilde{d_1})}=\begin{pmatrix} 4kN+\frac{2N^2ke_1}{(gk+1)r} \\ 0 \end{pmatrix}.$$

Moreover,

$$\begin{aligned} W_3^T G_{d_1}(E_3;\tilde{d_1}) &= (1,0)\begin{pmatrix} 0 \\ 0 \end{pmatrix}=0, \\ W_3^T DG_{d_1}(E_3;\tilde{d_1})V_3 &= (1,0)\begin{pmatrix} -k \\ 0 \end{pmatrix}=-k\neq 0, \\ W_3^T D^2G(E_3;\tilde{d_1})(V_3,V_3) &= (1,0)\begin{pmatrix} 4kN+\frac{2N^2ke_1}{(gk+1)r} \\ 0 \end{pmatrix}=4kN+\frac{2N^2ke_1}{(gk+1)r}\neq 0. \end{aligned}$$

Therefore, a transcritical bifurcation emerges at $E_3(0,k)$ when $d_1=\tilde{d_1}$.
(IV) Consider $\theta$ as the bifurcation parameter and let $\theta=\tilde{\theta}$. Then the characteristic roots of $J_4$ are 0 and $-\frac{\varepsilon\left((gn_4^+ +1)^2(k-2n_4^+)r-Ne_1k\right)}{k(gn_4^+ +1)^2}$. $V_4=\left(1,\frac{e_1n_4^+k(gn_4^+ +1)}{(gn_2^+ +1)^2(k-2n_4^+)r-Ne_1k}\right)^T$ and $W_4=(1,0)^T$ are selected as the eigenvectors of $J_4$ and $J_4^T$. Some calculations yield

$$\begin{aligned} G_\theta(E_4^+;\tilde{\theta}) &= \begin{pmatrix} \frac{u(u-N)}{N^2}(N(d_0-b_0)-\gamma_2 u) \\ 0 \end{pmatrix}_{(E_4^+;\tilde{\theta})}=\begin{pmatrix} 0 \\ 0 \end{pmatrix}, \\ DG_\theta(E_4^+;\tilde{\theta})V_4 &= \begin{pmatrix} \gamma_2u(2N-3u)+N(2u-N)(d_0-b_0) & 0 \\ 0 & 0 \end{pmatrix}\begin{pmatrix} 1 \\ \frac{e_1n_4^+k(gn_4^+ +1)}{(gn_4^+ +1)^2(k-2n_4^+)r-Ne_1k} \end{pmatrix}_{(E_4^+;\tilde{\theta})} \\ &= \begin{pmatrix} (c_0-a_0)N^2 \\ 0 \end{pmatrix}, \\ D^2G(E_4^+;\tilde{\theta})(V_4,V_4) &= \begin{pmatrix} 2\gamma_2(N-3u)+2N(d_0-b_0) \\ 0 \end{pmatrix}_{(E_4^+;\tilde{\theta})}=\begin{pmatrix} 2N(c_0-a_0-\gamma_2) \\ 0 \end{pmatrix}. \end{aligned}$$

Then,

$$\begin{aligned} W_4^T G_\theta(E_4^+;\tilde{\theta}) &= (1,0)\begin{pmatrix} 0 \\ 0 \end{pmatrix}=0, \\ W_4^T DG_\theta(E_4^+;\tilde{\theta})V_4 &= (1,0)\begin{pmatrix} -k \\ 0 \end{pmatrix}=-k\neq 0, \\ W_4^T D^2G(E_4^+;\tilde{\theta})(V_4,V_4) &= (1,0)\begin{pmatrix} 4kN+\frac{2N^2ke_1}{(gk+1)r} \\ 0 \end{pmatrix}=4kN+\frac{2N^2ke_1}{(gk+1)r}\neq 0. \end{aligned}$$

Therefore, we conclude that a transcritical bifurcation arises at $E_4^+(N,n_4^+)$ for the system (2.5) when $\theta=\tilde{\theta}$.
(V) Choose $\varepsilon$ as the bifurcation parameter. If $\varepsilon=\tilde{\varepsilon}$ and $\delta_7>0$, then $\mathrm{Det}(J^*)>0$ and $\mathrm{Tr}(J^*)=0$. In this case, the characteristic roots of (A.1) are $i\sqrt{\mathrm{Det}(J^*)}$ and $-i\sqrt{\mathrm{Det}(J^*)}$. Calculations yield

$$\left(\frac{\mathrm{dRe}\lambda}{\mathrm{d}\varepsilon}\right)_{\varepsilon=\tilde{\varepsilon},\lambda=i\sqrt{\mathrm{Det}(J^*)}} = r\left(1-\frac{2n^*}{k}\right)-\frac{e_1u^*}{(gn^*+1)^2}\neq 0.$$

Hopf bifurcation occurs at $E^*(u^*,n^*)$ because the transversality condition is satisfied. Accordingly, we have Theorem 3.2 as follows.

**Theorem 3.2**

*(I) A transcritical bifurcation appears at* $E_1(N,0)$ *if* $c_0=a_0$.
*(II) A transcritical bifurcation appears at* $E_2\left(\frac{N(d_0-b_0)}{a_0+d_0-b_0-c_0},0\right)$ *if* $r=\tilde{r}$.
*(III) A transcritical bifurcation appears at* $E_3(0,k)$ *if* $d_1=\tilde{d}_1$.
*(IV) A transcritical bifurcation appears at* $E_4^+(N,n_4^+)$ *if* $\theta=\tilde{\theta}$.
*(V) A Hopf bifurcation appears at* $E^*(u^*,n^*)$ *if* $\varepsilon=\tilde{\varepsilon}$ *and* $\delta_7>0$.

The dynamical properties, including stability and bifurcation of the temporal system (2.5), are presented in Table 2.

***Remark 3.1*** Substituting $g=0$ into the Holling II functional response system (2.5) yields the following linear consumption system:

$$\begin{cases}\dfrac{\mathrm{d}u}{\mathrm{d}t}=\dfrac{u}{N^2}(N-u)\left[((d_1-d_0-a_0+a_1-b_1+b_0+c_0-c_1)u\right.\\ \qquad\left.+N(d_0-d_1-b_0+b_1))n-\theta((b_0+c_0-d_0-a_0)u+N(d_0-b_0))\right],\\ \dfrac{\mathrm{d}n}{\mathrm{d}t}=\varepsilon\left(rn\left(1-\dfrac{n}{k}\right)-e_1nu\right).\end{cases}\tag{3.4}$$

We denote the equilibria of system (3.4) as $E_0^{'}(0,0)$, $E_1^{'}(N,0)$, $E_2^{'}\left(\frac{N(d_0-b_0)}{a_0+d_0-b_0-c_0},0\right)$, $E_3^{'}(0,k)$, $E_4^{'}\left(N,\frac{k(r-Ne_1)}{r}\right)$, and $E_\pm^*(u_\pm^*,n_\pm^*)$. The specific forms of $u_\pm^*$ and $n_\pm^*$ are $n_\pm^*=\frac{-\delta_3\pm\sqrt{\delta_3^2+4\delta_2\delta_4}}{2\delta_2}$ and $u_\pm^*=\frac{r(k-n_\pm^*)}{ke_1}$, respectively. $E_4^{'}\left(N,\frac{k(r-Ne_1)}{r}\right)$ exists when $r>Ne_1$. Define

$$\begin{aligned}
&e_1^+=\frac{r(k-n_+^*)}{kN},\ e_1^-=\frac{r(k-n_-^*)}{kN},\\
&n_4^{'}=\frac{k(r-Ne_1)}{r},\ \tilde{N}^{'}=\frac{r(k-2n_4^{'})}{e_1k},\\
&\tilde{a}_1^{'}=\frac{\theta(c_0-a_0)}{n_4^{'}}+a_0-c_0+c_1,\ \tilde{\varepsilon}^{'}=\frac{ku_\pm^*(N-u_\pm^*)(\theta\gamma_2-\gamma_1n_\pm^*)}{N^2[(2n_\pm^*-k)r+u_\pm^*e_1k]},\\
&\tilde{\theta}^{'}=\frac{(a_0-a_1-c_0+c_1)n_4^{'}}{a_0-c_0},\delta_3^{'}=(Ne_1\gamma_3-\gamma_1r)k-\theta r\gamma_2,\\
&\delta_5^{'}=\frac{u_\pm^*(N-u_\pm^*)}{N^2}(\gamma_2\theta-\gamma_1n_\pm^*),\ \delta_6^{'}=r\left(\frac{2n_\pm^*}{k}-1\right)+e_1u_\pm^*,\\
&\delta_7^{'}=(\gamma_2\theta-\gamma_1n_\pm^*)\left(r\left(1-\frac{2n_\pm^*}{k}\right)-e_1u_\pm^*\right)+(\gamma_1u_\pm^*+N\gamma_3)e_1n_\pm^*.
\end{aligned}$$

**Table 2** Existence and stability of equilibria and bifurcation of the temporal system (2.5). HB and TB represent Hopf bifurcation and transcritical bifurcation, respectively.

| Equilibrium | Existence | Stable | Saddle point | Unstable | Bifurcation |
|---|---|---|---|---|---|
| $E_0(0,0)$ | Always | — | $b_0 < d_0$ | $b_0 > d_0$ | — |
| $E_1(N,0)$ | Always | $c_0 < a_0$ and $r < Ne_1$ | $c_0 > (<)a_0$ and $r < (>)Ne_1$ | $c_0 > a_0$ and $r > Ne_1$ | TB, $c_0 = a_0$ |
| $E_2(\frac{N(d_0-b_0)}{a_0+d_0-b_0-c_0}, 0)$ | (H1) | $a_0 < c_0$ and $r < \tilde{r}$ | $a_0 > (<)c_0$ and $r < (>)\tilde{r}$ | $a_0 > c_0$ and $r > \tilde{r}$ | TB, $r = \tilde{r}$ |
| $E_3(0,k)$ | Always | $d_1 > \tilde{d}_1$ | $d_1 < \tilde{d}_1$ | — | TB, $d_1 = \tilde{d}_1$ |
| $E_4^+(N, n_4^+)$ | (H2)-(H3) | $a_1 > \tilde{a}_1$ and $N > \tilde{N}$ | $a_1 < (>)\tilde{a}_1$ and $N > (<)\tilde{N}$ | $a_1 < \tilde{a}_1$ and $N < \tilde{N}$ | TB, $\theta = \tilde{\theta}$ |
| $E_4^-(N, n_4^-)$ | (H4) | $a_1 > \hat{a}_1$ and $N > \hat{N}$ | $a_1 < (>)\hat{a}_1$ and $N > (<)\hat{N}$ | $a_1 < \hat{a}_1$ and $N < \hat{N}$ | — |
| $E^*(u^*, n^*)$ | (H5) | $\varepsilon\delta_6 > \delta_5$ and $\delta_7 > 0$ | $\delta_7 < 0$ | $\varepsilon\delta_6 < \delta_5$ and $\delta_7 > 0$ | HB, $\varepsilon = \tilde{\varepsilon}$ and $\delta_7 > 0$ |

**Table 3** Existence and stability of equilibria and bifurcation of the linear consumption system (3.4). HB and TB represent Hopf bifurcation and transcritical bifurcation, respectively.

| Equilibrium | Existence | Stable | Saddle point | Unstable | Bifurcation |
|---|---|---|---|---|---|
| $E_0^{'}(0,0)$ | Always | — | $b_0 < d_0$ | $b_0 > d_0$ | — |
| $E_1^{'}(N,0)$ | Always | $c_0 < a_0$ and $r < Ne_1$ | $c_0 > (<)a_0$ and $r < (>)Ne_1$ | $c_0 > a_0$ and $r > Ne_1$ | TB, $c_0 = a_0$ |
| $E_2^{'}(\frac{N(d_0-b_0)}{a_0+d_0-b_0-c_0}, 0)$ | (H1) | $a_0 < c_0$ and $r < \tilde{r}$ | $a_0 > (<)c_0$ and $r < (>)\tilde{r}$ | $a_0 > c_0$ and $r > \tilde{r}$ | TB, $r = \tilde{r}$ |
| $E_3^{'}(0,k)$ | Always | $d_1 > \tilde{d}_1$ | $d_1 < \tilde{d}_1$ | — | TB, $d_1 = \tilde{d}_1$ |
| $E_4^{'}(N, \frac{k(r-Ne_1)}{r})$ | $r > Ne_1$ | $a_1 > \tilde{a}_1^{'}$ and $N > \tilde{N}^{'}$ | $a_1 < (>)\tilde{a}_1^{'}$ and $N > (<)\tilde{N}^{'}$ | $a_1 < \tilde{a}_1^{'}$ and $N < \tilde{N}^{'}$ | TB, $\theta = \tilde{\theta}^{'}$ |
| $E_{\pm}^{*}, (u_{\pm}^{*}, n_{\pm}^{*})$ | (H6)-(H11) | $\varepsilon\delta_6^{'} > \delta_5^{'}$ and $\delta_7^{'} > 0$ | $\delta_7^{'} < 0$ | $\varepsilon\delta_6^{'} < \delta_5^{'}$ and $\delta_7^{'} > 0$ | HB, $\varepsilon = \tilde{\varepsilon}^{'}$ and $\delta_7^{'} > 0$ |

The positive equilibrium $E_+^*(u_+^*, n_+^*)$ exists if any of the following conditions hold.
**(H6)**: $\gamma_1 > 0$, $\delta_3^{'} < 0$, $\delta_3^{'2} + 4\delta_2\delta_4 > 0$, $e_1 > e_1^+$, and $k > n_+^*$.
**(H7)**: $\gamma_1 > 0$, $\delta_3^{'} > 0$, $\delta_4 > 0$, $e_1 > e_1^+$, and $k > n_+^*$.
**(H8)**: $\gamma_1 < 0$, $\delta_3^{'} > 0$, $\delta_3^{'2} + 4\delta_2\delta_4 > 0$, $\delta_4 > 0$, $e_1 > e_1^+$, and $k > n_+^*$.
Similarly, $E_-^*(u_-^*, n_-^*)$ exists under any of the following conditions.
**(H9)**: $\gamma_1 > 0$, $\delta_3^{'} < 0$, $\delta_3^{'2} + 4\delta_2\delta_4 > 0$, $\delta_4 < 0$, $e_1 > e_1^-$, and $k > n_-^*$.
**(H10)**: $\gamma_1 < 0$, $\delta_3^{'} > 0$, $\delta_3^{'2} + 4\delta_2\delta_4 > 0$, $e_1 > e_1^-$, and $k > n_-^*$.
**(H11)**: $\gamma_1 < 0$, $\delta_3^{'} < 0$, $\delta_4 < 0$, $e_1 > e_1^-$, and $k > n_-^*$.
By applying similar analytical techniques as utilized for system (2.5), we derive the conditions for the existence of the equilibria , stability, and bifurcation for system (3.4), as summarized in Table 3.

Comparing Tables 2 and 3 reveals that the nonlinear saturated functional response significantly influences the non-spatial dynamics of the system, leading to a richer set of dynamical behaviors. In the linear depletion system (3.4), at most four boundary equilibria can exist, whereas in the system with a nonlinear saturated functional response (2.5), up to five boundary equilibria are possible. Theoretically, system (3.4) can exhibit up to two interior equilibria, while system (2.5) can support up to three. Some of the boundary equilibrium expressions and all of the interior equilibrium expressions differ between the two systems, indicating that the nonlinear saturated functional response alters the evolutionary trajectories of both strategies and resources. Specifically, the inclusion of a nonlinear saturation effect introduces additional equilibrium configurations, thus expanding the range of potential evolutionary outcomes. Moreover, the nonlinear saturated functional response modifies the conditions for the existence, stability, and bifurcation of equilibria. This suggests that even when starting from identical initial conditions, the evolutionary trajectories of cooperation may diverge, ultimately leading to different long-term outcomes.

The system (3.4) incorporating a linear depletion term exhibits richer dynamical behavior than the model of Tilman et al. Specifically, system (3.4) can admit up to four boundary equilibria, exceeding the two boundary equilibria possible in the framework proposed by Tilman et al. (2020). From a mathematical analysis perspective, we explicitly derive the conditions for both transcritical and Hopf bifurcations, which are not addressed in the framework of Tilman et al. (2020). Moreover, the number of transcritical bifurcations associated with boundary equilibria is greater than that reported in previous studies. Consequently, even in the case $g = 0$, the system (3.4) with a linear depletion term allows for a wider range of potential evolutionary outcomes for both strategies and environmental resources.

The Hopf bifurcation for the system (2.5) exists, but the stability and direction concerning the Hopf bifurcation are still unknown. In order to ascertain the stability of the evolutionary direction and the final evolutionary outcome of the cooperators due to the relative timescale, the direction of the Hopf bifurcation and the stability of the periodic solution are investigated in the Appendix B. Based on this analysis, we obtain Theorem 3.3 as follows.

**Theorem 3.3** *(I) If $\xi_1(\tilde{\varepsilon}) < 0$ ($\xi_1(\tilde{\varepsilon}) > 0$), then the periodic solution is stable (unstable).*

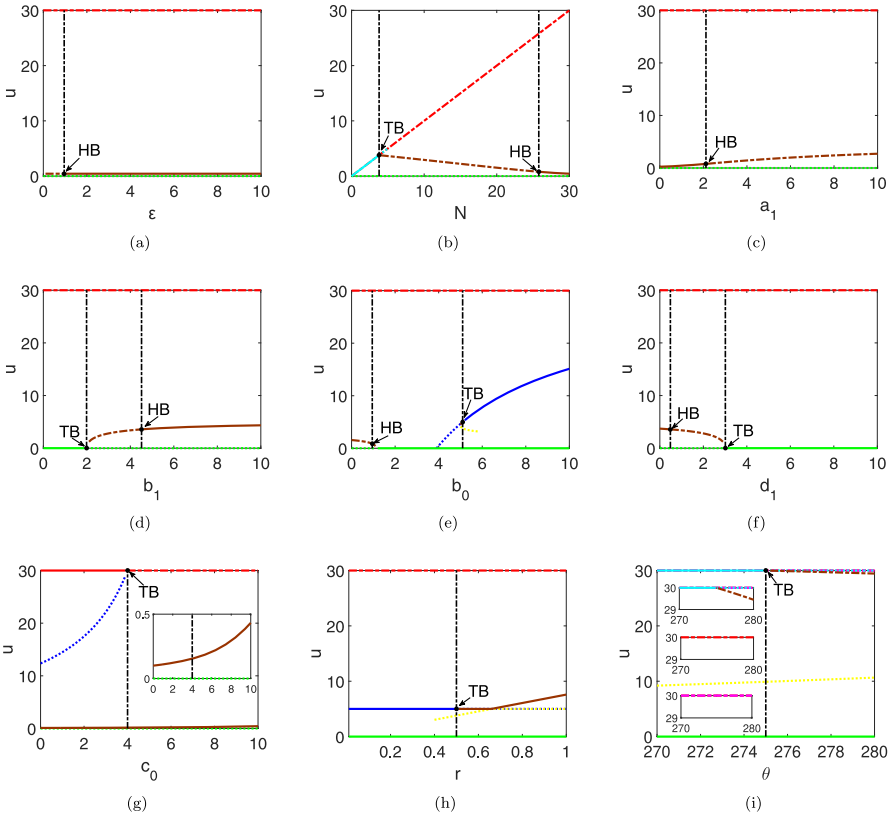


**Fig. 4** Existence and stability of equilibria, Hopf bifurcations, and transcritical bifurcations related to $\varepsilon$, $N$, $a_1, b_0, c_0, b_1, r, d_1$, and $\theta$ of the temporal system (2.5). The densities of the cooperators are depicted as red, blue, green, magenta, cyan, brown, and yellow curves for $E_1$, $E_2$, $E_3$, $E_4^-$, $E_4^+$, $E^*$, and $E_1^*$, respectively. The solid and dotted curves represent stable equilibria and saddle points, respectively. Dash-dotted curves are unstable focuses or nodes. TB and HB denote transcritical bifurcations and Hopf bifurcations, respectively, marked with black dots. Thresholds for the occurrence of transcritical bifurcations and Hopf bifurcations are indicated by black dash-dotted lines. The critical values corresponding to Theorem 3.2 for transcritical and Hopf bifurcations are calculated to be $c_0 = 4$, $\tilde{r} = 0.5$, $\tilde{d}_1 = 3.0128$, $\tilde{\theta} = 275$, and $\tilde{\varepsilon} = 0.9575$. The intervals in which the system appears to be bistable are $b_0 \in (5.1, 10)$, $r_0 \in (0.5, 1)$, $c_0 \in (0.9, 4)$, $r \in (0, 0.5)$, and $\theta \in (270, 275)$. Parameters: $\varepsilon = 2, a_1 = 1, a_0 = 4, b_0 = 1.1, b_1 = 2, c_0 = 10, c_1 = -4$, $d_0 = 3.9, d_1 = 3, r = 0.5, k = 4.7, e_1 = 0.1, g = 0.1, \theta = 3, N = 30$. (g) $d_0 = -0.1$ and remaining parameters are the same as above

*(II) If $\Gamma > 0$ ($\Gamma < 0$), then the Hopf bifurcation is supercritical (subcritical).*

Evolutionary results for the density of cooperators exhibit diverse trends with respect to the parameters $\varepsilon$, $N$, $a_1$, $b_0$, $c_0$, $b_1$, $r$, $d_1$, and $\theta$ (see Fig. 4). These outcomes are not solely determined by any single parameter. In Fig. 5, we further analyze the joint effects of multiple parameters on the evolutionary outcomes. Diverse evolutionary outcomes arise from the combined influence of multiple factors rather than from a single parameter alone. Fig. 4(a) illuminates the effect of the relative timescale on evolution. The relative timescale does not affect the stability of $E_1$ and $E_3$, which

are always unstable nodes and saddle points, respectively. When the relative time scale lies in the interval (0,0.9575), the internal equilibrium $E^*$ is unstable, and periodic solutions appear, as explained in detail in Figs. 6(a) and 7(b)(f). In this case, the cycle of cooperators and defectors prevails. In Fig. 7(f), the blue curve evolving from the inside and the magenta curve evolving from the outside eventually converge to the green closed curve, indicating that the periodic solution is stable. Regardless of the initial density of cooperators, the exact final evolutionary outcome is a cyclic oscillation of cooperators and defectors. System (2.5) remains stable at $E^*$ when the relative timescale exceeds the threshold value of 0.9575. Furthermore, relative timescales larger than the threshold do not affect the evolutionary consequences, with stable coexistence of cooperators and defectors.

Fig. 4(b) demonstrates the relationship between the density of players in the population and the density of cooperators. The transcritical bifurcation and Hopf bifurcation occur at $N = 3.7925$ and $N = 25.7890$, respectively. Variations in player density will not change the fact that $E_3$ is a saddle point. The density of cooperators rises with player density when player density is limited to a lower level. Once the player density exceeds the threshold for transcritical bifurcation, the system undergoes a periodic solution, with cooperators and defectors coexisting in oscillation. Cooperators and defectors coexist stably as $N$ lies in the interval (25.7890,30). Notice that the increase in player density is detrimental to the existence of cooperators if the player density exceeds the critical value of the transcritical bifurcation.

Fig. 4(c)-(g) examine the role of payoffs from players' encounters on the evolution of cooperators. Whether in rich or poor resources, there will be some benefit to the cooperator in terms of an increase in the cooperator's earnings when the cooperator meets other players. When cooperators meet, the density of cooperators increases as the cooperators' payoffs $a_1$ increase cooperators' density increases. When $a_1$ is greater than its threshold, a stable periodic solution emerges and cooperators and defectors cycle to dominate the population. Surprisingly, increasing the payoffs of cooperators does not necessarily always promote their survival, but instead may even lead to their extinction. When a cooperator meets a defector in an abundance of resources, the cooperator will become extinct if its payoff is relatively small. Further enhancing the payoffs of the cooperators, the cooperators can survive when $b_1$ is greater than the transcritical bifurcation threshold of 1.9872. The Hopf bifurcation arises at $b_1 = 4.5154$. Periodic solutions appear, and cooperators and defectors oscillate to coexist when $b_1$ exceeds the critical value of its Hopf bifurcation. The blue curve from the inside and the magenta curve from the outside ultimately tend to a green curve, which indicates that the periodic solution is stable. If the cooperator's payoff $b_0$ is small, the cooperator and defector oscillations coexist and show a decreasing trend as $b_0$ increases. The Hopf bifurcation and the transcritical bifurcation emerge at $b_0 = 0.95$ and $b_0 = 5.1$, respectively. The bistability phenomenon, i.e., the fact that both $E_3$ and $E_2$ are stable, exists in the interval $b_0 \in (5.1, 10)$. On this occasion, the initial density of cooperators has a decisive influence on whether the cooperators survive or perish. If the initial density of the cooperators is not appropriate, even if it increases the cooperator's payoff $b_0$, then the choice of cooperative strategy is not attractive to the player, and the cooperators eventually become extinct. The Hopf bifurcation and the transcritical bifurcation appears at $d_1 = 0.4846$ and $d_1 = 3.0128$, respectively.

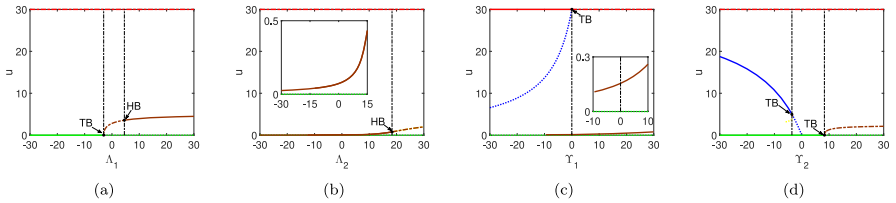


**Fig. 5** The combination of parameters in the payoff matrix, that is, incentive parameters $\Lambda_1$, $\Lambda_2$, $\Upsilon_1$, and $\Upsilon_2$, induces bistability, transcritical bifurcations, and Hopf bifurcations. The densities of the cooperators are depicted as red, blue, green, brown, and yellow curves for $E_1$, $E_2$, $E_3$, $E^*$, and $E_1^*$, respectively. The solid and dotted curves represent stable equilibria and saddle points, respectively. Dash-dotted curves are unstable focuses or nodes. TB and HB denote transcritical bifurcations and Hopf bifurcations, respectively, marked with black dots. Thresholds for the occurrence of transcritical bifurcations and Hopf bifurcations are indicated by black dash-dotted lines. Transcritical bifurcations and Hopf bifurcations occur at $\Lambda_1 = -3.0384$, $\Lambda_1 = 4.5462$, $\Lambda_2 = 18.3573$, $\Upsilon_1 = -9.5$, $\Upsilon_2 = -3.6$, and $\Upsilon_2 = 8.2941$. The intervals in which the system (2.5) appears to be bistable are $\Upsilon_1 \in (-9.5, 0)$ and $\Upsilon_2 \in (-30, -3.6)$. Parameters: $\varepsilon = 2$, $a_1 = 1$, $b_0 = 1.1$, $b_1 = 2$, $c_0 = 10$, $r = 0.5$, $k = 4.7$, $e_1 = 0.1$, $g = 0.1$, $\theta = 3$, $N = 30$

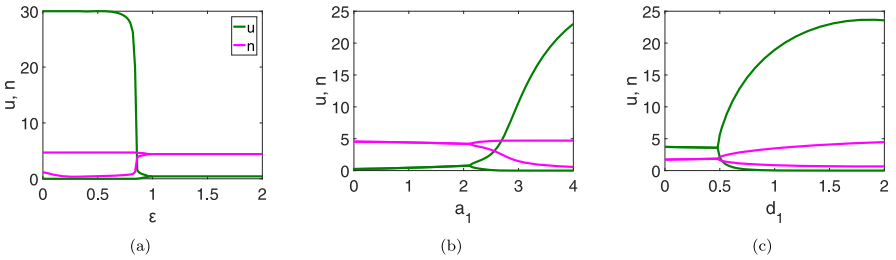


**Fig. 6** Hopf bifurcation diagram of the temporal system (2.5) regarding $\varepsilon$, $a_1$, and $d_1$. (a) System is unstable if $\varepsilon \in (0, 0.9575)$ and is stable if $\varepsilon > 0.9575$. Hopf bifurcation occurs at $\varepsilon = \tilde{\varepsilon} = 0.9575$. (b) The system is stable when $a_1 < 2.1191$. If $a_1 \in (2.1191, 4)$, then the periodic solution appears and the system becomes unstable. Hopf bifurcation appears if $a_1 = 2.1191$. (c) Hopf bifurcation emerges when $d_1 = 0.4846$. The system is stable when $d_1$ lies in interval (0,0.4846) and is unstable when $d_1$ lies in interval (0.4846,2)

Unsurprisingly, increasing the payoffs of defectors can reduce the chances of survival or even lead to the extinction of cooperators when defectors encounter each other. The transcritical bifurcation emerges when $c_0 = 4$. The phenomenon of bistability, i.e., $E_1$ and $E^*$ are stable, appears when $c_0$ lies in the interval (0,4). The initial state of the cooperator determines whether the cooperator will monopolize the population or coexist with defectors. Surprisingly, increasing the payoffs of the defectors instead favors the cooperators when $c_0$ exceeds the critical value of the transcritical bifurcation.

Three types of bistability phenomena emerge in Fig. 4(h) and (i). $E_3$ and $E_2$ are stable when $r \in (0, 0.5)$. The transition of stability from $E_2$ to $E^*$ is at $r = 0.5$, after which $E^*$ and $E_3$ are stable simultaneously. $E_4^+$ and $E_3$ are stable if $\theta$ is in the interval (270,275). The initial choice of strategy made by the players in the population determines whether the cooperators survive or become extinct. Large growth rates favor the viability of cooperators.

Fig. 5 illustrates the impact of incentives on the evolutionary outcomes of cooperation. In Fig. 5(a), transcritical and Hopf bifurcations occur at $\Lambda_1 = -3.0384$ and $\Lambda_1 = 4.5462$, respectively. When the incentive $\Lambda_1$ is less than $-3.0384$, cooperation

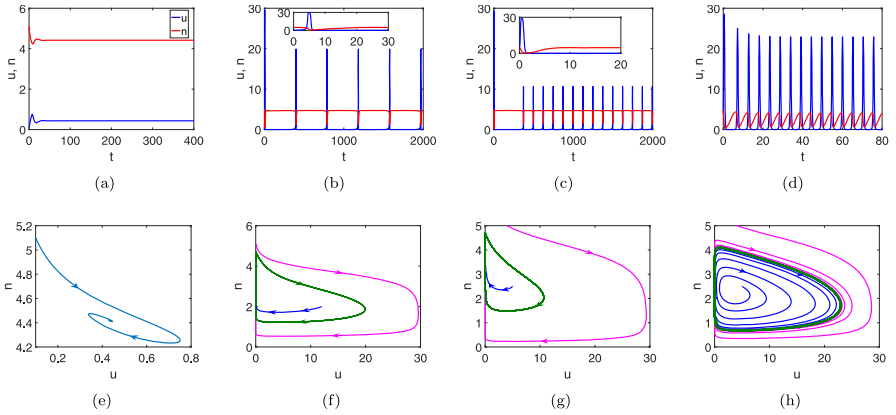


**Fig. 7** Temporal evolution of resources and cooperators (first row), as well as the corresponding phase trajectories (second row). (a), (e) $E^*$ is stable. (b),(f) $\varepsilon = 0.84$, a stable periodic solution occurs near $E^*$. (c), (g) The choice of $a_1 = 3$ leads to $E^*$ being unstable and a stable periodic solution emerging. (d), (h) Choosing $d_1 = 1.5$ yields a stable periodic solution arising around $E^*$

is not attractive to players, and no individuals in the population choose to cooperate. As the incentive increases, enthusiasm for cooperation is stimulated, leading to oscillatory coexistence between cooperators and defectors. When $\Lambda_1$ exceeds the Hopf bifurcation threshold, oscillations disappear and a stable coexistence of strategies emerges. In Fig. 5(b), a Hopf bifurcation arises at $\Lambda_2 = 18.3573$. As $\Lambda_2$ increases, the incentive for cooperation grows stronger, resulting in an upward trend in the density of cooperators. The elevation of $\Lambda_1$ and $\Lambda_2$ serves to facilitate the mobilization of players toward cooperation. In Fig. 5(c), when $\Upsilon$ lies within the interval $(-9.5, 0)$, both $E_1$ and $E^*$ are stable, and the evolutionary outcome depends on the initial condition. A transcritical bifurcation occurs at $\Upsilon_1 = 0$. When $\Upsilon_1$ is small (i.e., negative), cooperators dominate the entire population. As $\Upsilon_1$ increases, defectors emerge and the cooperation level declines sharply. In particular, when $\Upsilon_1$ is negative, cooperators are more likely to dominate; when $\Upsilon_1$ is positive, the chance for cooperation to persist becomes minimal. In Fig. 5(d), both $E_2$ and $E_3$ are stable when $\Upsilon_2$ is in the range $(-30, -3.6)$. Transcritical bifurcations occur at $\Upsilon_2 = -3.6$ and $\Upsilon_2 = 8.2941$. Overall, increasing $\Upsilon_1$ or $\Upsilon_2$ tends to undermine the prevalence of cooperation.

Fig. 8 explores the combined effects of various parameters on the density of cooperators and the stock of resources. In this analysis, cooperators interact in environments with both poor and rich resources, allowing us to contrast how changes in cooperator payoffs in these differing resource conditions impact their density and resource availability (Fig. 8(a)-(d)). The results show that cooperator payoffs have a more pronounced effect in resource-rich environments compared to resource-poor ones. This is evident in the vertical changes in cooperator density, which are more significant than the horizontal shifts. When the parameter $a_1$–representing cooperator payoffs in resource-rich environments–is initially small, even a slight increase in $a_1$ leads to a steady rise in cooperator density. As $a_1$ increases further, we observe a transition between Region I and Region II, indicating a shift from stable to unstable equilibria

($E_*$). In resource-rich environments, cooperators benefit from high payoffs, enabling them to achieve higher densities. However, this increase in density does not prevent the periodic extinction of cooperators, suggesting that other factors continue to drive fluctuations in their population. Interestingly, when $a_1$ remains constrained to lower values, increasing the payoffs for cooperators in resource-poor environments unexpectedly reduces their density. In this context, cooperators become more efficient at capturing resources, which leads to an abundance of supplies. This resource surplus, in turn, causes players to become more inert, increasing the likelihood that they will switch to a defection strategy. As a result, the population experiences a rise in defection, and cooperation becomes less favorable.

The effects of cooperators' payoffs during encounters between cooperators and defectors on the evolution of cooperation across different resource abundance levels are depicted in Fig. 8(e)-(h). When the payoff parameter $b_1$–which represents the payoffs from encounters in resource-rich environments–is small, neither adjusting the value of $b_1$ nor $b_0$ (the payoff from encounters in resource-poor environments) alters the outcome that cooperators will eventually go extinct. However, when the payoffs for cooperators encountering defectors in rich resources are moderately increased, cooperators can periodically reach maximum density, temporarily boosting their population. Yet, an uncontrolled increase in these payoffs paradoxically results in a decline in cooperator density, which hampers their ability to reproduce and maintain their presence in the population. Interestingly, when the value of $b_1$ is kept moderate, increasing $b_0$-the payoff for cooperators encountering defectors in resource-poor environment–leads to a reduction in cooperator density. This suggests that in poor resource settings, raising cooperators' payoffs does not promote cooperation, as the scarcity of resources makes it more costly for cooperators to access and utilize these resources. Even when cooperators' earnings increase in these conditions, the overall resource limitation discourages players from adopting cooperative strategies, as the benefits do not outweigh the challenges posed by resource scarcity.

In Fig. 8(i)-(l), we investigate the role of defector payoffs during encounters between defectors and their impact on the evolution of cooperation. When the payoff parameter $d_1$–representing the payoffs from defector encounters in resource–rich environments–remains high, changing the values of $b_0$ or $b_1$ (payoffs from cooperators encountering defectors in resource-poor or rich environments, respectively) does not affect the eventual extinction of cooperators. However, increasing the payoffs for defectors leads to an initial decline in cooperator density, followed by a cyclical turnover between cooperators and defectors. While cooperators are unable to escape periodic extinction, their population can reach increasingly higher densities as long as $d_1$ remains small and fixed. This cyclical dynamic highlights that, even in the face of fluctuating populations, cooperators can periodically recover, albeit temporarily. Interestingly, reducing the payoffs from defector-defector encounters, whether in resource-rich or resource-poor environments, encourages players to adopt cooperative strategies. By diminishing the rewards for defectors in these encounters, the system creates incentives for cooperation to persist, thereby promoting the long-term continuation of cooperative behavior within the population. This suggests that lowering defector payoffs can effectively shift the balance towards cooperation, even in resource-scarce conditions.

In Fig. 8(m)-(p), we examine the roles of the resource growth rate and resource consumption rate on the evolution of cooperators. Region I, which occupies a significantly larger area than Region III, highlights the dominant influence of the resource consumption rate over the resource growth rate in shaping the evolutionary dynamics of cooperation. Regardless of how the resource growth rate is adjusted, cooperators are driven toward extinction when the resource consumption rate is high. In contrast, cooperators can reach and maintain high densities only when the consumption or depletion rate of resources is relatively low. Under these conditions, cooperators can avoid periodic extinction and persist in the population. The results suggest that small resource consumption rates, combined with high resource growth rates, create favorable conditions for the spread of cooperative strategies. These conditions enable cooperators to thrive and maintain large population densities, ensuring the sustainability of cooperative behavior over time.

In Fig. 8(q) and (r), the system reaches a stable positive equilibrium, where cooperators and defectors coexist. In scenarios where defectors and cooperators interact in resource-abundant environments, reducing the payoffs for defectors has the effect of energizing cooperators, boosting their density. Interestingly, in environments with moderate resource scarcity, increasing defector payoffs unexpectedly leads to an increase in cooperator density. As resources become more limited, the population faces a shortage of necessary supplies for survival and reproduction. This scarcity triggers a survival instinct among players, motivating more individuals to adopt cooperative strategies to collectively replenish resources. Additionally, small improvements in player density further support the prevalence of cooperators. However, slight changes in payoff factors do not significantly alter the overall evolutionary outcomes, suggesting that certain key parameters, such as player density and resource availability, play a more crucial role in determining the dynamics between cooperators and defectors.

The effects of player density and baseline payoffs on the evolutionary outcomes of cooperator density and resource stock are revealed in Fig. 8(s) and (t). The density of cooperators is positively facilitated by the density of players if baseline payoffs are kept small. In this case, whatever the value of the baseline payoff is taken does not shake the final evolution of the cooperators and resources. Cooperators eventually become extinct once baseline payoffs are limited to large values. No amount of changing player density and baseline payoffs is going to change the fact that defectors fill the population. Small baseline payoffs and large player densities favorably motivate players to choose to cooperate.

Predicting the outcome of evolution by consulting only a single factor is limiting, and it is crucial to consider the effect of parameter interactions on evolution. In some cases, small payoffs of cooperators and defectors contribute to the survival of cooperators. In region I, small $a_0$ and $b_0$ help cooperators from extinction if the values of $a_1$ and $b_1$ are kept constant. Similarly, lowering $c_1$ helps cooperators survive if $c_0$ is held constant. There are also cases where large payoffs in cooperators and defectors facilitate the attainment of high densities by cooperators, although the cooperators are unable to avoid periodic extinctions. In Region II, keeping $a_0$ constant, an increase in $a_1$ can assist cooperators in reaching high densities, and defectors can also periodically dominate the population (Fig. 8(a)-(d)). In Region II of Fig. 8(i)-(l), increasing $d_0$ leads to a density of cooperators that can be gradually maximized when $d_1$ maintains

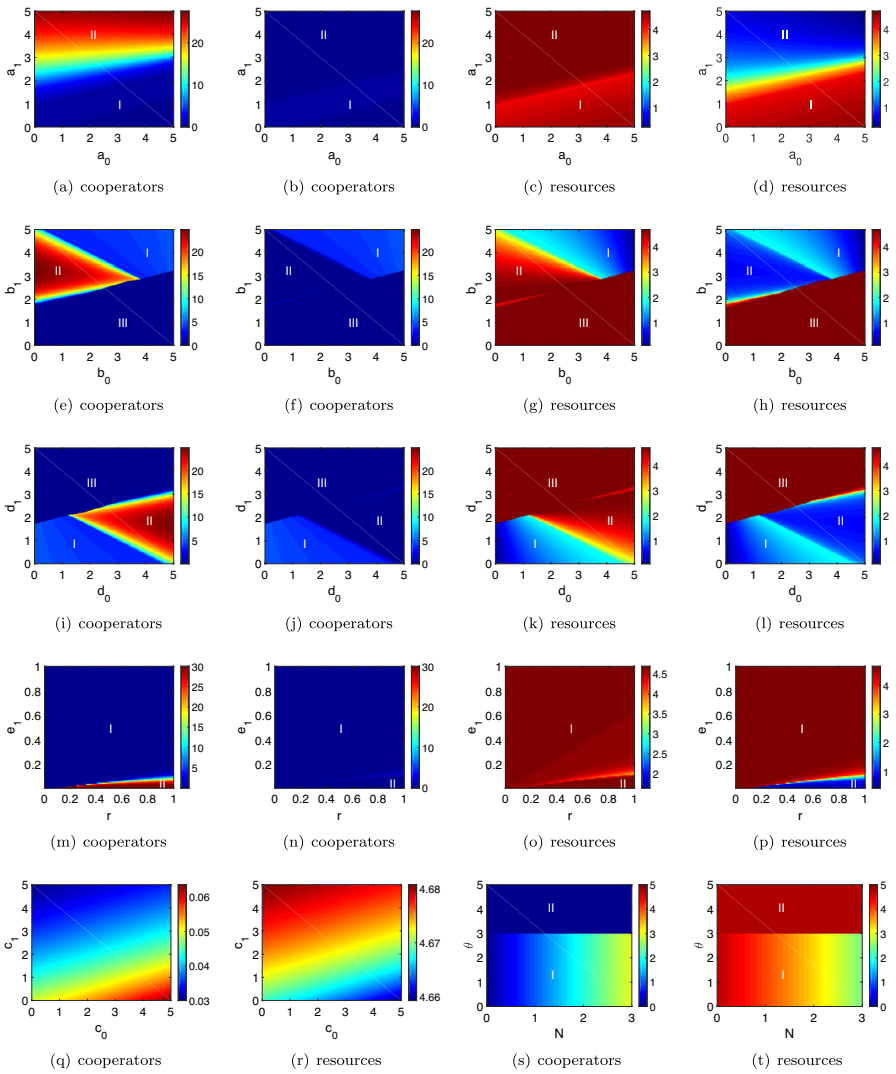


**Fig. 8** Multiple evolutionary outcomes for resources and cooperators triggered by two-dimensional parameters. (a)-(p) Regions I, II, and III indicate stable $E^*$, unstable $E^*$, and stable $E_3$, respectively. $E^*$ is unstable and periodic solutions occur in region II. Region II in the first and third columns denotes the maximum values of cooperator density and resource stock after a long evolutionary period, respectively. Region II in the second and fourth columns corresponds to the minimum values of cooperator density and resource stock, respectively. (q), (r) $E^*$ is stable. (s),(t) Regions I and II correspond to the basins of attraction for $E_4^+$ and $E_3$, respectively

a moderate value. Notably, sometimes, changing player payoffs does not have any effect on evolutionary outcomes. In Region III, whether varying cooperators' payoffs or defectors' payoffs in poor or rich resources, cooperators eventually become extinct. Raising the payoffs of cooperators and lowering the payoffs of defectors does not

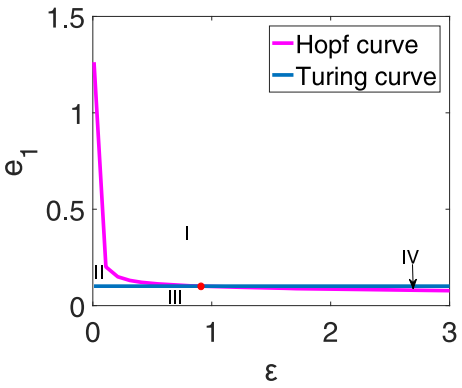


**Fig. 9** Turing-Hopf bifurcation diagram in the $\varepsilon - e_1$ plane. The Turing-Hopf bifurcation occurs at $(\varepsilon, e_1) = (0.91, 0.11)$ marked with a red dot

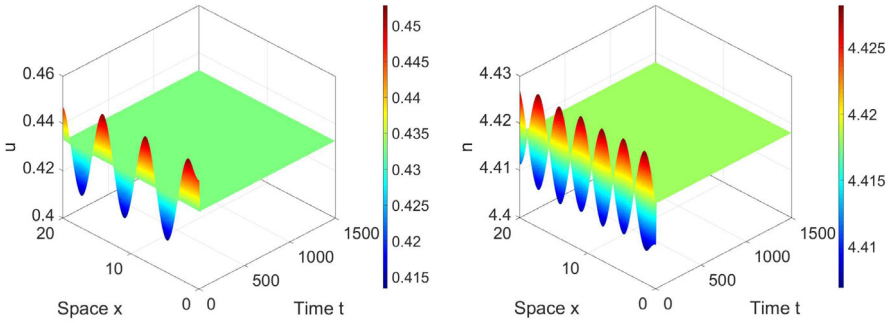


(a) cooperators (b) resources

**Fig. 10** Evolution of cooperators and resources with space $x$ and time $t$. The steady state $E^*$ is stable when $\varepsilon = 2 > \varepsilon^* = 0.9141$. The initial conditions are $u(x, 0) = 0.4326 + 0.01\sin x$ and $n(x, 0) = 4.4180 + 0.01\sin x$

always boost the density of cooperators and, in some cases, discourages players from choosing a cooperative strategy.

## 4 Dynamics of diffusion system (2.6)

In this section, we explore spatial dynamical properties including local stability, Hopf bifurcation and Turing instability for the diffusion system (2.6). Note that we assume that cooperators perform unbiased diffusion in a two-dimensional spatial domain. A derivation of the resulting Fickian diffusion term under constant density is provided in Appendix C.

### 4.1 Local stability

Obviously, the equilibria $E_0(0, 0)$, $E_1(N, 0)$, $E_2(u_2, 0)$, $E_3(0, k)$, $E_4^+(N, n_4^+)$, $E_4^-(N, n_4^-)$, and $E^*(u^*, n^*)$ of the temporal system (2.5) also satisfy the spatial system (2.6). We consider a two-dimensional domain $\Omega$ defined as $\{\mathbf{x} = (x, y) | 0 < x <$

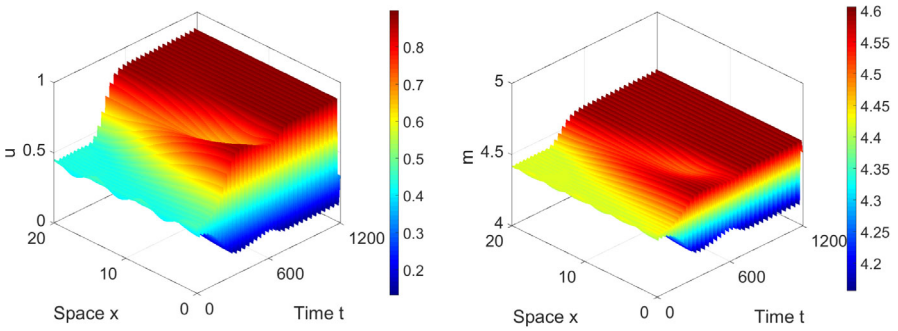


(a) cooperators (b) resources

**Fig. 11** Evolution of cooperators and resources with space $x$ and time $t$. Spatially homogeneous periodic solution appears when $\varepsilon = 0.9 < \varepsilon^* = 0.9141$. The initial conditions are $u(x,0) = 0.4326 + 0.01\sin x$ and $n(x,0) = 4.4180 + 0.01\sin x$

$M, 0 < y < M\}$ whose boundary is $\partial\Omega$. Then,

$$\begin{cases} \nabla^2 \mathbf{V} + m^2 \mathbf{V}, & \mathbf{x} \in \Omega, \\ \dfrac{\partial \mathbf{V}}{\partial \eta} = 0, & \mathbf{x} \in \partial\Omega, \end{cases}$$

has eigenfunctions

$$\mathbf{V}_{s,v}(\mathbf{x}) = \mathbf{H}_{s,v} \cos\frac{s\pi x}{M} \cos\frac{v\pi y}{M}, \; m^2 = \pi^2 \left( \frac{s^2}{M^2} + \frac{v^2}{M^2} \right),$$

where $\mathbf{x} = (x, y)$, $s$ and $v$ are integers, and $\mathbf{H}_{s,v}$ is a Fourier coefficient. For the system (2.6), the stability of the constant steady states $E_0(0,0)$, $E_1(N,0)$, $E_2(u_2,0)$, $E_3(0,k)$, $E_4^+(N,n_4^+)$, $E_4^-(N,n_4^-)$, and $E^*(u^*,n^*)$ is summarized with the following theorem.

**Theorem 4.1** *(I) The steady state $E_0(0,0)$ is always spatially unstable.*

*(II) The steady state $E_1(N,0)$ is spatially stable if $c_0 < a_0$ and $r < Ne_1$; while $E_1(N,0)$ is spatially unstable if $c_0 > a_0$ or $r > Ne_1$.*

*(III) The steady state $E_2(u_2,0)$ is spatially stable if $a_0 < c_0$ and $r < \tilde{r}$; while $E_1(N,0)$ is spatially unstable if $a_0 > c_0$ or $r > \tilde{r}$.*

*(IV) The steady state $E_3(0,k)$ is spatially stable if $d_1 > \tilde{d}_1$; $E_3(0,k)$ is spatially unstable if $d_1 < \tilde{d}_1$.*

*(V) The steady state $E_4^+(N,n_4^+)$ is spatially stable if $a_1 > \tilde{a}_1$ and $N > \tilde{N}$; while $E_4^+(N,n_4^+)$ is spatially unstable if $a_1 < \tilde{a}_1$ or $N < \tilde{N}$.*

*(VI) The steady state $E_4^-(N,n_4^-)$ is spatially stable if $a_1 > \hat{a}_1$ and $N > \hat{N}$; while $E_4^-(N,n_4^-)$ is spatially unstable if $a_1 < \hat{a}_1$ or $N < \hat{N}$.*

*(VII) The steady state $E^*(u^*,n^*)$ is spatially stable if $\delta_5 < 0$, $\delta_6 > 0$, and $\delta_7 > 0$.*

***Proof*** See Appendix D. □

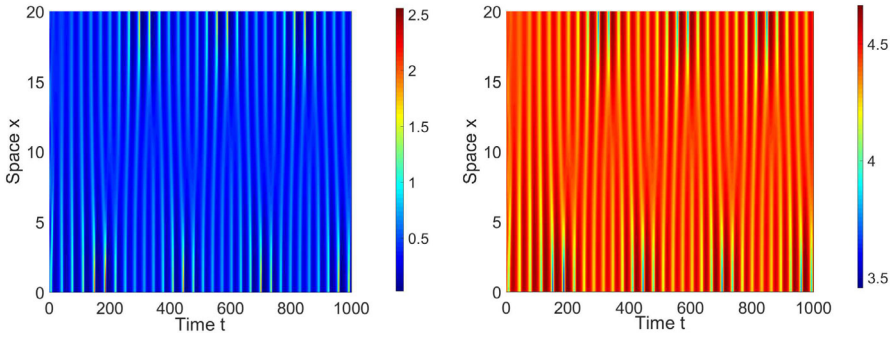


(a) cooperators (b) resources

**Fig. 12** Evolution of cooperators and resources with space $x$ and time $t$. Spatially heterogeneous periodic solutions appear

### 4.2 Turing instability

Next, we derive the conditions under which the steady state $E^*(u^*, n^*)$ of (D.3) is destabilized due to heterogeneous perturbations of small amplitudes in the two-dimensional square domain $\Omega$. For this purpose, we assume that the conditions in Theorem 3.1 (VII) that allow the equilibrium $E^*(u^*, m^*)$ to be stable hold. For the non-zero wavenumber $m$, Turing instability can only arise for $\widetilde{\mathrm{Det}}(m^2) < 0$ since $\widetilde{\mathrm{Tr}}(m^2) < 0$ holds. For convenience, define

$$\psi(m^2) := \mathrm{Det}(m^2) = d_u d_n m^4 - (j_{11} d_n + j_{22} d_u) m^2 + j_{11} j_{22} - j_{21} j_{12}. \tag{4.1}$$

The equilibrium $E^*(u^*, n^*)$ of system (2.5) is stable, hence $\mathrm{Det}(J^*) = j_{11} j_{22} - j_{21} j_{12} > 0$. According to (4.1), $\psi(m^2) < 0$ is possible if

$$\varpi(d_u, d_m) := j_{11} d_n + j_{22} d_u > 0. \tag{4.2}$$

According to (4.2) and $\mathrm{Tr}(J^*) = j_{11} + j_{22} < 0$, one can know that $d_u \neq d_m$ and $j_{11} j_{22} < 0$. We have $j_{12} > 0$ since $\mathrm{Det}(J^*) = j_{11} j_{22} - j_{21} j_{12} > 0$ and $j_{21} < 0$. The minimum value of $\psi(m^2)$ at $m^2_{\min}$ is

$$\min_m \psi(m^2) = j_{11} j_{22} - j_{21} j_{12} - \frac{(j_{11} j_{22} - j_{21} j_{12})^2}{4 d_u d_m},$$

where

$$m^2_{\min} = \frac{j_{11} d_n + j_{22} d_u}{2 d_u d_v}.$$

According to $\min_m \psi(m^2) = 0$, we have

$$\frac{(j_{11} d_n + j_{22} d_u)^2}{4 d_u d_n} = j_{11} j_{22} - j_{21} j_{12}.$$

Let

$$\begin{aligned}\Upsilon(d_u, d_n) :=&(j_{11}d_n + j_{22}d_u)^2 - 4d_u d_m(j_{11}j_{22} - j_{21}j_{12})\\ =&j_{11}^2 d_n^2 + j_{22}^2 d_u^2 + 2(2j_{12}j_{21} - j_{11}j_{22})d_u d_n.\end{aligned}$$

Denote $\varphi = \frac{d_n}{d_u}$, then we have

$$\Upsilon(d_u, d_n) = j_{11}^2\varphi^2 + 2(2j_{12}j_{21} - j_{11}j_{22})\varphi + j_{22}^2 = 0.$$

According to $\varpi(d_u, d_m) = 0$, we obtain

$$\varphi = -\frac{j_{22}}{j_{11}} \triangleq \varphi^*.$$

Since $j_{12} > 0$, $j_{21} < 0$, and $\mathrm{Det}(J^*) > 0$, we obtain

$$4(2j_{12}j_{21} - j_{11}j_{22})^2 - 4j_{11}^2 j_{22}^2 = 16j_{21}j_{12}(j_{21}j_{12} - j_{11}j_{22}) > 0.$$

Therefore, the equation $\Upsilon(g_u, d_n) = 0$ has the following two positive roots

$$\begin{aligned}\varphi_1 =&\frac{j_{11}j_{22} - 2j_{12}j_{21} + \sqrt{(2j_{12}j_{21} - j_{11}j_{22})^2 - j_{11}^2 j_{22}^2}}{j_{11}^2},\\ \varphi_2 =&\frac{j_{11}j_{22} - 2j_{12}j_{21} - \sqrt{(2j_{12}j_{21} - j_{11}j_{22})^2 - j_{11}^2 j_{22}^2}}{j_{11}^2}.\end{aligned}$$

Obviously,

$$0 < \varphi_2 < \varphi^* < \varphi_1.$$

We know that $\min_m \psi(m^2) < 0$ and $\varpi(d_u, d_m) > 0$ when $\varphi = \frac{d_n}{d_u} > \varphi_1$. Thus, the steady state $E^*(u^*, n^*)$ is spatially unstable which means that Turing instability arises. Let $d_n^c = d_u\varphi_c$ and then the critical wavenumber is given by

$$m_c^2 = \frac{j_{22}d_u + j_{11}d_u^c}{2d_u d_n^c}.$$

Thus, we obtain the following Theorem 4.2

**Theorem 4.2** *Assume that $\varepsilon\delta_6 > \delta_5$ and $\delta_7 > 0$. Turing instability driven by diffusion occurs near the steady state $E^*(u^*, n^*)$ if $\varphi = \frac{d_n}{d_u} > \varphi_1$.*

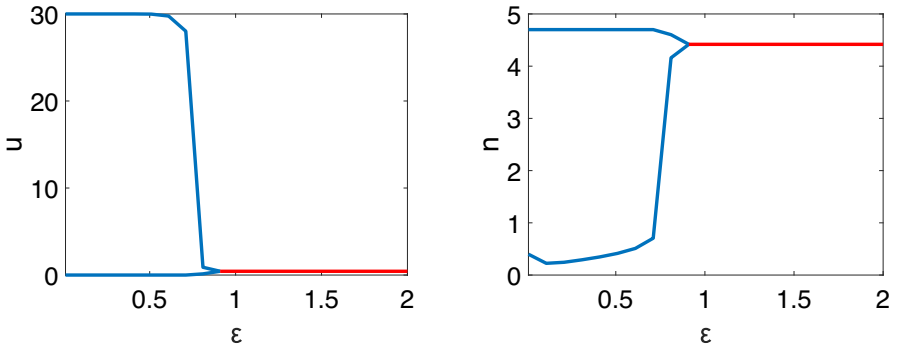


(a) cooperators (b) resources

**Fig. 13** Dependence of cooperator density and resource stock on relative timescales for system (2.6). When the value of $\varepsilon$ falls within the intervals indicated by the blue curve and the red line, respectively, system (2.6) exhibits periodic solutions and remains spatially stable. Hopf bifurcation occurs when $\varepsilon = \varepsilon^* = 0.9141$

### 4.3 Hopf bifurcation

If $\widetilde{\mathrm{Tr}}(m^2) = 0$ and $\widetilde{\mathrm{Det}}(m^2) > 0$, then (D.3) has pure imaginary roots. Denote

$$\varepsilon^* = \tilde{\varepsilon} - \frac{(d_u + d_n)m^2}{\delta_6}.$$

If $\varepsilon = \varepsilon^*$, then $\mathrm{Tr}(m^2) = 0$. One can see that $\varepsilon^*\delta_6 > j_{11}d_n$ enables $(d_n j_{11} + j_{22}d_u)|_{\varepsilon=\varepsilon^*} < 0$. Further, $\delta_7 > 0$ such that $\mathrm{Det}(J^*)|_{\varepsilon=\varepsilon^*} = j_{11}j_{22} - j_{12}j_{21} > 0$. Hence, $\widetilde{\mathrm{Det}}(m^2)|_{\varepsilon=\varepsilon^*} > 0$ if $\varepsilon^*\delta_6 > j_{11}d_n$ and $\delta_7 > 0$. From (D.3), we have

$$\mathrm{Re}\left[\frac{\mathrm{d}\lambda}{\mathrm{d}\varepsilon}\right]_{\varepsilon=\varepsilon^*} = r\left(\frac{1}{2} - \frac{n^*}{k}\right) - \frac{e_1 u^*}{2(1+gn^*)^2} \neq 0.$$

The Hopf bifurcation appears at $\varepsilon = \varepsilon^*$ because the transversality condition holds. Therefore, we have the following theorem.

**Theorem 4.3** *The system (2.6) undergoes Hopf bifurcation at $\varepsilon = \varepsilon^*$ if $\varepsilon^*\delta_6 > j_{11}d_n$ and $\delta_7 > 0$.*

### 4.4 Turing-Hopf bifurcation

Next we we investigate the existence of the Turing-Hopf bifurcation. Denote

$$\gamma_4 = r(1 - \frac{2n^*}{k}),\ \gamma_5 = \frac{u^*}{(gn^*+1)^2},\ \gamma_6 = \frac{n^*}{1+gn^*},\ \gamma_7 = j_{11}d_n + \varepsilon\gamma_4 d_u - j_{11}\varepsilon\gamma_4.$$

Setting $\widetilde{\mathrm{Det}}(m^2) = 0$ yields

$$d_u d_n m^4 - (j_{11}d_n + \varepsilon(\gamma_4 - e_1\gamma_5)d_u)m^2 + j_{11}\varepsilon(\gamma_4 - e_1\gamma_5) + j_{12}e_1\gamma_6\varepsilon = 0. \quad (4.3)$$

If $d_u d_n > \gamma_7$ and $\gamma_6 > \frac{\gamma_5(j_{11}-1)}{j_{11}}$, then the Hopf bifurcation curve $\varepsilon = \varepsilon^*$ cannot interact with the Turing bifurcation curve. When $d_u d_n < \gamma_7$ and $\gamma_6 > \frac{\gamma_5(j_{11}-1)}{j_{11}}$, substituting $\varepsilon = \varepsilon^*$ into (4.3) yields

$$e_1(m) = \frac{(j_{11}d_n + \varepsilon\gamma_4 d_u)m^2 - d_u d_n m^4 - j_{11}\varepsilon\gamma_4}{\varepsilon(d_u\gamma_5 m^2 - j_{11}\gamma_5 + j_{12}\gamma_6)},\ m \in [1, m^*],$$

in which

$$m^* = \left[\frac{j_{11}d_n + \varepsilon\gamma_4 d_u + \sqrt{(j_{11}d_n + \varepsilon\gamma_4 d_u)^2 - 4d_u d_n j_{11}\varepsilon\gamma_4}}{d_u d_n}\right],$$

and $[\cdot]$ is the integer part. Let

$$f(p) = -j_{11}\varepsilon\gamma_4 + (j_{11}d_n + \varepsilon\gamma_4 d_u)p - d_u d_n p^2,\ p \in [1, m^{*2}].$$

Calculations yield $f'(p) \geq 0$ for $p \leq p^*$ and $f'(p) < 0$ for $p > p^*$, where

$$p^* = j_{11}\gamma_5 - j_{12}\gamma_6 + \frac{\sqrt{d_u^2 d_n^2 (j_{11}\gamma_5 - j_{12}\gamma_6)^2 + d_u d_n \gamma_5 (j_{12}\gamma_6(j_{11}d_n + \gamma_4\varepsilon) - j_{11}^2 d_n\gamma_5)}}{d_u d_n}.$$

Let

$$m_* = \begin{cases} 1, & \text{if } p^* \leq 1, \\ [\sqrt{p^*}], & \text{if } e_1(1 + [\sqrt{p^*}]) \leq e_1([\sqrt{p^*}]),\ 1 < \sqrt{p^*} < m^*, \\ 1 + [\sqrt{p^*}], & \text{if } e_1([\sqrt{p^*}]) \leq e_1(1 + [\sqrt{p^*}]),\ 1 < \sqrt{p^*} < m^*. \end{cases}$$

There exists $p_*$ such that $e_1^* = e(m_*) = \max\limits_{1\leq m\leq m^*} e_1(m)$. Thus, the Turing-Hopf bifurcation appears at the point

$$(e_1^*, \varepsilon^*) = \left(\frac{(j_{11}d_n + \varepsilon^*\gamma_4 d_u)m_*^2 - d_u d_n m_*^4 - j_{11}\varepsilon^*\gamma_4}{\varepsilon^*(d_u\gamma_5 m_*^2 - j_{11}\gamma_5 + j_{12}\gamma_6)}, \varepsilon^*\right).$$

Therefore, we obtain the following Theorem 4.4.

**Theorem 4.4** *The system (2.6) undergoes Turing-Hopf bifurcation at* $(e_1, \varepsilon) = (e_1^*, \varepsilon^*)$ *if* $d_u d_n < \gamma_7$ *and* $\gamma_6 > \frac{\gamma_5(j_{11}-1)}{j_{11}}$.

***Remark 4.1*** Following a similar analytical procedure, we analyze the spatial stability and identify the conditions for Turing-Hopf bifurcation of system (2.6) in the case when $g = 0$, as summarized in Table 5. The explicit expressions of the mathematical terms in Table 5 are presented below.

$$j_{11}^{'} = \frac{u_\pm^*(N - u_\pm^*)}{N^2}(\gamma_2\theta - \gamma_1 n_\pm^*),\ j_{12}^{'} = \frac{u^*(N - u^*)}{N^2}(N\gamma_3 - \gamma_1 u^*),$$

**Table 4** Stability and Turing-Hopf bifurcation of the diffusion system (2.6).

| Steady state | Spatially stable | Spatially unstable | Turing-Hopf bifurcation |
|---|---|---|---|
| $E_0(0,0)$ | — | Always | — |
| $E_1(N,0)$ | $c_0 < a_0$ and $r < Ne_1$ | $c_0 > a_0$ or $r > Ne_1$ | — |
| $E_2(u_2,0)$ | $a_0 < c_0$ and $r < \tilde{r}$ | $a_0 > c_0$ or $r > \tilde{r}$ | — |
| $E_3(0,k)$ | $d_1 > \tilde{d}_1$ | $d_1 < \tilde{d}_1$ | — |
| $E_4^+(N,n_4^+)$ | $a_1 > \tilde{a}_1$ and $N > \tilde{N}$ | $a_1 < \tilde{a}_1$ or $N < \tilde{N}$ | — |
| $E_4^-(N,n_4^-)$ | $a_1 > \hat{a}_1$ and $N > \hat{N}$ | $a_1 < \hat{a}_1$ or $N < \hat{N}$ | — |
| $E^*(u^*,n^*)$ | $\delta_5 < 0, \delta_6 > 0$, and $\delta_7 > 0$ | — | $d_u d_n < \gamma_7, \gamma_6 > \frac{\gamma_5(j_{11}-1)}{j_{11}}, (e_1,\varepsilon) = (e_1^*,\varepsilon^*)$ |

**Table 5** Stability and Turing-Hopf bifurcation of the diffusion system (2.6) when $g = 0$.

| Steady state | Spatially stable | Spatially unstable | Turing-Hopf bifurcation |
|---|---|---|---|
| $E_0^{'}(0,0)$ | — | Always | — |
| $E_1{}'(N,0)$ | $c_0 < a_0$ and $r < Ne_1$ | $c_0 > a_0$ or $r > Ne_1$ | — |
| $E_2{}'(u_2,0)$ | $a_0 < c_0$ and $r < \tilde{r}$ | $a_0 > c_0$ or $r > \tilde{r}$ | — |
| $E_3{}'(0,k)$ | $d_1 > \tilde{d}_1$ | $d_1 < \tilde{d}_1$ | — |
| $E_4^{'}(N,n_4^{'})$ | $a_1 > \tilde{a}_1^{'}$ and $N > \tilde{N}^{'}$ | $a_1 < \tilde{a}_1^{'}$ or $N < \tilde{N}^{'}$ | — |
| $E_{\pm}^{*}(u_{\pm}^{*},n_{\pm}^{*})$ | $\delta_5^{'} < 0$, $\delta_6^{'} > 0$, and $\delta_7^{'} > 0$ | — | $d_u d_n < \gamma_7$, $\gamma_6^{'} > \frac{\gamma_5^{'}(j_{11}^{'}-1)}{j_{11}^{'}}$, $(e_1,\varepsilon) = (\hat{e}_1^{*},\hat{\varepsilon}^{*})$ |

$$\gamma_4^{'} = r(1 - \frac{2n_{\pm}^*}{k}),\ \gamma_5^{'} = u_{\pm}^*,\ \gamma_6^{'} = n_{\pm}^*,\ \gamma_7^{'} = j_{11}^{'} d_n + \varepsilon\gamma_4^{'} d_u - j_{11}^{'}\varepsilon\gamma_4^{'},$$

$$\hat{\varepsilon}^* = \tilde{\varepsilon}^{'} - \frac{(d_u + d_n)m^{2^{'}}}{\delta_6},\ \hat{e}_1^* = \frac{(j_{11}^{'} d_n + \hat{\varepsilon}^*\gamma_4^{'} d_u)m_*^2 - d_u d_n m_*^4 - j_{11}^{'}\hat{\varepsilon}^*\gamma_4^{'}}{\hat{\varepsilon}^*(d_u\gamma_5^{'} m_*^2 - j_{11}\gamma_5^{'} + j_{12}^{'}\gamma_6^{'})}.$$

From Tables 4 and 5, it is evident that incorporating a nonlinear saturated functional response into the diffusion system results in significantly richer spatial dynamical behaviors compared to a system with a linear depletion term. Firstly, the nonlinear saturation introduces more steady states: the system with a nonlinear saturated functional response can exhibit up to nine steady states, whereas the system with a linear depletion term has at most seven. Secondly, the expressions for the positive steady states differ substantially between the two systems, which leads to distinct evolutionary outcomes in terms of strategies and resource levels. Moreover, the spatial stability conditions of the two systems are not identical. This implies that, under the same parameter settings, the systems may exhibit divergent spatial evolutionary processes and outcomes. Finally, the criteria for the onset of Turing-Hopf bifurcations also differ between the two systems, indicating that even under identical parameters, the spatial distributions of strategies and resources may vary considerably due to the form of the functional response. Moreover, while our analysis systematically contrasts the spatial dynamics arising from nonlinear and linear functional responses, it is also important to place this work in the broader research context. Specifically, we investigate the dynamical properties of diffusion systems with linear depletion terms, whereas Tilman et al. (2020) primarily focused on the dynamical properties of temporal systems rather than spatial distributions.

The Turing-Hopf bifurcation is revealed in Figs. 9-13 and the conditions for the presence of the Turing-Hopf bifurcation are provided by Theorem 4.4. Table 4 succinctly summarizes the conditions for Turing-Hopf bifurcation and steady-state spatial stability. The Hopf bifurcation occurs at $\tilde{\varepsilon}$ and $\varepsilon^*$ for the temporal system (2.5) and the diffusion system (2.6), respectively, which reveals that diffusion causes the Hopf bifurcation to occur earlier, as detailed in Fig. 6(a) and Fig. 13.

The Turing and Hopf bifurcation curves delineated in Fig. 9 separate the plane into four regions. The steady state $E^*$ depicted in Fig. 10 is ultimately spatially stable, and the parameters adopted in the figure correspond to the region I of Fig. 9, which illustrates the fact that the relative timescale does not alter the final evolutionary outcome if the relative timescale is larger than its threshold. If the values of the parameters originate from region II of Fig. 9, then the diffusion system manifests itself like a spatially homogeneous periodic solution appearing as detailed in Fig. 11. The values of the parameters falling in region II of Fig. 9 are consistent with the elaboration of Theorem 4.4. The diffusion system undergoes a Turing-Hopf bifurcation near the steady state $E^*$, and the heterogeneous periodic solutions arise, as illustrated in Fig. 12.

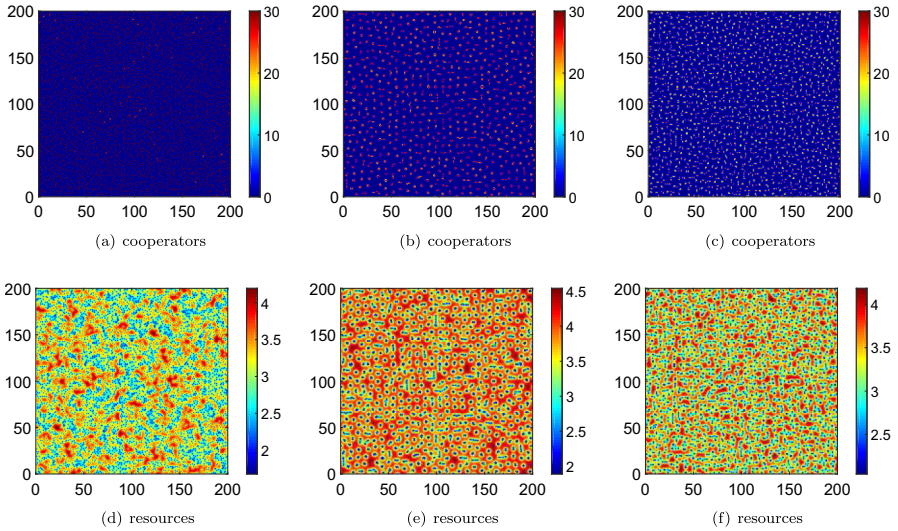


**Fig. 14** Spatial distribution of cooperators and resources with $d_u = 0.01$ (column I), $d_u = 0.5$ (column II), and $d_u = 1$ (column III). The initial heterogeneous distributions are $u(x, y, 0) = u^\star + 0.01\cos\frac{2\pi x}{200}\cos\frac{2\pi y}{200}$ and $n(x, y, 0) = n^\star + 0.01\cos\frac{2\pi x}{200}\cos\frac{2\pi y}{200}$, where $(u^\star, n^\star)$ is the homogeneous steady state. The diffusion coefficient $d_n = 10$ and other parameters are adopted from Fig. 4

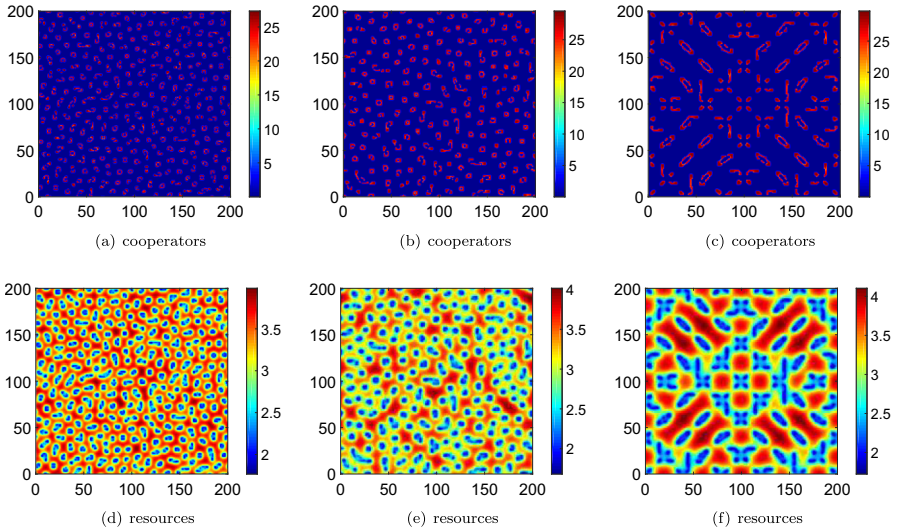


**Fig. 15** Spatial distribution of cooperators and resources with $d_n = 30$ (column I), $d_n = 60$ (column II), and $d_n = 100$ (column III). The diffusion coefficient $d_u = 0.1$ and other parameters and initial values are identical to those in Fig. 14

## 5 Pattern formation

This section further investigates the fascinating spatial distributions of cooperator densities and resource stocks induced by diffusion, relative timescales, and other parameters. Figs. 14-18, Fig. 20, and Fig. 23 present various stationary patterns and interesting chaotic patterns. To compare the evolutionary results concerning cooperators and resources for well-mixed and heterogeneous situations, the parameters of Figs. 14-25 are taken from Fig. 4.

### 5.1 Pattern formation induced by spatial diffusion

Spatial diffusion induces Turing instability, facilitating the transition from spatially homogeneous to heterogeneous stationary distributions of cooperators and resources. Figs. 14 and 15 examine the influence of the diffusion coefficients $d_u$ and $d_n$ on the spatial distribution of cooperator density and resource stock. When the conditions of Theorem 4.2 are met, varying diffusion coefficients generate intricate Turing patterns. At lower diffusion rates, cooperators primarily form isolated spots, with a few connected by thin stripes. Resources tend to accumulate around cooperators, but resource availability is limited in areas directly occupied by cooperators due to their consumption. As the diffusion coefficient of cooperators increases, they cluster into more structured formations, such as polygons and bars. These regions are surrounded by more abundant resources, indicating improved access to resources with greater cooperator mobility. However, when the diffusion rate becomes too high, the polygons dissolve, and cooperators become more diffusely distributed. As shown in Fig. 19(a), the overall level of cooperation initially declines and then increases with rising cooperator diffusion rates. This suggests that indiscriminately increasing the diffusion rate does not necessarily promote cooperation. An optimal diffusion rate enhances cooperator clustering and resource use, while slower diffusion encourages the adoption of cooperative strategies.

Fig. 15 shows the diverse spatial distribution of cooperators and resources due to different diffusion rates of resources. Cooperators exhibit a mixed pattern of speckled, semi-annular, and annular formations when the resource spreads slowly. Large spots, half-rings, and rings comprise the mixed pattern. As resource mobility increases, the spatial alignment between cooperators and resources becomes more intricate. Cooperators tend to cluster more tightly in order to remain within effective proximity to mobile resources. Further increasing the diffusion coefficient of the resource, cooperators agglomerate to form a mixed pattern of solid irregular spots, strips, and unclosed loops. Interestingly, the patterns of cooperators and resources are complementary, meaning that the cooperators are located in places where resources are scarce due to the capture of resources by the cooperators, and resources surround the cooperators. Notably, as shown in Fig. 19(b), increasing the resource diffusion rate initially promotes higher cooperator density, but excessive diffusion ultimately inhibits cooperation. The diffusion rate of cooperators and resources not only affects the patterns of spots and stripes but also influences the players' choice of strategies and the availability of resources, thus impacting the sustainability of the population.

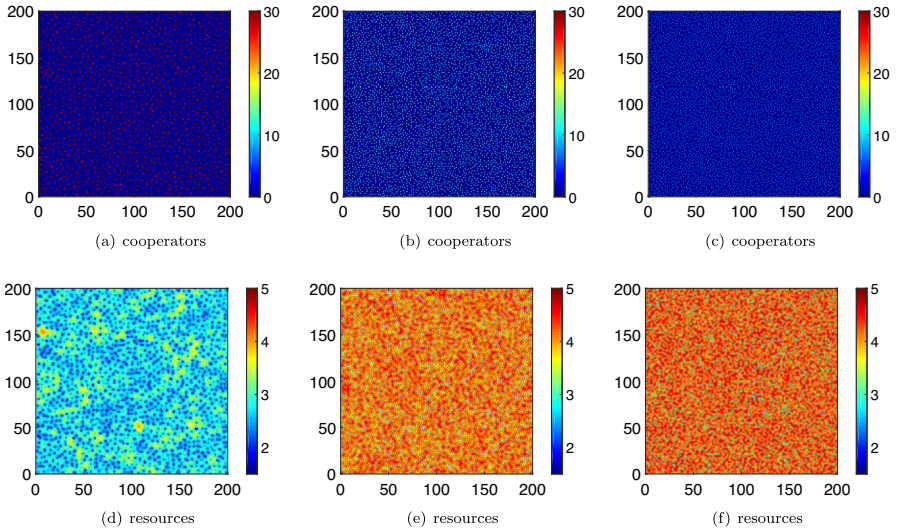


**Fig. 16** Spatial distribution of cooperators and resources with $\varepsilon = 0.95$ (column I), $\varepsilon = 10$ (column II), and $\varepsilon = 15$ (column III). The values of $d_u$ and $d_n$ are 0.1 and 10, respectively. The initial values and other parameters are selected from Fig. 14

### 5.2 Pattern formation induced by relative timescale

In Fig. 16, we investigate the influence of relative timescales on the spatial distributions of cooperators and resource densities. When resources evolve more slowly than cooperators ($\varepsilon < 1$), cooperators form dense stripes and patches. As the cooperator evolution rate slows relative to resources ($\varepsilon > 1$), the cooperator population becomes more diffuse, with most cooperators standing alone or forming small clusters of short stripes. In this scenario, resource preservation improves, and cooperators exhibit a relatively loose distribution, as shown in the third column of Fig. 16. In the temporal model, changes in the relative timescale do not affect the ultimate outcome of cooperator density and resource stock once the critical threshold is reached. However, in the diffusion model, variations in relative timescales give rise to diverse spatial patterns of cooperator and resource densities. Rapid resource turnover facilitates better resource preservation, and a higher relative timescale leads to a more dispersed distribution of cooperators. This increased spatial separation weakens cooperative clustering and reduces access to shared resources, ultimately leading to lower cooperator densities, in alignment with the findings in Fig. 19(c).

### 5.3 Pattern formation induced by player density

The effect of changes in total player density on cooperator density and resource stock is illustrated in Fig. 17. In the first column, a portion of the cooperators form clusters in the shape of rectangles and rounded rectangles, while another portion appears as thick spots and thick stripes. As total player density increases, the spatial pattern transitions

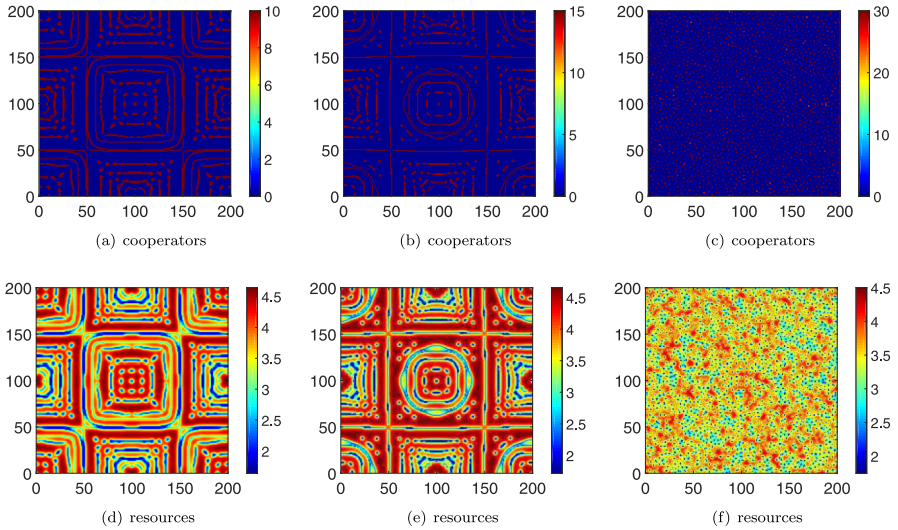


**Fig. 17** Spatial distribution of cooperators and resources with $N = 10$ (column I), $N = 15$ (column II), and $N = 30$ (column III). Note that the parameters and initial states for this figure and Fig. 18 are taken from Fig. 16

from thick stripes and spots to thinner stripes and finer spots. Interestingly, while the overall spatial arrangement of cooperators and resources remains similar, their density magnitudes are inverted. At higher total player densities, the stripes dissipate, and cooperators are dispersed more evenly across space, appearing primarily as isolated spots. This pattern shift from broad stripes to fine speckles reflects the tendency of higher total player density to induce a more spatially diffuse distribution of cooperators. Fig. 19(d) shows that increasing total player density generally supports cooperation. At low total player densities, cooperators tend to form spatial clusters, which facilitates effective resource use. In contrast, under high player density, such spatial clustering becomes less pronounced as cooperators are more uniformly distributed.

### 5.4 Pattern formation induced by growth rate of resources

In Fig. 18, we explore how varying the growth rate of resources impacts the evolution and distribution of cooperators within an ecosystem. At first, when the resource growth rate is low, cooperators are loosely scattered, forming small, isolated patches. Their limited aggregation results in weaker exploitation pressure on local resources. This mild level of interaction allows resources to regenerate steadily, maintaining a relatively stable supply. However, as the growth rate of resources increases, a counterintuitive pattern emerges. One might expect faster regeneration to result in a greater resource stock, yet the overall resource abundance declines. This decline can be attributed to the adaptive spatial response of cooperators to the elevated resource availability. As shown in Fig. 19(e), a higher resource growth rate supports a larger cooperator population, which in turn intensifies spatial exploitation.

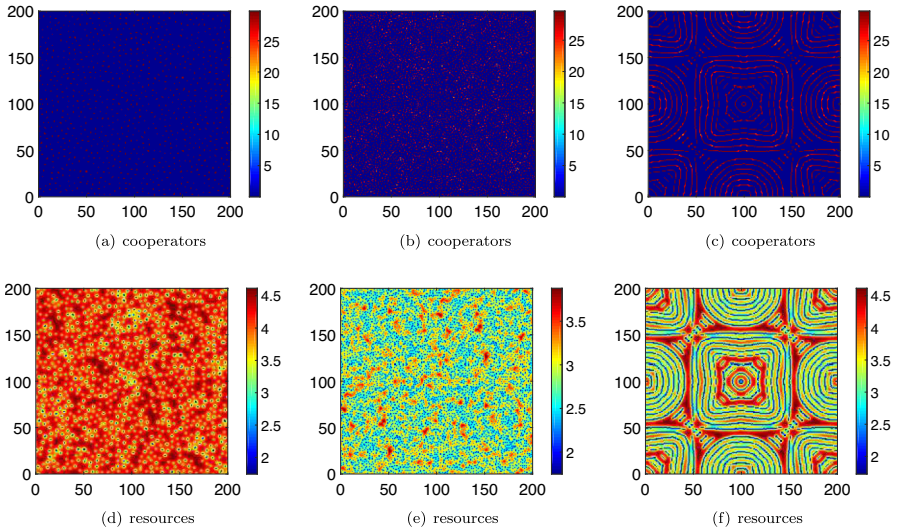


**Fig. 18** Spatial distribution of cooperators and resources with $r = 0.4$ (column I), $r = 0.6$ (column II), and $r = 0.8$ (column III)

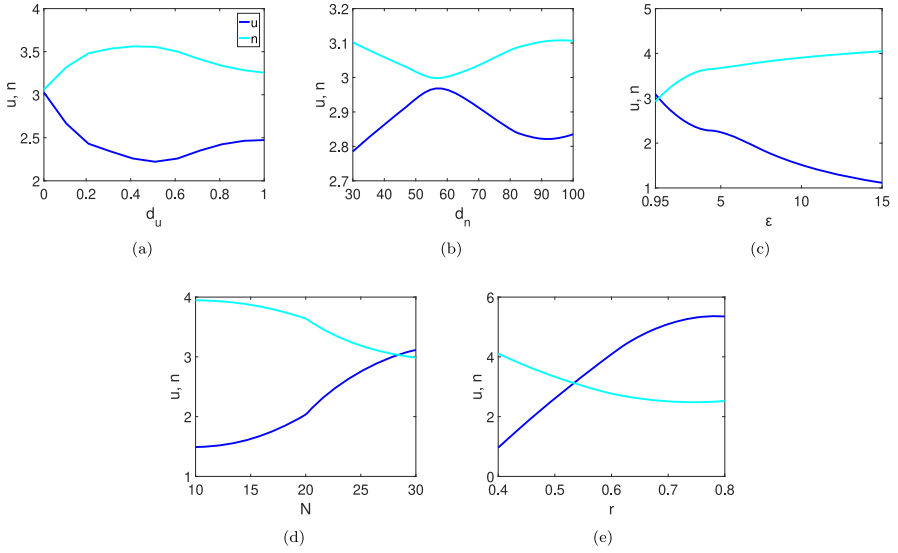


**Fig. 19** Dependence of the aggregate level of cooperation and the resource stock on the parameters $d_u$, $d_n$, $\varepsilon$, $N$, and $r$. The blue and cyan curves indicate the spatially averaged densities of cooperators and resources, respectively

Cooperators begin to concentrate in regions with abundant resources, leading to more aggressive local harvesting and accelerated depletion. As the growth rate continues to rise, the spatial distribution of cooperators further evolves. They organize into more regular and compact structures–rectangular patches, circular clusters, and stripe-

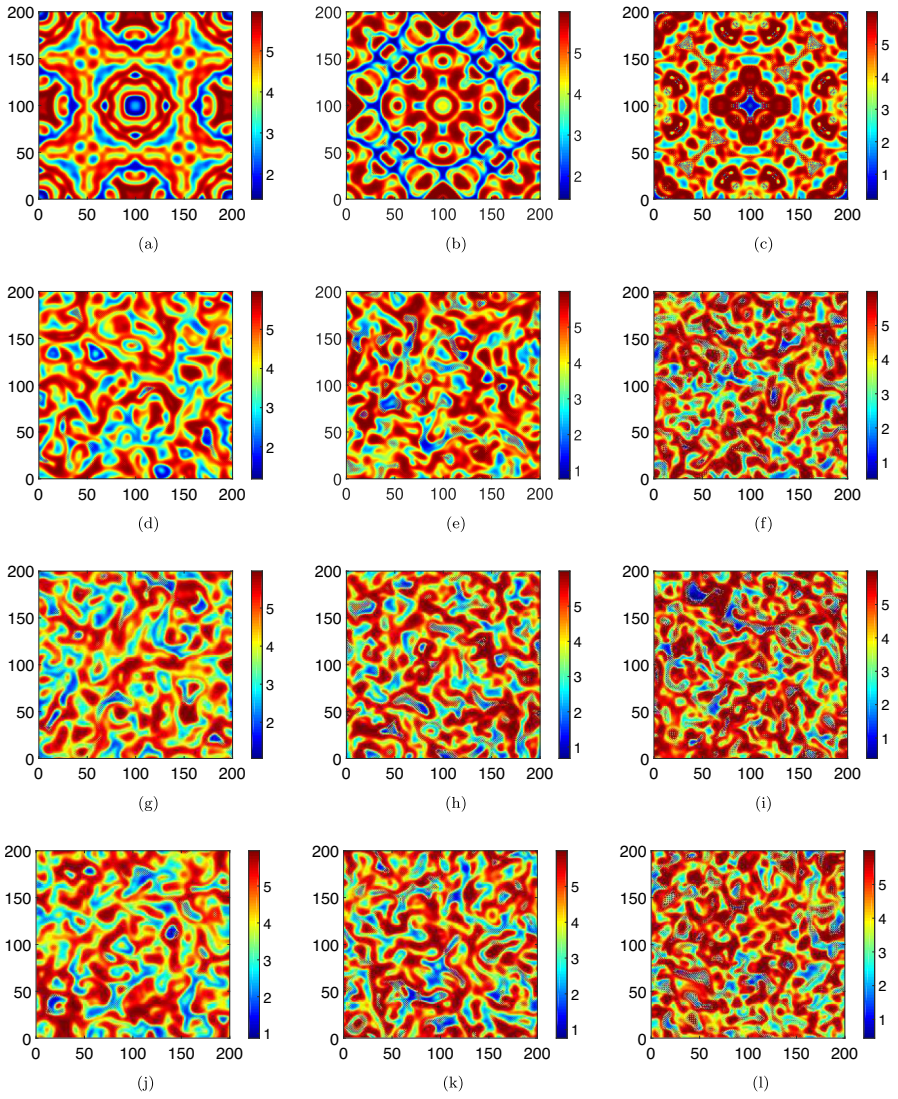


**Fig. 20** Pattern evolution of cooperators and resources with $a_1 = 10$ (column I), $a_1 = 12$ (column II), and $a_1 = 15$ (column III). The first row, the second row, the third row, and the fourth row show the spatial distribution at times $t = 100$, $t = 1000$, $t = 5000$, and $t = 10000$, respectively

like arrangements–which reflect their adaptive redistribution in response to changing environmental conditions. Interestingly, despite the intensification of exploitation, the resources remain at a certain stock level, as the rate of regeneration eventually offsets some of the increase in consumption. This balance ensures the coexistence of cooperators and renewable resources. Ultimately, increasing the resource growth rate facilitates a more spatially organized and persistent presence of cooperators, contribut-

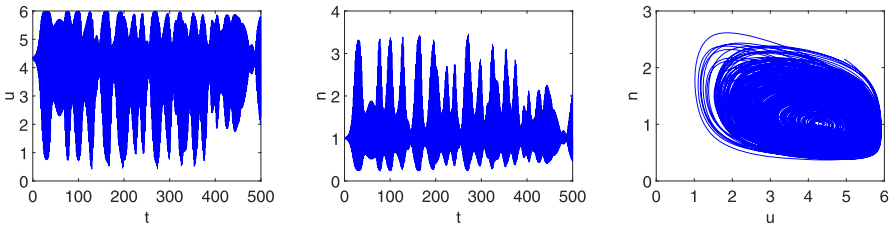


(a) cooperators (b) resources (c) phase portrait in $u$-$n$ plane

**Fig. 21** Chaotic behavior appears with $a_1 = 10$ at location (100,100)

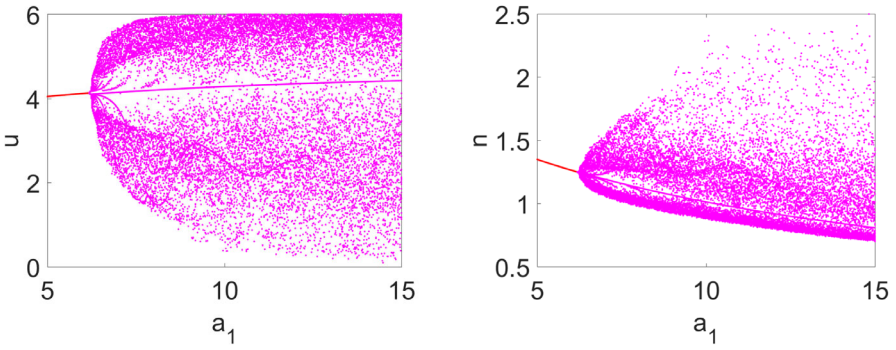


(a) cooperators (b) resources

**Fig. 22** Chaos induced by $a_1$ at location (100,100). The red curve means that the system (2.6) is spatially stable. The magenta part suggests that chaos appears for the system (2.6)

ing to system-level stability through dynamic feedback between resource availability and cooperator adaptation.

## 6 Chaos induced by payoffs

The influence of the payoffs $a_1$ and $c_0$ on the temporal and spatial evolution of cooperators is depicted in Figs. 20 and 23. Cooperators exhibit irregular, disorderly spatial distributions over time, highlighting the chaotic spatiotemporal dynamics induced by changes in $a_1$ and $c_0$. Interestingly, in the early stages of evolution, cooperators form spatially centrosymmetric and axisymmetric patterns. However, as the system evolves, these patterns break down into irregular configurations, particularly in the middle and later stages of evolution. While changes in payoff parameters do not prevent the emergence of chaotic behavior, they influence the specific form of spatial distribution among cooperators in these later stages. A comparison of different spatial distributions of cooperators at the same evolutionary stage, under varying payoff conditions, shows that increasing payoffs during cooperator encounters in resource-rich environments leads to higher cooperator densities. When cooperators encounter each other with small payoffs in abundant resources, the system settles into a stationary pattern, with cooperative behavior stabilizing in space after prolonged evolution. However,

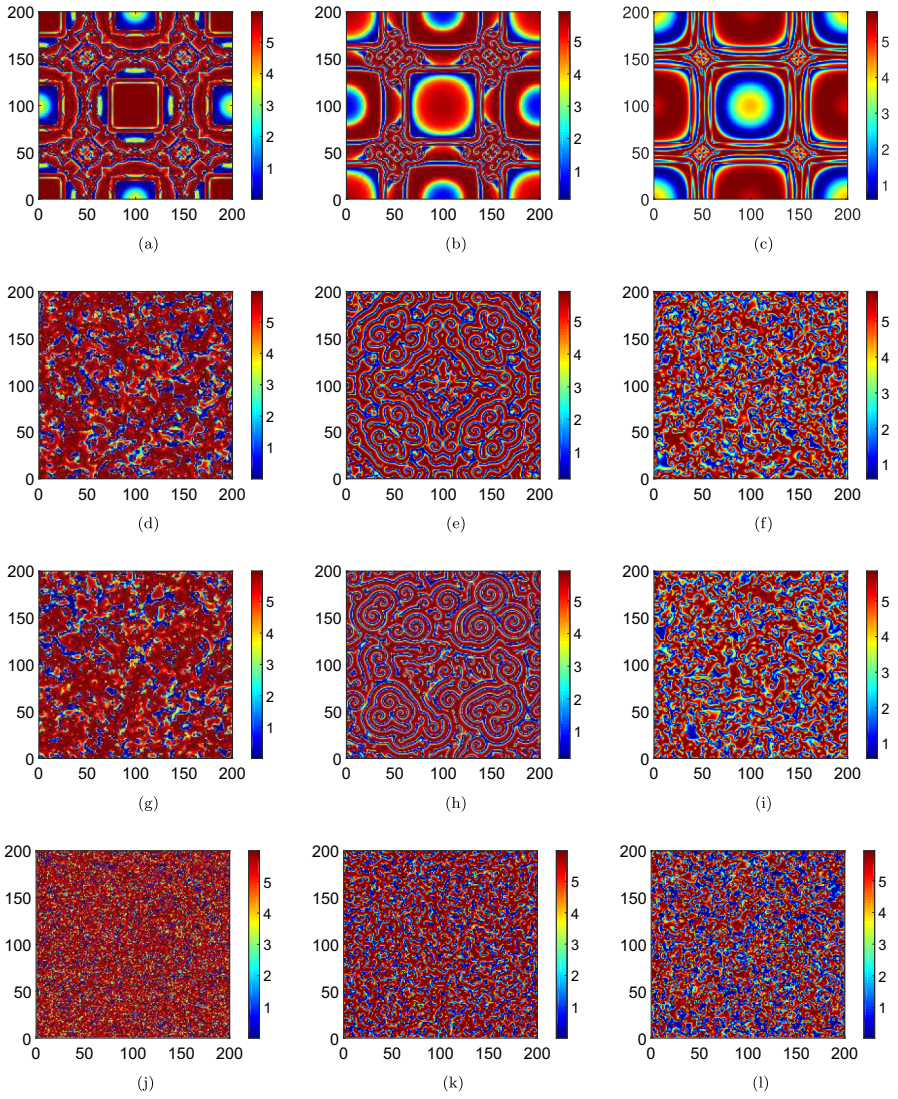


**Fig. 23** Pattern evolution of cooperators and resources with with $c_0 = 4.3$ (column I), $c_0 = 4.8$ (column II), and $c_0 = 5.5$ (column III). The first row, the second row, the third row, and the fourth row show the spatial distribution at times $t = 100$, $t = 1000$, $t = 5000$, and $t = 10000$, respectively

increasing the payoffs between cooperators triggers a transition from stationary to chaotic patterns. This variation in payoffs introduces uncertainty into the evolutionary trajectory of cooperation. Regardless of whether the system involves diffusion or not, raising cooperator payoffs consistently supports the continuation and growth of cooperative behavior. In contrast to the temporal system, the diffusion system exhibits a wider range of spatial patterns, including both chaotic and static distributions. A comparison between the temporal and spatial systems reveals that the diffusion of

cooperators and resources contributes to the emergence of both chaotic and stationary patterns in the spatial distribution of cooperative behavior.

Fig. 21 illustrates the chaotic dynamics of cooperators and resources through time series and phase trajectories. Cooperator densities and resource stocks exhibit disordered oscillations over time, signaling the onset of chaotic behavior. Notably, the cooperator density never reaches zero, indicating the persistent coexistence of cooperators and defectors. Similarly, resource levels remain above zero throughout the evolutionary process, ensuring that resources are consistently available to sustain the population. The phase trajectories of cooperator densities and resource stocks do not converge to an equilibrium or a limit cycle but instead evolve erratically, further confirming the presence of chaos. As cooperator payoffs fluctuate, the system transitions from a homogeneous distribution to chaotic dynamics, as demonstrated in Fig. 22. In the diffusion system, spatial stability is observed when the value of $a_1$ lies within the interval indicated by the red curve. In contrast to the temporal system, once $a_1$ surpasses its threshold, complex chaotic patterns emerge, corresponding to the magenta region. In Fig. 26(a), the maximum Lyapunov exponent shifts from negative to positive as $a_1$ increases, marking the transition of the system (2.6) from spatial stability to chaos. Negative maximum Lyapunov exponents imply spatial stability when the brown line is below the blue line. Once the maximum Lyapunov exponent exceeds the threshold at $a_1 = 6.18$, chaos ensues. The parameter values used in Figs. 20 and 21 correspond to the magenta region of Fig. 22, where cooperators and defectors coexist with a continuous supply of resources.

Fig. 23 reveals intriguing results regarding the spatio-temporal evolution of strategies in response to changing payoffs during defector-cooperator interactions. Players form spatial distributions centered around rectangles and circles, with cooperators displaying regular, axisymmetric, and centrosymmetric patterns in the early stages of evolution. When the payoffs from defector-cooperator encounters are moderate, cooperators tend to cluster at the core and four corners of the system. However, if defector payoffs increase, cooperators abandon these regions and migrate to the center of the four edges. As evolution progresses, the symmetrical distribution breaks down, and cooperators adopt increasingly complex and irregular spatial arrangements. This gradual shift from rectangular and circular aggregations to pinstripes and spots reflects a more dispersed spatial distribution of cooperators as evolution progresses. Elevated defector payoffs entice players to adopt defection strategies, undermining cooperation by reducing cooperator density. In the temporal system, altering defector payoffs leads to a definitive evolutionary outcome for cooperator density. However, in the spatial system, the diffusion of players and resources induces highly unpredictable and irregular spatial distributions of cooperator density as evolution proceeds.

The erratic evolution and oscillatory behavior of cooperators and resources over time, as shown in Fig. 24, reveal the emergence of chaotic dynamics within the diffusion system. The irregular and unpredictable movements of the phase trajectories of both cooperators and resources, which neither stabilize at equilibrium nor settle into periodic orbits as evolution progresses, are strong indicators of chaotic behavior. Further supporting this, the positive maximum Lyapunov exponent, shown in Fig. 26(b), confirms the chaotic nature of the system. Specifically, the system described by equation (2.6) remains stable when the purple curve lies above the blue line. However,

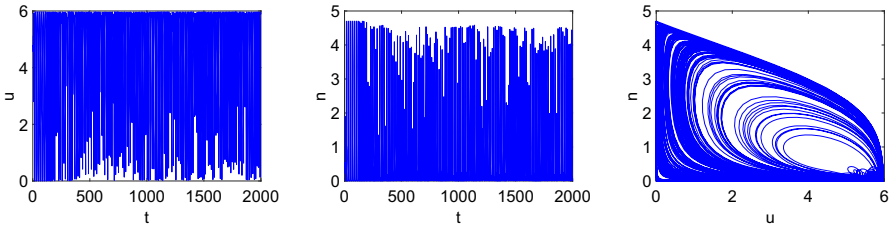


(a) cooperators (b) resources (c) phase portrait in $u$-$n$ plane

**Fig. 24** Chaotic behavior appears with $c_0 = 4.1$ at location (100,100)

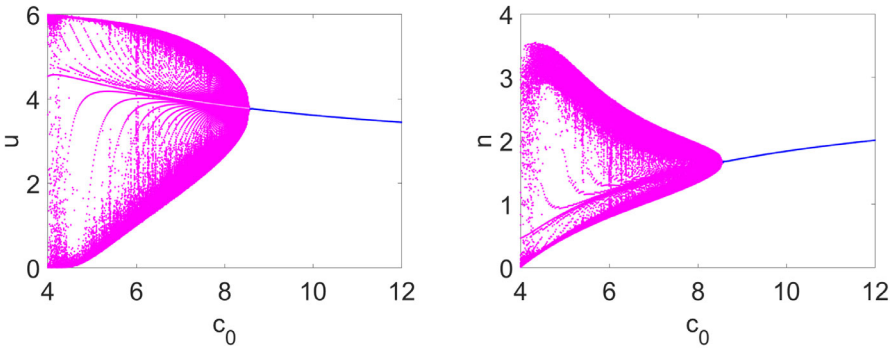


(a) cooperators (b) resources

**Fig. 25** Chaos induced by $c_0$ at location (100,100). The blue curve means that the system (2.6) is spatially stable. The magenta part suggests that chaos appears for the system (2.6)

as the parameter $c_0$ exceeds its critical threshold value of $c_0 = 8.58$, the system transitions into chaos. This shift is marked by the emergence of positive maximal Lyapunov exponents, signaling the onset of chaotic dynamics. In this chaotic regime, defectors have the potential to dominate the system, occupying nearly the entire spatial domain, while cooperators struggle to gain an evolutionary advantage. The magenta regions in Fig. 25 correspond to these chaotic phases within the diffusion system, during which defectors can potentially outcompete cooperators and take control of the population. However, as the payoffs for defectors exceed their thresholds during interactions with cooperators, the chaotic behavior subsides, leading to a more predictable and stable dynamic. The blue line in Fig. 26(b) indicates a spatially stable system where defectors and cooperators can coexist in a stable arrangement. In this context, small payoffs for defectors allow them to exploit all available resources, granting them dominance within the diffusion system. By contrast, in the temporal system, these small payoffs are insufficient for defectors to capture all resources, as they do in the spatial model. While increasing the payoffs for defectors discourages cooperative behavior among players, it simultaneously prevents defectors from monopolizing all the resources, leading to a more balanced distribution of strategies.

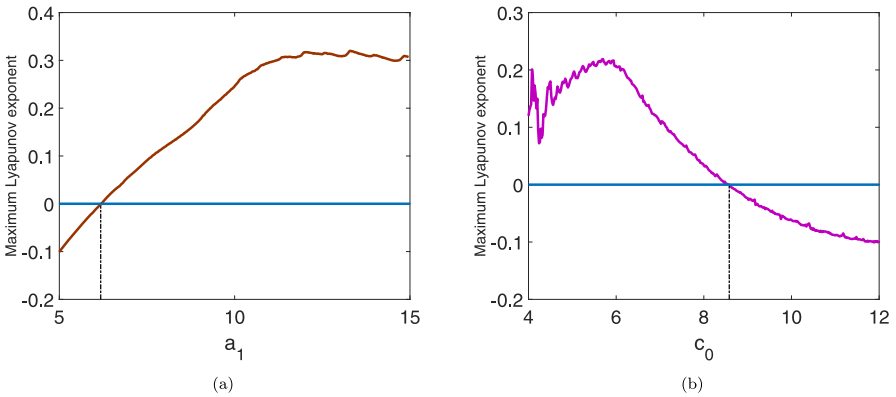


**Fig. 26** Maximum Lyapunov exponents with respect to $a_1$ and $c_0$. The blue line represents a value of zero, and its intersections with the brown and purple lines mark the thresholds of $a_1 = 6.18$ and $c_0 = 8.58$, respectively, as indicated by the black vertical dashed lines. The system (2.6) enters a chaotic state when the maximum Lyapunov exponents corresponding to $a_1$ and $c_0$ respectively are positive within a certain range

## 7 Discussion

In this paper, we investigate two types of models that integrate replicator dynamics with resource feedback mechanisms. The first model considers a well-mixed environment, where interactions between cooperators and defectors occur uniformly. In contrast, the second model incorporates spatial diffusion, acknowledging the non-uniform spatial distribution of cooperators and defectors. The fitness of both cooperators and defectors in these systems is influenced by several factors, including the stock of resources, baseline payoffs, and payoff matrices that differentiate between resource-poor and resource-rich conditions. In both the temporal and diffusion systems, we examine key parameters such as relative timescales, payoff structures, total player density, resource growth rates, and baseline payoffs. The dynamics of the temporal system are outlined in Figs. 1-8, while the spatial diffusion system's evolutionary outcomes are detailed in Figs. 9-26.

Our findings highlight that each of these parameters significantly impacts the strategic evolution of cooperators and defectors. Notably, in contrast to previous multiscale analyses (Bertram and Rubin 2017; Heggerud et al. 2020), we observe that relative timescales play a crucial role in triggering Hopf bifurcations, with bifurcations in the spatial diffusion system occurring at an earlier stage compared to the temporal system. In contrast to models where cooperation promotes sustainable resource use, our framework captures scenarios in which cooperation may intensify the extraction of environmental resources, potentially degrading the environment. This phenomenon is not merely theoretical: in certain real-world systems, increased cooperation correlates with overuse of shared resources. For example, coordinated irrigation efforts among farmers can lead to excessive groundwater depletion (Giordano and Villholth 2007). In biological contexts, cooperative hunting among species like chimpanzees (Gilby et al. 2015) or group-attacking fish (Herbert-Read et al. 2016) may heighten pres-

sure on prey populations. Similarly, mutualistic interactions, such as ants protecting aphids (Stadler and Dixon 2005) for honeydew, can indirectly harm plant health due to overextraction of sap by aphids. These examples underscore that the environmental consequences of cooperation depend critically on the ecological and strategic context, and our model offers a complementary perspective to frameworks where cooperators are assumed to act more sustainably.

A particularly interesting discovery is that in the temporal system, cooperators and resources exhibit stable periodic oscillations when payoffs exceed certain threshold values. However, in the spatial diffusion system, these payoffs lead to chaotic dynamics rather than periodic solutions. This results in irregular spatial patterns and temporal evolutions of cooperators and resources. Additionally, we investigate the effects of both individual parameters and parameter interactions on the evolution of strategies. For each system, we explore a range of dynamical behaviors, including the existence of equilibria, local stability, bi-stability, multi-stability, and various types of bifurcations–such as transcritical and Hopf bifurcations in the temporal system, and spatial stability, Turing instability, Hopf bifurcation, and Turing-Hopf bifurcation in the spatial diffusion system.

Compared to the linear resource consumption assumed in previous work (Tilman et al. 2020), our model incorporates a saturated functional response, resulting in significantly richer dynamical behaviors in both non-spatial and spatiotemporal contexts. First, while Tilman et al. (2020) identified at most two boundary equilibria and two internal equilibria, our model supports up to six boundary equilibria and three internal equilibria. This expansion reflects a wider range of potential evolutionary outcomes for both strategies and environmental resources. Second, beyond the bistability observed by Tilman et al. (2020), we uncover not only bistability but also tri-stability, and we derive analytical conditions for the existence of three bistable and two tri-stable configurations. These findings suggest that, depending on the initial conditions, our system can exhibit a broader array of evolutionary pathways for strategies and resource levels, as illustrated by two distinct tri-stable scenarios. Third, we rigorously identify the conditions under which transcritical and Hopf bifurcations occur, and further determine the direction and stability of the resulting periodic solutions. Our results demonstrate that variations in payoff parameters, intrinsic growth rates, and baseline payoffs can produce qualitatively different evolutionary dynamics. Fourth, whereas previous studies focused on ordinary differential equation (ODE) frameworks, we extend the analysis to include spatial diffusion. This allows us to explore complex spatial phenomena, such as spatial stability, Hopf bifurcations, Turing-Hopf bifurcations, and pattern formation. Fifth, our model also captures payoff-induced chaotic dynamics, adding another layer of complexity to the system's behavior. To support these findings, we present a comprehensive mathematical analysis and develop a unified theoretical framework that integrates both ODE and partial differential equation (PDE) perspectives. Overall, our study offers a holistic approach to understanding the interplay between strategic behavior and resource dynamics in mixed and spatially structured environments, contributing substantially to the broader field of eco-evolutionary game theory.

The existence and stability of equilibria offer critical insights into potential evolutionary outcomes, especially regarding the sustainability of resources and the persistence of cooperative strategies. While much of the previous research has con-

centrated on identifying factors conducive to the development of cooperation, this study adds depth by highlighting some lesser-known influences that foster cooperation. Specifically, we find that increasing the initial density of cooperators, enhancing the growth rate of resources, and lowering the initial stock of resources all positively contribute to promoting cooperative behavior. In systems with spatial heterogeneity, small payoffs for defectors can induce chaotic dynamics, creating opportunities for cooperators to dominate the system. For multi-parameter systems, focusing solely on individual parameters limits the understanding of cooperation. Instead, considering the interaction of multiple parameters is essential for accurately predicting evolutionary processes and outcomes. For instance, the effect of total player density on cooperation is complex, showing no consistent positive or negative trend. A critical factor in this interaction is the parameter $\theta$. When $\theta$ is small, increasing player density can incentivize cooperation. However, when $\theta$ is large, even substantial adjustments to player density will not prevent the extinction of cooperators.

Several counterintuitive phenomena emerge when examining the interactions between the payoff matrices for resource-rich and resource-poor conditions. Generally, one would expect that increasing the payoffs for cooperators would enhance their competitive edge. However, our findings show that in some scenarios, raising the payoffs–whether from encounters between cooperators or between cooperators and defectors–can actually hinder cooperative survival. Similarly, while increasing defector payoffs typically encourages defection, in resource-poor environments, this can have the opposite effect, allowing cooperators to survive and thrive. In the diffusion system, when cooperators encounter each other in resource-abundant areas, increasing their payoffs can shift the dynamic from one where cooperators hold an advantage to one characterized by chaotic coexistence between cooperators and defectors. Furthermore, in systems exhibiting bi- or multi-stability, the initial condition–such as the initial density of cooperators and the initial stock of resources–play a crucial role in determining evolutionary outcomes. Diverse scenarios can unfold from different initial conditions, ranging from the stable coexistence of cooperators and defectors to the dominance or extinction of cooperators. Therefore, accurately predicting evolutionary outcomes requires careful consideration not only of the parameter values but also of the initial states of cooperators and resources. These initial conditions, alongside the interaction of key factors, are pivotal in shaping the long-term dynamics of the system.

This study builds upon the seminal work of Cheng et al. (2024) by advancing the theoretical understanding of cooperation in systems characterized by mutual feedback between strategic behaviors and environmental resources across both temporal and spatial dimensions. Both models address the dynamical properties of temporal systems–such as stability and bifurcation–as well as those of spatial systems, including spatial stability, Turing-Hopf bifurcations, pattern formation, and chaotic dynamics. Several fundamental distinctions, however, set our model apart from theirs. First, the two models are intrinsically different in terms of resource dynamics. Cheng et al. (2024) considered a decaying resource produced by cooperators and consumed linearly by all individuals in the population. In contrast, our model incorporates a renewable resource that grows logistically and is consumed directly by cooperators. Second, the feedback mechanisms differ markedly. While the earlier model adopts a linear resource consumption framework, our model incorporates a Holling Type II functional response

to more accurately capture the nonlinear and saturating nature of resource exploitation–offering a more biologically grounded depiction of eco-evolutionary feedback. Third, the equilibrium structures diverge significantly. The model proposed by Cheng et al. (2024) supports at most two boundary equilibria and two interior equilibria, with only bistability observed. In contrast, our model allows for up to six boundary equilibria and three interior equilibria, giving rise to three distinct types of bistability and two forms of tristability. This structural complexity leads to a broader array of possible evolutionary outcomes for both strategies and environmental resources. Fourth, bifurcation behavior also shows notable differences. Our model exhibits a richer spectrum of bifurcation types, including more extensive transcritical bifurcations. Particularly important is the bifurcation behavior triggered by cooperator–defector interactions. In our framework, the payoff to cooperators when interacting with defectors can induce Hopf bifurcations and give rise to oscillatory dynamics. By contrast, the previous model under similar conditions only generated transcritical bifurcations. Furthermore, in our model, payoffs obtained by defectors interacting with each other–previously insufficient to elicit Hopf bifurcations–are now capable of generating periodic solutions, further underscoring the model's dynamic richness. Fifth, from a biological standpoint, the evolutionary outcomes differ profoundly between the two models due to both the number and the mathematical expressions of equilibrium points. The presence of tristability in our model enables a wider range of potential outcomes under identical conditions. Additionally, the differences in bifurcation conditions and diversity of bifurcation types imply that the same parameter variations may lead to qualitatively different evolutionary trajectories of cooperation.

Diffusion effects reveal nuanced influences on cooperation and spatial organization that fundamentally diverge from the model proposed by Cheng et al. (2024). In their framework, increasing the diffusion rate of cooperators typically undermines cooperation, as their wider dispersion weakens local interactions and disrupts spatial clustering. Conversely, higher diffusion rates of resources tend to promote cooperation but simultaneously reduce spatial aggregation. In contrast, our model uncovers more intricate dynamics. Specifically, increasing the diffusion rate of cooperators initially suppresses cooperation but ultimately facilitates it, while spatial clustering of cooperators shows the opposite trend–first increasing and then decreasing. For resource diffusion, we observe the reverse pattern: cooperation is initially enhanced but later inhibited as diffusion increases, whereas spatial clustering of cooperators steadily improves. These findings underscore a critical departure from previous conclusions: simply increasing the diffusivity of resources or reducing the mobility of cooperators does not lead to a monotonic enhancement of cooperation. Instead, cooperation is maximized only under appropriate tuning of diffusion parameters, highlighting the complex interplay between spatial processes and nonlinear feedbacks in resource consumption embedded in our model. For both spatial diffusion models, the number of steady states in our framework is larger, and the spatial stability conditions for these equilibria differ substantially from those in Cheng et al. (2024), reflecting profound differences in spatial evolutionary outcomes. Furthermore, in the case of payoff-induced chaos, the spatial distribution at the early stage of evolution can still exhibit symmetry; however, in our model, this symmetric pattern disappears markedly earlier than in the model of Cheng et al. (2024), indicating a faster breakdown of spatial order. A

key innovation of our framework is the explicit incorporation of the intrinsic growth rate of resources. This not only ensures sustainable resource levels but also significantly enhances the stability of cooperation–an ecological mechanism absent in prior models. Finally, although both models exhibit Turing–Hopf bifurcations and chaotic dynamics, our model identifies novel parameter-induced pathways to chaos (e.g., via parameter $c_0$) and uncovers previously unobserved chaotic regimes. Notably, we find that chaos arises when certain parameters are relatively small, which contrasts with earlier findings where large parameter values were typically associated with chaos. Most importantly, we provide theoretical confirmation of chaos through computation of the maximum Lyapunov exponent, addressing a critical gap left in earlier studies. In summary, by introducing nonlinear feedbacks, more complex equilibrium structures, and biologically grounded resource dynamics, our model significantly expands the theoretical landscape of prior work, offering a more comprehensive and ecologically realistic framework for understanding the evolution of cooperation under resource feedbacks.

This paper presents theorems for temporal and diffusion systems that state the conditions for the existence of equilibria, bi-stability, multi-stability, Hopf bifurcation, transcritical bifurcation, and Turing-Hopf bifurcation, to facilitate the understanding of and analysis of these two types of systems. We develop a mathematical framework and employ various mathematical methods to explore the complex spatio-temporal dynamics of evolutionary game systems with resource feedback under well-mixed and unevenly distributed environmental conditions. This theoretical framework aids in accurately predicting the evolution of cooperation and resource reserves in biological systems and ecosystems in which resources are renewable and acquired by cooperators. As an initial exploration into partial differential evolutionary game systems driven by reaction-diffusion processes, our work opens avenues for future research. Key areas for further investigation include the impact of spatial memory (Wang and Salmaniw 2023), environmental noise (Feng et al. 2021), and time delays (Yuan and Meng 2022; Wang et al. 2024) on the evolution of cooperation in eco-evolutionary games. Additionally, incorporating multi-strategy games, variable population sizes, and multi-game (Cheng and Meng 2023) dynamics into spatio-temporal diffusion models is a critical direction for advancing this field.

## A Proof of Theorem 3.1

***Proof*** (I) The Jacobian matrix corresponding to $E_0(0, 0)$ is

$$J_0 = \begin{pmatrix} \theta(b_0 - d_0) & 0 \\ 0 & r\varepsilon \end{pmatrix}.$$

The eigenvalues are $r\varepsilon > 0$ and $\theta(b_0 - d_0)$. $E_0(0, 0)$ is a saddle point when $b_0 < d_0$. $E_0(0, 0)$ is an unstable node when $b_0 > d_0$.

(II) The Jacobian matrix of $E_1(N, 0)$ is given by

$$J_1 = \begin{pmatrix} \theta(c_0 - a_0) & 0 \\ 0 & \varepsilon(r - Ne_1) \end{pmatrix}.$$

The two eigenvalues are $\theta(c_0 - a_0)$ and $\varepsilon(r - Ne_1)$. When $c_0 < a_0$ and $r < Ne_1$, both eigenvalues are less than zero, then $E_1(N, 0)$ is a stable node. On the contrary, $E_1(N, 0)$ is an unstable node when $c_0 > a_0$ and $r > Ne_1$. Moreover, one of the two eigenvalues is greater than zero and the other is less than zero when $c_0 > a_0$ and $r < Ne_1$, or $c_0 < a_0$ and $r > Ne_1$. In such case, $E_1(N, 0)$ is a saddle point.
(III) The Jacobian matrix at $E_2(u_2, 0)$ is

$$J_2 = \begin{pmatrix} \frac{\theta(d_0-b_0)(a_0-c_0)}{a_0+d_0-b_0-c_0} & \frac{N(d_0-b_0)(a_0-c_0)}{(a_0-c_0-b_0+d_0)^3}((c_1-d_1)(a_0-c_0)+(a_1-c_1)(d_0-b_0)) \\ 0 & \varepsilon(r-\tilde{r}) \end{pmatrix},$$

where $u_2 = \frac{N(d_0-b_0)}{a_0+d_0-b_0-c_0}$. The eigenvalues of $J_2$ are $\frac{\theta(d_0-b_0)(a_0-c_0)}{a_0+d_0-b_0-c_0}$ and $\varepsilon(r-\tilde{r})$, whose signs depend on $a_0 - c_0$ and $r - \tilde{r}$, respectively, since $\frac{\theta(d_0-b_0)}{a_0+d_0-b_0-c_0} > 0$ and $\varepsilon > 0$. If $a_0 < c_0$ and $r < \tilde{r}$, then $E_2(u_2, 0)$ is a stable node. Conversely, $E_2(u_2, 0)$ is an unstable node if $a_0 > c_0$ and $r > \tilde{r}$. For the rest, $E_2(u_2, 0)$ is a saddle point.
(IV) The Jacobian matrix with respect to $E_3(0, k)$ is

$$J_3 = \begin{pmatrix} k(\tilde{d}_1 - d_1) & 0 \\ -\frac{e_1 k\varepsilon}{gk+1} & -r\varepsilon \end{pmatrix},$$

$k(\tilde{d}_1 - d_1)$ and $-r\varepsilon < 0$ are the eigenvalues of the above matrix. The sign of $\tilde{d}_1 - d_1$ determines the stability of $E_3(0, k)$. $E_3(0, k)$ is a stable node when $d_1 > \tilde{d}_1$. When $d_1 < \tilde{d}_1$, $E_3(0, k)$ is a saddle point.
(V) The Jacobian matrix corresponding to $E_4^+(N, n_4^+)$ is given by

$$J_4^+ = \begin{pmatrix} (\tilde{a}_1 - a_1)n_4^+ & 0 \\ -\frac{e_1\varepsilon n_4^+}{gn_4^+ + 1} & \frac{\varepsilon}{e_1}(\tilde{N} - N)(gn_4^+ + 1)^2 \end{pmatrix},$$

The eigenvalues $(\tilde{a}_1 - a_1)n_4^+$ and $\frac{\varepsilon}{e_1}(\tilde{N} - N)(gn_4^+ + 1)^2$ of $J_4^+$ are less than zero when $a_1 > \tilde{a}_1$ and $N > \tilde{N}$. Under this condition, $E_4^+(N, n_4^+)$ is a stable node. If $a_1 < \tilde{a}_1$ and $N < \tilde{N}$, then $E_4^+(N, n_4^+)$ is an unstable node. In other cases, $E_4^+(N, n_4^+)$ is a saddle point.
(VI) The Jacobian matrix of $E_4^-(N, n_4^-)$ is

$$J_4^- = \begin{pmatrix} (\hat{a}_1 - a_1)n_4^- & 0 \\ -\frac{e_1\varepsilon n_4^-}{gn_4^- + 1} & \frac{\varepsilon}{e_1}(\hat{N} - N)(gn_4^- + 1)^2 \end{pmatrix},$$

Similarly to the analysis of $E_4^+(N, n^+)$, we easily conclude that $E_4^-(N, n^-)$ is a stable node when $a_1 > \hat{a}_1$ and $N > \hat{N}$. If $a_1 < \hat{a}_1$ and $N < \hat{N}$, then $E_4^-(N, n^-)$ is an unstable node. In the remaining cases, $E_4^-(N, n^-)$ is a saddle point.
(VII) The Jacobian matrix with respect to the internal equilibrium $E^*(u^*, n^*)$ is given by

$$J^* = \begin{pmatrix} j_{11} & j_{12} \\ j_{21} & j_{22} \end{pmatrix},$$

where

$$\begin{aligned} j_{11} =& \frac{u^*(N-u^*)}{N^2}(\gamma_2\theta - \gamma_1 n^*),\ j_{12} = \frac{u^*(N-u^*)}{N^2}(N\gamma_3 - \gamma_1 u^*), \\ j_{21} =& -\frac{e_1 n^* \varepsilon}{gn^*+1},\ j_{22} = \varepsilon\left(r\left(1-\frac{2n^*}{k}\right) - \frac{e_1 u^*}{(gn^*+1)^2}\right). \end{aligned}$$

The characteristic equation is

$$\lambda^2 - \mathrm{Tr}(J^*)\lambda + \mathrm{Det}(J^*) = 0, \tag{A.1}$$

where $\mathrm{Tr(J^*)} = j_{11} + j_{22}$ and $\mathrm{Det}(J^*) = j_{11}j_{22} - j_{21}j_{12}$. Define Some calculations yield $\mathrm{Tr}(J^*) < 0$ ($\mathrm{Tr}(J^*) > 0$) if $\varepsilon\delta_6 > \delta_5$ ($\varepsilon\delta_6 < \delta_5$). If $\delta_7 > 0$ ($\delta_7 < 0$), then $\mathrm{Det}(J^*) > 0$ ($\mathrm{Det}(J^*) < 0$). The sign of $\mathrm{Tr}(J^*)$ and $\mathrm{Det}(J^*)$ determines the stability of $E^*(u^*, n^*)$. Therefore, if $\varepsilon\delta_6 > \delta_5$ and $\delta_7 > 0$, then $E^*(u^*, n^*)$ is a stable node or focus. $E^*(u^*, n^*)$ is a saddle point when $\delta_7 < 0$. $E^*(u^*, n^*)$ is an unstable node or focus if $\varepsilon\delta_6 < \delta_5$ and $\delta_7 > 0$. □

## B Proof of Theorem 3.3

Let $\tilde{u} = u - u^*$ and $\tilde{n} = n - n^*$. $u$ and $n$ are still utilized to denote $\tilde{u}$ and $\tilde{n}$, respectively, for convenience. Then, system (2.5) becomes

$$\begin{cases} \dfrac{\mathrm{d}u}{\mathrm{d}t} = \dfrac{(u+u^*)}{N^2}(N-u-u^*)\big[((d_1-d_0-a_0+a_1-b_1+b_0+c_0-c_1)(u+u^*) \\ \qquad +N(d_0-d_1-b_0+b_1))(n+n^*) - \theta((b_0+c_0-d_0-a_0)(u+u^*)+N(d_0-b_0))\big], \\ \dfrac{\mathrm{d}n}{\mathrm{d}t} = \varepsilon\left(r(n+n^*)\left(1-\dfrac{n+n^*}{k}\right) - \dfrac{e_1(n+n^*)}{1+g(n+n^*)}(u+u^*)\right). \end{cases} \tag{B.1}$$

For (B.1) employing the Taylor series at $E^*(u^*, n^*)$ yields

$$\begin{pmatrix} u_t \\ n_t \end{pmatrix} = J^* \begin{pmatrix} u \\ n \end{pmatrix} + \begin{pmatrix} h(u,n,\varepsilon) \\ z(u,n,\varepsilon) \end{pmatrix}, \tag{B.2}$$

where

$$h(u,n,\varepsilon) = h_1u^2 + h_2un + h_3u^3 + h_4u^2n + \cdots,$$

$$z(u,n,\varepsilon) = z_1 un + z_2 n^2 + z_3 un^2 + z_4 n^3 + \cdots,$$

with

$$\begin{aligned}
h_1 &= \frac{1}{N^2}\left[3(\gamma_1 n^* - \theta\gamma_2)u^* + (\theta(d_0 - b_0) - \gamma_3 n^* - \gamma_1 N + \theta\gamma_2)N\right],\\
h_2 &= \frac{1}{N^2}\left[3\gamma_1 u^{*2} - 2u^* N(\gamma_1 + \gamma_3) + N^2\gamma_3\right],\\
h_3 &= \frac{\gamma_1 n^* - \theta\gamma_2}{N^2},\ h_4 = \frac{3\gamma_1 u^* - N(\gamma_1 + \gamma_3)}{N^2},\\
z_1 &= -\frac{\varepsilon e_1}{(1+gn^*)^2},\ z_2 = \varepsilon\left[\frac{e_1 u^* g}{(1+gn^*)^3} - \frac{r}{k}\right],\\
z_3 &= \frac{\varepsilon e_1 g}{(1+gn^*)^3},\ z_4 = -\frac{\varepsilon e_1 u^* g^2}{(1+gn^*)^4}.
\end{aligned}$$

The eigenvalues of $J^*$ are $\lambda_{11} = \phi + i\varrho$ and $\lambda_{12} = \phi - i\varrho$, where $\phi = \frac{\mathrm{Tr}(J^*)}{2}$ and $\varrho = \sqrt{\mathrm{Det}(J^*) - \left(\frac{\mathrm{Tr}(J^*)}{2}\right)^2}$. If $\mathrm{Tr}^2(J^*) < 4\mathrm{Det}(J^*)$,then $\lambda_{11}$ and $\lambda_{12}$ are complex conjugate. Specifically, when $\varepsilon = \varepsilon^*$, $\lambda_{11} = i\varrho$ and $\lambda_{12} = -i\varrho$ are purely imaginary numbers. Then, the eigenvector of $J^*$ corresponding to $\lambda_{11,12}$ is

$$\zeta = \begin{pmatrix} 1 \\ \zeta_1 - \zeta_2 i \end{pmatrix},$$

in which $\zeta_1 = \frac{\phi - j_{11}}{j_{12}}$ and $\zeta_2 = -\frac{\varrho}{j_{12}}$.
Let

$$H = \begin{pmatrix} 1 & 0 \\ \zeta_1 & \zeta_2 \end{pmatrix}.$$

With the transformation

$$\begin{pmatrix} u \\ n \end{pmatrix} = H \begin{pmatrix} p \\ q \end{pmatrix},$$

(B.2) is rewritten as

$$\begin{pmatrix} \frac{\mathrm{d}p}{\mathrm{d}t} \\ \frac{\mathrm{d}q}{\mathrm{d}t} \end{pmatrix} = \begin{pmatrix} \phi & -\varrho \\ \varrho & \phi \end{pmatrix} \begin{pmatrix} p \\ q \end{pmatrix} + \begin{pmatrix} K(p,q) \\ S(p,q) \end{pmatrix}, \tag{B.3}$$

where

$$\begin{aligned}
K(p,q) &= k_1 p^2 + k_2 pq + k_3 p^3 + k_4 p^2 q + \cdots,\\
S(p,q) &= s_1 p^2 + s_2 pq + s_3 q^2 + s_4 p^3 + s_5 pq^2 + s_6 p^2 q + s_7 q^3 + \cdots,
\end{aligned}$$

with

$$k_1 = h_1 + h_2\zeta_1,\ k_2 = h_2\zeta_2,\ k_3 = h_3 + h_4\zeta_1,\ k_4 = h_4\zeta_2,$$

$$s_1 = z_1\zeta_1 + z_2\zeta_1^2,\ s_2 = z_1\zeta_1\zeta_2 + 2\zeta_1\zeta_2 z_2,\ s_3 = z_2\zeta_2,$$
$$s_4 = z_4\zeta_1^3 + z_3\zeta_1^2,\ s_5 = z_3\zeta_2^2 + 3z_4\zeta_1\zeta_2^2,\ s_6 = 2z_3\zeta_1\zeta_2 + 3z_4\zeta_1^2\zeta_2,\ s_7 = z_4\zeta_2^3.$$

Transforming (B.3) with polar coordinates yields

$$\begin{cases} \dfrac{\mathrm{d}r_0}{\mathrm{d}t} = \phi'(\tilde{\varepsilon})(\varepsilon - \tilde{\varepsilon})r_0 + \xi_1(\tilde{\varepsilon})r_0^3 + \cdots, \\ \dfrac{\mathrm{d}\theta_0}{\mathrm{d}t} = \varrho(\tilde{\varepsilon}) + \varrho'(\tilde{\varepsilon})(\varepsilon - \tilde{\varepsilon}) + \xi_2(\tilde{\varepsilon})r_0^2 + \cdots. \end{cases}$$

Next we determine the positivity and negativity of $\xi_1(\tilde{\varepsilon})$.

$$\begin{aligned} \xi_1(\tilde{\varepsilon}) = &\frac{1}{16}\left[K_{ppp} + K_{pqq} + S_{ppq} + S_{qqq}\right]_{(0,0,\tilde{\varepsilon})} + \frac{1}{16\varrho(\tilde{\varepsilon})}\left[K_{pq}(K_{pp} + K_{qq})\right. \\ &\left. - S_{pq}(S_{pp} + S_{qq}) - K_{pp}S_{pp} + K_{qq}S_{qq}\right]_{(0,0,\tilde{\varepsilon})}, \end{aligned}$$

where

$$\begin{aligned} &K_{ppp}(0,0,\tilde{\varepsilon}) = 6k_3,\ K_{pqq}(0,0,\tilde{\varepsilon}) = 0,\ K_{qqq}(0,0,\tilde{\varepsilon}) = 0, \\ &S_{ppq}(0,0,\tilde{\varepsilon}) = 2\left(\frac{2\zeta_1\zeta_2\tilde{\varepsilon}e_1 g}{(1+gn^*)^3} - \frac{3\varepsilon^* e_1 u^* g^2\zeta_1^2\zeta_2}{(1+gn^*)^4}\right), \\ &S_{qqq}(0,0,\tilde{\varepsilon}) = -\frac{6\zeta_2^3\tilde{\varepsilon}e_1 u^* g^2}{(1+gn^*)^4}, \\ &K_{pq}(0,0,\tilde{\varepsilon}) = k_2,\ K_{pp}(0,0,\tilde{\varepsilon}) = 2k_1,\ K_{qq}(0,0,\tilde{\varepsilon}) = 0, \\ &S_{pq}(0,0,\tilde{\varepsilon}) = -\frac{\tilde{\varepsilon}e_1\zeta_1\zeta_2}{(1+gn^*)^2} + 2\tilde{\varepsilon}\zeta_1\zeta_2\left(\frac{e_1 u^* g}{(1+gn^*)^3} - \frac{r}{k}\right), \\ &S_{pp}(0,0,\tilde{\varepsilon}) = \tilde{\varepsilon}\zeta_1\left(\frac{e_1 u^* g\zeta_1}{(1+gn^*)^3 - \frac{r\zeta_1}{k}} - \frac{e_1}{(1+gn^*)^2}\right), \\ &S_{qq}(0,0,\tilde{\varepsilon}) = 2\tilde{\varepsilon}\zeta_2\left(\frac{e_1 u^* g}{(1+gn^*)^3} - \frac{r}{k}\right). \end{aligned}$$

Denote $\Gamma = -\frac{\xi_1(\tilde{\varepsilon})}{\phi'(\tilde{\varepsilon})}$. The stability of the periodic solution depends on $\xi_1(\tilde{\varepsilon})$. $\Gamma$ determines the direction of the Hopf bifurcation. Thus, we obtain Theorem 3.3.

## C Derivation of the Fickian diffusion term

Based on the mean-field logic commonly used in spatial ecological modeling (Durrett and Levin 1994), we derive the Fickian diffusion term below. We assume that the total population density at each spatial location remains constant and is denoted by $N$. Let $u(x, y, t)$ represent the density of cooperators at spatial location $(x, y)$ and time $t$, while $N - u(x, y, t)$ represents the density of defectors. We assume that, at each short time

interval, cooperators undergo unbiased, random movements between a focal location $(x, y)$ and its four immediate neighboring sites: to the right $(x + \Delta x, y)$, to the left $(x - \Delta x, y)$, upward $(x, y + \Delta y)$, and downward $(x, y - \Delta y)$. The same symmetric movement rule applies to defectors. For simplicity, we focus on the dynamics of cooperators only. We perform a second-order Taylor expansion of $u(x, y, t)$ around the focal point $(x, y)$ in both directions:

$$
\begin{aligned}
u(x + \Delta x, y, t) &= u(x, y, t) + \Delta x \frac{\partial u}{\partial x} + \frac{(\Delta x)^2}{2} \frac{\partial^2 u}{\partial x^2} + \cdots, \\
u(x - \Delta x, y, t) &= u(x, y, t) - \Delta x \frac{\partial u}{\partial x} + \frac{(\Delta x)^2}{2} \frac{\partial^2 u}{\partial x^2} + \cdots, \\
u(x, y + \Delta y, t) &= u(x, y, t) + \Delta y \frac{\partial u}{\partial y} + \frac{(\Delta y)^2}{2} \frac{\partial^2 u}{\partial y^2} + \cdots, \\
u(x, y - \Delta y, t) &= u(x, y, t) - \Delta y \frac{\partial u}{\partial y} + \frac{(\Delta y)^2}{2} \frac{\partial^2 u}{\partial y^2} + \cdots.
\end{aligned}
$$

The net change in the density of cooperators at $(x, y)$ due to symmetric random movement is proportional to the inflow from the four neighboring sites minus the outflow from the focal site. That is,

$$
\begin{aligned}
\Delta u(x, y, t) \propto [&u(x + \Delta x, y, t) + u(x - \Delta x, y, t) \\
&+ u(x, y + \Delta y, t) + u(x, y - \Delta y, t) - 4u(x, y, t)].
\end{aligned}
$$

Substituting the Taylor expansions and simplifying, we obtain

$$
\Delta u(x, y, t) \propto (\Delta x)^2 \frac{\partial^2 u}{\partial x^2} + (\Delta y)^2 \frac{\partial^2 u}{\partial y^2}.
$$

Letting $\Delta x = \Delta y = \varrho$, dividing by a small time increment $\Delta t$, and defining the diffusion coefficient $D = \frac{\varrho^2}{2\Delta t}$, we arrive at the diffusion equation:

$$
\frac{\partial u}{\partial t} = D \left( \frac{\partial^2 u}{\partial x^2} + \frac{\partial^2 u}{\partial y^2} \right) = D \nabla^2 u.
$$

This concludes the derivation of the standard Fickian diffusion term in two spatial dimensions. The result justifies our use of the Laplacian operator $\nabla^2 u$ in the reaction-diffusion model under the assumption of random movement and constant total density.

## D Proof of Theorem 4.1

***Proof*** Linearization of the system (2.6) at any steady state $E(u, m)$ yields

$$\begin{cases} \dfrac{\partial \mathbf{P}}{\partial t} = \mathcal{L}\mathbf{P} := D_1 \nabla^2 \mathbf{P} + \tilde{J}\mathbf{P}, & \mathbf{x} \in \Omega, \\ \dfrac{\partial \mathbf{P}}{\partial \eta} = 0, & \mathbf{x} \in \partial\Omega, \\ \partial \mathbf{P}(\mathbf{x}, 0) = \mathbf{P}_0(\mathbf{x}), & \mathbf{x} \in \Omega, \end{cases} \tag{D.1}$$

where

$$\tilde{J} = \begin{pmatrix} \tilde{j}_{11} & \tilde{j}_{12} \\ \tilde{j}_{21} & \tilde{j}_{22} \end{pmatrix}, \mathbf{P} = \begin{pmatrix} \tilde{u} - u \\ \tilde{n} - n \end{pmatrix}, D_1 = \begin{pmatrix} d_u & 0 \\ 0 & d_n \end{pmatrix},$$

with

$$\begin{aligned} \tilde{j}_{11} =& \frac{1}{N^2}\left[3(\gamma_1 n - \theta\gamma_2)u^2 + 2(\theta(d_0 - b_0) - \gamma_3 n - \gamma_1 n + \theta\gamma_2)Nu - N^2(\theta(d_0 - b_0) - \gamma_3 n)\right] \\ \tilde{j}_{12} =& \frac{u(N-u)}{N^2}(N\gamma_3 - \gamma_1 u), \\ \tilde{j}_{21} =& -\frac{e_1 n\varepsilon}{gn+1}, \\ \tilde{j}_{22} =& \varepsilon\left(r\left(1 - \frac{2n}{k}\right) - \frac{e_1 u}{(gn+1)^2}\right). \end{aligned}$$

Find the solution $\mathbf{V}_{s,v}(\mathbf{x})$ of (D.1) in the following form

$$\mathbf{V}_{s,v}(\mathbf{x}, t) = \sum_{s,v} \mathbf{H}_{s,v} e^{\lambda(m^2)t} \cos\frac{s\pi x}{M} \cos\frac{v\pi y}{M}. \tag{D.2}$$

Substituting (D.2) into (D.1) yields the following characteristic equation

$$\lambda^2 - \widetilde{\mathrm{Tr}}(m^2)\lambda + \widetilde{\mathrm{Det}}(m^2) = 0, \tag{D.3}$$

where

$$\begin{aligned} \widetilde{\mathrm{Tr}}(m^2) &= -m^2(d_u + d_n) + \tilde{j}_{11} + \tilde{j}_{22}, \\ \widetilde{\mathrm{Det}}(m^2) &= d_u d_n m^4 - (\tilde{j}_{11} d_n + \tilde{j}_{22} d_u)m^2 + \tilde{j}_{11}\tilde{j}_{22} - \tilde{j}_{21}\tilde{j}_{12}. \end{aligned}$$

(I) If $E(u, n) = E_0(0, 0)$, then the eigenvalues of (D.3) are $\lambda_{1m} = \theta(b_0 - d_0) - d_u m^2$ and $\lambda_{2m} = r\varepsilon - d_n m^2$. Clearly, there exists $m = 0$ such that $\lambda_{20} = r\varepsilon > 0$. Thus, $E_0(0, 0)$ is spatially unstable.
(II) If $E(u, n) = E_1(N, 0)$, then $\lambda_{1m} = \theta(c_0 - a_0) - d_u m^2$ and $\lambda_{2m} = \varepsilon(r - Ne_1) - d_n m^2$ are eigenvalues of (D.3). $\lambda_{1m} < 0$ and $\lambda_{2m} < 0$ hold for all wavenumbers $m$ when $c_0 < a_0$ and $r < Ne_1$. In this case, $E_1(N, 0)$ is spatially stable. When $c_0 > a_0$ or $r > Ne_1$, $\lambda_{10} > 0$ or $\lambda_{20} > 0$ is valid, then $E_1(N, 0)$ is spatially unstable.

(III) If $E(u,n)=E_2(u_2,0)$, then (D.3) has eigenvalues $\lambda_{1m}=\frac{\theta(d_0-b_0)(a_0-c_0)}{a_0+d_0-b_0-c_0}-d_um^2$ and $\lambda_{2m}=\varepsilon(r-\tilde{r})-d_nm^2$. For all wavenumbers $m$, both $\lambda_{1m}<0$ and $\lambda_{2m}<0$ are true when $a_0<c_0$ and $r<\tilde{r}$, so $E_2(u_2,0)$ is spatially stable. However, when $a_0>c_0$ or $r>\tilde{r}$, $E_2(u_2,0)$ is spatially unstable since there exists $m=0$ making $\lambda_{10}>0$ or $\lambda_{20}>0$.
(IV) If $E(u,n)=E_3(0,k)$, then the two eigenvalues of (D.3) are $\lambda_{1m}=k(\tilde{d_1}-d_1)-d_um^2$ and $\lambda_{2m}=-r\varepsilon-d_nm^2$. If $d_1>\tilde{d_1}$,then $\lambda_{1m}<0$ and $\lambda_{2m}<0$ are valid for all $m$. For $m=0$, $\lambda_{10}=k(\tilde{d_1}-d_1)>0$ if $d_1<\tilde{d_1}$. Such a situation, $E_3(0,k)$ is spatially unstable.
(V) If $E(u,n)=E_4^+(N,n_4^+)$, then the eigenvalues of (D.3) are $\lambda_{1m}=(\tilde{a_1}-a_1)n_4^+-d_um^2$ and $\lambda_{2m}=\frac{\varepsilon}{e_1}(\tilde{N}-N)(gn_4^++1)^2-d_mm^2$. $\lambda_{1m}<0$ and $\lambda_{2m}<0$ are true when $a_1>\tilde{a_1}$ and $N>\tilde{N}$. Hence, $E_4^+(N,n_4^+)$ is spatially stable. For $m=0$, there is $\lambda_{10}=(\tilde{a_1}-a_1)n_4^+>0$ or $\lambda_{20}=\frac{\varepsilon}{e_1}(\tilde{N}-N)(gn_4^++1)^2>0$ when $a_1<\tilde{a_1}$ or $N<\tilde{N}$. Then, $E_4^+(N,n_4^+)$ is spatially unstable.
(VI) If $E(u,n)=E_4^-(N,n_4^-)$, then the eigenvalues of (D.3) are $\lambda_{1m}=(\tilde{a_1}-a_1)n_4^--d_um^2$ and $\lambda_{2m}=\frac{\varepsilon}{e_1}(\tilde{N}-N)(gn_4^-+1)^2-d_mm^2$. The process of analyzing the stability of the steady state $E_4^-(N,n_4^-)$ is similar to that of $E_4^-(N,n_4^+)$, and we will not describe it in detail here.
(VII) If $E(u,n)=E^*(u^*,n^*)$, then $\tilde{J}|_{E=E^*}=J^*$. $\delta_5<0$ and $\delta_6>0$ guarantee that $j_{11}<0$ and $j_{22}<0$, then $\widetilde{\mathrm{Tr}}(m^2)<0$ holds. Furthermore, $\widetilde{\mathrm{Det}}(m^2)>0$ when $\delta_7>0$. Therefore, $E^*(u^*,n^*)$ is spatially stable when $\delta_5<0$, $\delta_6>0$, and $\delta_7>0$. In this case, Turing instability is impossible. This completes the proof. □

**Acknowledgements** The research of Haihui Cheng was partially supported by the National Natural Science Foundation of China (No.12271308) and the China Scholarship Council. The research of Hao Wang was partially supported by the Natural Sciences and Engineering Research Council of Canada (Individual Discovery Grant RGPIN-2020-03911 and Discovery Accelerator Supplement Award RGPAS-2020-00090) and the Canada Research Chairs program (Tier 1 Canada Research Chair Award). The research of Xinzhu Meng was partially supported by the National Natural Science Foundation of China (No.12271308).

**Availability of data and material** Data sharing not applicable to this article as no datasets were generated or analysed during the current study.

## Declarations

**Conflicts of interest** All authors certify that they have no affiliations with or involvement in any organization or entity with any financial interest or non-financial interest in the subject matter or materials discussed in this manuscript.

## References

Alfarano S, Lux T, Wagner F (2005) Estimation of agent-based models: The case of an asymmetric herding model. Comput Econ 26(1):19–49. https://doi.org/10.1007/s10614-005-6415-1

Auger P, Bravo de la Parra R, Morand S, Sanchez E (2002) A predator-prey model with predators using hawk and dove tactics. Math Biosci 177–178:185–200. https://doi.org/10.1016/s0025-5564(01)00112-2

Bertram R, Rubin JE (2017) Multi-timescale systems and fast-slow analysis. Math Biosci 287:105–121. https://doi.org/10.1016/j.mbs.2016.07.003

Boesch C (1994) Cooperative hunting in wild chimpanzees. Anim Behav 48(3):653–667. https://doi.org/10.1006/anbe.1994.1285

Cantrell RS, Cosner C (2004) Spatial ecology via reaction-diffusion equations. John Wiley & Sons

Cheng H, Meng X (2023) Evolution of cooperation in multigame with environmental space and delay. Biosystems 223:104801. https://doi.org/10.1016/j.biosystems.2022.104801

Cheng H, Meng X, Hayat T, Hobiny A (2022) Dynamics analysis for a prey–predator evolutionary game system with delays. Dyn Games and Appl 14(2):480–507. https://doi.org/10.1007/s13235-022-00464-w

Cheng H, Meng X, Hayat T, Hobiny A (2023) Multistability and bifurcation analysis for a three-strategy game system with public goods feedback and discrete delays. Chaos, Solitons & Fractals 175:114011. https://doi.org/10.1016/j.chaos.2023.114011

Cheng H, Sysoeva L, Wang H, Yuan H, Zhang T, Meng X (2024) Evolution of cooperation in spatio-temporal evolutionary games with public goods feedback. Bull Math Biol 86(6):67. https://doi.org/10.1007/s11538-024-01296-y

Dugatkin LA (2001) Model systems in behavioral ecology: integrating conceptual, theoretical, and empirical approaches, vol 23. Princeton University Press

Durrett R, Levin S (1994) The importance of being discrete (and spatial). Theor Popul Biol 46(3):363–394. https://doi.org/10.1006/tpbi.1994.1032

Feng T, Charbonneau D, Qiu Z, Kang Y (2021) Dynamics of task allocation in social insect colonies: scaling effects of colony size versus work activities. J Math Biol 82(5):42. https://doi.org/10.1007/s00285-021-01589-z

Garay J, Cressman R, Mori TF, Varga T (2018) The ess and replicator equation in matrix games under time constraints. J Math Biol 76(7):1951–1973. https://doi.org/10.1007/s00285-018-1207-0

Gilby IC, Machanda ZP, Mjungu DC, Rosen J, Muller MN, Pusey AE, Wrangham RW (2015) 'impact hunters' catalyse cooperative hunting in two wild chimpanzee communities. Philos Trans Roy Soc B Biol Sci 370(1683):20150005. https://doi.org/10.1098/rstb.2015.0005

Giordano M, Villholth KG (2007) The agricultural groundwater revolution: opportunities and threats to development, vol 3. CABI

Gordon DM (2010) Ant encounters: interaction networks and colony behavior. Princeton University Press. https://doi.org/10.1515/9781400835447

Gou W, Jin Z, Wang H (2023) Hopf bifurcation for general network-organized reaction-diffusion systems and its application in a multi-patch predator-prey system. J Differ Equ 346:64–107. https://doi.org/10.1016/j.jde.2022.11.026

Halatek J, Frey E (2018) Rethinking pattern formation in reaction–diffusion systems. Nat Phys 14(5):507–514. https://doi.org/10.1038/s41567-017-0040-5

Haselhuhn MP, Mellers BA (2005) Emotions and cooperation in economic games. Brain Res Cogn Brain Res 23(1):24–33. https://doi.org/10.1016/j.cogbrainres.2005.01.005

Hastings A, Cuddington K, Davies KF, Dugaw CJ, Elmendorf S, Freestone A, Harrison S, Holland M, Lambrinos J, Malvadkar U, Melbourne BA, Moore K, Taylor C, Thomson D (2004) The spatial spread of invasions: new developments in theory and evidence. Ecol Lett 8(1):91–101. https://doi.org/10.1111/j.1461-0248.2004.00687.x

Hauert C, Saade C, McAvoy A (2019) Asymmetric evolutionary games with environmental feedback. J Theor Biol 462:347–360. https://doi.org/10.1016/j.jtbi.2018.11.019

Heggerud CM, Wang H, Lewis MA (2020) Transient dynamics of a stoichiometric cyanobacteria model via multiple-scale analysis. SIAM J Appl Math 80(3):1223–1246. https://doi.org/10.1137/19m1251217

Herbert-Read JE, Romanczuk P, Krause S, Strömbom D, Couillaud P, Domenici P, Kurvers RHJM, Marras S, Steffensen JF, Wilson ADM, Krause J (2016) Proto-cooperation: group hunting sailfish improve hunting success by alternating attacks on grouping prey. Proceedings of the Royal Society B Biological Sciences 283(1842):20161671. https://doi.org/10.1098/rspb.2016.1671

Hofbauer J, Sigmund K (1998) Evolutionary games and population dynamics. Cambridge University Press

Jiang Y, Wang X, Liu L, Wei M, Zhao J, Zheng Z, Tang S (2023) Nonlinear eco-evolutionary games with global environmental fluctuations and local environmental feedbacks. PLoS Comput Biol 19(6):e1011269. https://doi.org/10.1371/journal.pcbi.1011269

Jousset A, Eisenhauer N, Materne E, Scheu S (2013) Evolutionary history predicts the stability of cooperation in microbial communities. Nat Commun 4(1):2573. https://doi.org/10.1038/ncomms3573

Keeling MJ, Rohani P (2011) Modeling infectious diseases in humans and animals. Princeton University Press
Kittle AM, Anderson M, Avgar T, Baker JA, Brown GS, Hagens J, Iwachewski E, Moffatt S, Mosser A, Patterson BR, Reid DE, Rodgers AR, Shuter J, Street GM, Thompson ID, Vander Vennen LM, Fryxell JM (2015) Wolves adapt territory size, not pack size to local habitat quality. J Anim Ecol 84(5):1177–86. https://doi.org/10.1111/1365-2656.12366
Kolk A, Pinkse J (2005) Business responses to climate change: Identifying emergent strategies. Calif Manage Rev 47(3):6–20. https://doi.org/10.2307/41166304
Lenoir A, D'Ettorre P, Errard C, Hefetz A (2001) Chemical ecology and social parasitism in ants. Annu Rev Entomol 46:573–99. https://doi.org/10.1146/annurev.ento.46.1.573
Lin YH, Weitz JS (2019) Spatial interactions and oscillatory tragedies of the commons. Phys Rev Lett 122(14):148102. https://doi.org/10.1103/PhysRevLett.122.148102
Lion S (2018) Theoretical approaches in evolutionary ecology: Environmental feedback as a unifying perspective. Am Nat 191(1):21–44. https://doi.org/10.1086/694865
Lyon BE, Eadie JM (2008) Conspecific brood parasitism in birds: A life-history perspective. Annu Rev Ecol Evol Syst 39(1):343–363. https://doi.org/10.1146/annurev.ecolsys.39.110707.173354
MacNulty DR, Smith DW, Mech LD, Vucetich JA, Packer C (2012) Nonlinear effects of group size on the success of wolves hunting elk. Behav Ecol 23(1):75–82. https://doi.org/10.1093/beheco/arr159
Manna K, Volpert V, Banerjee M (2021) Pattern formation in a three-species cyclic competition model. Bull Math Biol 83(5):52. https://doi.org/10.1007/s11538-021-00886-4
Mosser AA, Kosmala M, Packer C (2015) Landscape heterogeneity and behavioral traits drive the evolution of lion group territoriality. Behav Ecol 26(4):1051–1059. https://doi.org/10.1093/beheco/arv046
Nanda M, Durrett R (2017) Spatial evolutionary games with weak selection. Proc Natl Acad Sci USA 114(23):6046–6051. https://doi.org/10.1073/pnas.1620852114
Newth D, Cornforth D (2009) Asynchronous spatial evolutionary games. Biosystems 95(2):120–9. https://doi.org/10.1016/j.biosystems.2008.09.003
Nordhaus W (2015) Climate clubs: Overcoming free-riding in international climate policy. Am Econ Rev 105(4):1339–1370. https://doi.org/10.1257/aer.15000001
Nowak MA, May RM (1992) Evolutionary games and spatial chaos. Nature 359(6398):826–829. https://doi.org/10.1038/359826a0
Nowak MA, Sigmund K (2004) Evolutionary dynamics of biological games. Sci 303(5659):793–9. https://doi.org/10.1126/science.1093411
Press MC, Phoenix GK (2005) Impacts of parasitic plants on natural communities. New Phytol 166(3):737–51. https://doi.org/10.1111/j.1469-8137.2005.01358.x
Rand DG, Nowak MA (2013) Human cooperation. Trends Cogn Sci 17(8):413–25. https://doi.org/10.1016/j.tics.2013.06.003
Riehl C, Frederickson ME (2016) Cheating and punishment in cooperative animal societies. Philos Trans Roy Soc London B Biol Sci 371(1687):20150090. https://doi.org/10.1098/rstb.2015.0090
Scheel D, Packer C (1991) Group hunting behaviour of lions: a search for cooperation. Anim Behav 41(4):697–709. https://doi.org/10.1016/s0003-3472(05)80907-8
Schoener TW (1983) Field experiments on interspecific competition. Am Nat 122(2):240–285. https://doi.org/10.1086/284133
Schreiber SJ, Killingback TP (2013) Spatial heterogeneity promotes coexistence of rock-paper-scissors metacommunities. Theor Popul Biol 86:1–11. https://doi.org/10.1016/j.tpb.2013.02.004
Smith JM (1982) Evolution and the Theory of Games. Cambridge University Press, Cambridge. https://doi.org/10.1017/CBO9780511806292
Song Y, Jiang H, Liu QX, Yuan Y (2017) Spatiotemporal dynamics of the diffusive mussel-algae model near turing-hopf bifurcation. SIAM J Appl Dyn Syst 16(4):2030–2062. https://doi.org/10.1137/16m1097560
Stadler B, Dixon AF (2005) Ecology and evolution of aphid-ant interactions. Annu Rev Ecol Evol Syst 36(1):345–372. https://doi.org/10.1146/annurev.ecolsys.36.091704.175531
Szabó G, Szolnoki A (2012) Selfishness, fraternity, and other-regarding preference in spatial evolutionary games. J Theor Biol 299:81–87. https://doi.org/10.1016/j.jtbi.2011.03.015
Tilman AR, Watson JR, Levin S (2016) Maintaining cooperation in social-ecological systems. Thyroid Res 10(2):155–165. https://doi.org/10.1007/s12080-016-0318-8
Tilman AR, Plotkin JB, Akcay E (2020) Evolutionary games with environmental feedbacks. Nat Commun 11(1):915. https://doi.org/10.1038/s41467-020-14531-6

Tilman D (1982) Resource competition and community structure. Princeton University Press
Valdaliso JM, Wilson JR (2015) Strategies for shaping territorial competitiveness. Routledge, Oxford
van Veelen M (2011) The replicator dynamics with n players and population structure. J Theor Biol 276(1):78–85. https://doi.org/10.1016/j.jtbi.2011.01.044
Wagner CE, Saad-Roy CM, Grenfell BT (2022) Modelling vaccination strategies for covid-19. Nat Rev Immunol 22(3):139–141. https://doi.org/10.1038/s41577-022-00687-3
Wang C, Yuan S, Wang H (2022) Spatiotemporal patterns of a diffusive prey-predator model with spatial memory and pregnancy period in an intimidatory environment. J Math Biol 84(3):12. https://doi.org/10.1007/s00285-022-01716-4
Wang H, Salmaniw Y (2023) Open problems in pde models for knowledge-based animal movement via nonlocal perception and cognitive mapping. J Math Biol 86(5):71. https://doi.org/10.1007/s00285-023-01905-9
Wang W, Zhou M, Fan X, Zhang T (2024) Global dynamics of a nonlocal pde model for lassa haemorrhagic fever transmission with periodic delays. Comput Appl Math 43(3):140. https://doi.org/10.1007/s40314-024-02662-1
Weitz JS, Eksin C, Paarporn K, Brown SP, Ratcliff WC (2016) An oscillating tragedy of the commons in replicator dynamics with game-environment feedback. Proc Natl Acad Sci USA 113(47):E7518–E7525. https://doi.org/10.1073/pnas.1604096113
Wilkinson GS (1984) Reciprocal food sharing in the vampire bat. Nature 308(5955):181–184. https://doi.org/10.1038/308181a0
Yamin D, Jones FK, DeVincenzo JP, Gertler S, Kobiler O, Townsend JP, Galvani AP (2016) Vaccination strategies against respiratory syncytial virus. Proc Natl Acad Sci USA 113(46):13239–13244. https://doi.org/10.1073/pnas.1522597113
Yang J, Yuan S, Zhang T (2021) Complex dynamics of a predator–prey system with herd and schooling behavior: with or without delay and diffusion. Nonlinear Dyn 104(2):1709–1735. https://doi.org/10.1007/s11071-021-06343-0
Yong JC, Choy BKC (2021) Noncompliance with safety guidelines as a free-riding strategy: An evolutionary game-theoretic approach to cooperation during the covid-19 pandemic. Front Psychol 12:646892. https://doi.org/10.3389/fpsyg.2021.646892
Yuan H, Meng X (2022) Replicator dynamics of division of labor games with delayed payoffs in infinite populations. Chaos, Solitons & Fractals 158:112058. https://doi.org/10.1016/j.chaos.2022.112058
Yuan S, Xu C, Zhang T (2013) Spatial dynamics in a predator-prey model with herd behavior. Chaos 23(3):033102. https://doi.org/10.1063/1.4812724